Annual Report 2015

HI Jena

Helmholtz Institute Jena

Helmholtz Institute Jena
Fröbelstieg 3
07743 Jena
www.hi-jena.de

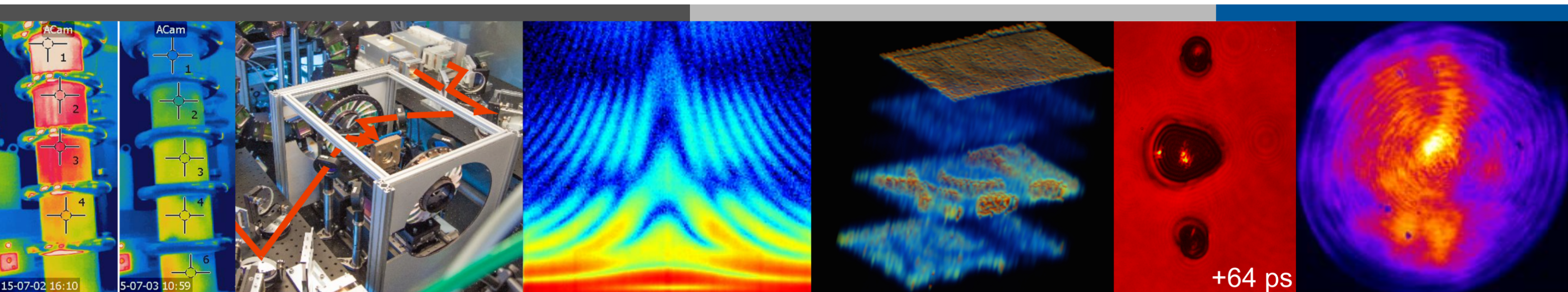

seit 1558

Helmholtz Institute Jena

Annual Report 2015

Imprint
Publisher: Helmholtz Institute Jena, Fröbelstieg 3, 07746 Jena, Germany, April 2016
Editors: Daniel Seipt and Marc M. Günther

Contents

Photon and Particle Spectroscopy 39

Theory 63

Publications 77

Foreword

Seven years after its foundation in 2009, the Helmholtz Institute Jena (HI-Jena) being an external research institute of GSI at Darmstadt has now established itself as a well-known research institution in the fields of high-power laser development, laser-particle acceleration and the spectroscopy and detection of high-energy photon and particle beams. With its location at the campus of the Friedrich Schiller University Jena (FSU), the HI Jena forms a recognized 'bridge' between the GSI Helmholtz Centre for Heavy Ion Research in Darmstadt and the Helmholtz Centres DESY in Hamburg, and HZDR at Dresden-Rossendorf.

A particularly important cornerstone of the year 2015 was the inauguration of the new JETI 200 laser system, which increases significantly the research infrastructure available at the Helmholtz Institute and will have a huge impact on the institute's ongoing research program. This Annual Report for the year 2015 highlights recent achievements in the experimental and theoretical research programs of the institute, with just emphasizing one particular milestone: After a significant upgrade of the laser system POLARIS has been carried out in 2015, its maximum output energy after the final amplifier could be increased by more than a factor of three. The achieved pulse energy of 54.16 Joules sets a new world record for fully diode-pumped, high-power laser systems.

Since the last year 2015, the HI-Jena is now part also of the HGF Program Oriented Funding, POF III, with an active involvement in the in-house research topic *Extreme States of Matter: From cold ions to hot plasmas* of the program *From Matter to Materials and Life* and the subtopics *Novel Accelerator Concepts and Detector Technologies and Systems* within the program *Matter and Technology*. The participation in POF and the long-term funding in this program helped to establish the visibility of the HI Jena within the Helmholtz Association. Moreover, the third-party funding has been increased significantly during the last two years, with one main focus on the APPA research program.

The *Research School for Advanced Photon Science* of the Helmholtz Institute (RS-APS) has gained increasing visibility during the last years. Meanwhile, about 35 participating students are enrolled in the School with almost 50% being supported by 3rd party funding. In September 2015 another lecture week on the topic *(Laser) Spectroscopy of Stored and Trapped Ions* took place, jointly organized by the RS-APS and by the Helmholtz Graduate School HGS-HIRe. These activities help to educate the next-generation of scientists in strong-field physics, an important part of the scientific program of the HI Jena and of particular relevance for future research at HGF's forthcoming large-scale facilities FAIR and XFEL. This success would not have been possible without the great effort of all members of the HI-Jena as well as the enthusiasm and support of the colleagues at the FSU and all partner research institutions.

Research School of Advanced Photon Science of the Helmholtz Institute Jena

G. Weber[1,2], R. Märtin[1,2], Ch. Spielmann[3], and Th. Stöhlker[1,2,3]
[1]HI-Jena, Jena, Germany; [2]GSI, Darmstadt, Germany; [3]IOQ, University Jena, Jena, Germany

Among the most important tasks of the Helmholtz Institute Jena is the education and support of young scientists. The Research School of Advanced Photon Science (RS-APS) provides structured PhD education adapted to the research profile and organizational structure of the HI Jena. Emphasis is given to research being relevant for the international FAIR project in Darmstadt and the European XFEL facility in Hamburg, both being currently in the construction phase.

In 2015 about 35 PhD students were participating in the program of the research school. By now more than 15 students with third-party funding have decided to join RS-APS to profit from the structured PhD education alongside the 20 stipend holders directly financed by the graduate school. The significant increase in the number of participants just three years after its official inauguration in 2012 is a great success. The doctoral students were supervised by 14 principal investigators belonging directly to the Helmholtz Institute Jena or to institutes of the cooperating University Jena. Besides their doctoral work the students have the possibility to participate in the academic program which is offered directly by the Helmholtz Institute Jena and moreover they have access to the broad spectrum of courses provided by the cooperating graduate programs.

The regular on-site seminars of the Research School provide the students either a platform for presenting their recent results or meeting distinguished researchers in the field. Additionally in 2014 almost half of the students of the HI Jena participated in dedicated soft skill block courses offered by HGS-HIRe focusing on the strengthening the core competencies of young researchers. Furthermore students of the Helmholtz Institute attended so-called Power Weeks by HGS-HIRe. A Power Week is focused on a particular science topic. In contrast to a lecture week it is not interdisciplinary and therefore allows discussions on a much deeper level. In addition transferable skill courses offered on site by the graduate academy Jena have been visited, e.g. qualification in academic teaching.

One major event in 2015 was the third joint HGS-HIRe and RS-APS Lecture Week which took place in Buchenau Manor from September 13th to 18th. The whole week 18 students from RS-APS and HGS-HIRe dealt intensively with “(Laser) Spectroscopy of Stored and Trapped Ions”. The PhD students have been supervised by the lecturers Yuri Litvinov (FAIR/GSI), Wilfried Nörtershäuser (TU Darmstadt/GSI), Jan Rothhardt HI Jena) and Andrey Surzhykov (HI Jena).

Figure 1: Participants of the joint lecture week at Haus Ebersberg

The Research School of the HI Jena is not only supporting its students financially through scholarships but also every student has its own annual travel budget which he can spend individually. In 2015 more than two third of the doctoral candidates took use of this money for visiting international workshops and conferences to present their research results.

High Power Laser Development

Beam profile improvement by means of a new pump extension in the 4th POLARIS amplifier*

S. Keppler[#,1], M. Hellwing[1], M. Hornung[1,2], F. Schorcht[2], A. Kessler[2], H. Liebetrau[1], J. Hein[1,2], and M. C. Kaluza[1,2]

[1]Institute of Optics and Quantum Electronics, FSU Jena, Germany; [2]Helmholtz-Institute Jena, Germany

The ongoing development of the POLARIS laser system in particular towards higher laser pulse energies and shorter pulse durations, is motivated by the prospect of new and more sophisticated experiments in the field of laser-driven particle acceleration. However, increasing the laser pulse energy to higher levels mandatorily requires a smooth and homogenous beam profile. Here, the current limitation is the 4th POLARIS amplifier A4.

Within A4 the pump profile is composed by a number of individual diode spots while the main pulse is amplified in a multi-pass arrangement. With this architecture, even small variations of the pump profile and the pump induced spatial phase aberrations directly lead to inhomogeneities of the spatial pulse profile. Here, the major challenge is the optimal arrangement of the different pump spots, which vary considerably in size and intensity. For the optimization of the individual positions, an „adaptive strategy“-algorithm was applied. This routine is a genetic algorithm that varies the positions of the recorded single pump spots randomly and thus generates mutations which were evaluated with respect to a defined figure of merit. Here, we used a target profile defined by a 4th-order Super-Gaussian function [1].

However, the final homogeneity not only depends on the position of the several spots, but also on their size and total number with respect to the desired pump area. During the operation of POLARIS over the last years, some of the diode stacks had to be replaced. The new stacks provide a better focussability which led to a degradation of the pump profile homogeneity. Smaller spots led to high-frequency spatial modulations and thus, small indentions which are visible in Fig. 1a) and b). Furthermore, by the limited steepness of the pump profile edges the seed beam becomes smaller and smaller during the amplification within the several passes. This “spatial profile narrowing” is compensated by a high input divergence of the seed beam. The free space propagation of the high divergent seed beam and the small inhomogeneities of the pump profile eventually lead to a deep dent of the beam profile, which is visible in Fig. 1c. The symmetry of the beam profile is associated to a symmetric vertical flipping of the profile with every pass during the amplification.

To overcome this problem, a newly developed pump extension was implemented into the existing pump architecture of the 4th POLARIS amplifier. Eight additional stacks, pair-wise polarization coupled, were focussed into the amplifying media by $f = 300$ mm achromatic lenses. The fine adjustment of the individual spot positions is realized by a specially developed mirror mount, which fits exactly into the existing circular lens array. The additional pump spots were positioned in the center of the pump profile to directly compensate for the dent of the beam profile by a slightly increased gain. Fig. 1b) shows the pump profile homogenized by the pump extension. The appropriate beam profile is depicted in Fig. 1d). For a complete compensation of the profile dent, the additional stacks operate at a current of 35A, which corresponds to 12% of the full power of each diode stack. However, from Fig. 1d) it is evident, that the spot positions of the additional stacks have to be optimized further in order to realize an optimal seed beam for the final amplifier A5.

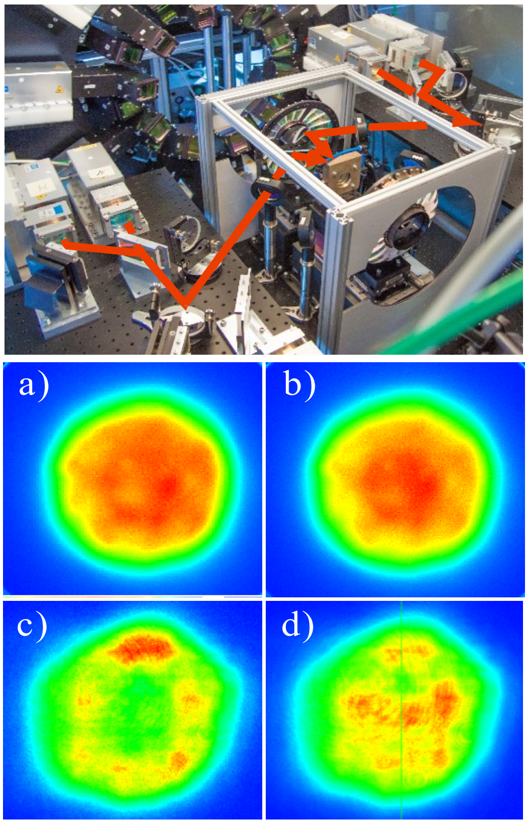

Figure 1: Photo of the newly developed pump extension (upper picture); measured pump profile without (a) and with (b) the pump extension; amplified beam profile of the A4 without (c) and with (d) pump extension.

* Work supported by the European Commissions (EC) 7th Framework Programme (LASERLAB-EUROPE, grant no. 228334) and the Bundesministerium für Bildung und Forschung (BMBF) (03ZIK445 and 03ZIH531).

#Sebastian.Keppler@uni-jena.de

References

[1] S. Keppler et al. Proc. SPIE **8780**, 87800I-1

Diode-Pumped, Chirped-Pulse-Amplification of POLARIS Laser Pulses to 54 J

M. Hornung[1,2,#], H. Liebetrau[2], S. Keppler[2], A. Kessler[1], J. Körner[2], G.A. Becker[2], J. Polz[2], M. Reuter[2], F. Schorcht[1], M. Hellwing[2], J. Hein[1,2], M.C. Kaluza[1,2]

[1]Helmholtz Institute Jena, Germany; [2]Institute of Optics and Quantum Electronics, Jena, Germany.

In 2015, we have performed an extensive upgrade of the POLARIS laser system in order to reach higher pulse energies and shorter pulse durations. Before this upgrade, the most powerful pulses reached a pulse energy of 20.3 J (before compression, 14 J on target) with a spectral bandwidth of 11 nm (FWHM). These pulses could be compressed to a minimum pulse duration of 143 fs (FWHM).

To achieve higher pulse energies we have optimized all multi-pass amplifiers (A2.5, A3, A4 and A5) of POLARIS [1]. A newly developed relay-imaging amplifier with 20 passes replaced the formerly used A2.5 and A3. The fourth amplifier A4 was optimized in its optical setup with respect to the near-field profile. Finally, the design of the last amplifier A5 [2] was changed from a 9- to a 17-pass configuration. Simultaneously, the A5 pump profile was enlarged in order to allow larger diameter pulses to be amplified.

Parallel to the changes in the multipass architecture, the laser was optimized to amplify pulse with a broader spectrum to achieve a shorter pulse duration. A newly developed front-end [3] was installed, the stretcher configuration was changed and spectral shaping capabilities were installed in the regenerative amplifier A2 and in front of A3.

The new A3 is capable of delivering laser pulses with 750 mJ pulse energy in an excellent near-field profile and a spectral bandwidth of 26 nm. These pulses were used as the seed pulses for the amplifier A4. In A4, eight additional laser diode stacks (in total 48) were installed and used to pump the active material specifically to compensate for thermally induced aberrations. In connection with an optimized multi pass setup, 9 passes instead of 10, a significantly improved near-field profile is available for seeding the A5.

In A5, a couple of changes were made in order to reach higher pulse energies. The active material ($Yb:CaF_2$) with a relatively low damage threshold of approx. 4 J/cm^2 was replaced by an new sample with a damage threshold exceeding 10 J/cm^2. The circular pump profile, which is formed by spots from 120 laser diode stacks [2], was enlarged from 35 mm to 42 mm (FWHM). Furthermore, the 30 4-channel laser diode drivers were upgraded to deliver temporally longer electric pulses, which was required to exploit the potential of $Yb:CaF_2$. The pump pulse duration could be increased from 2.7 ms to 4 ms. This leads to a total pump energy of 1.2 kJ. The measured fluorescence light at 1030 nm wavelength of the pump profile is shown in Fig. 1 a). The multi pass setup was entirely redesigned to finally allow for 17 passes (instead of 9) for amplification. This was achieved by using one single pass and 8 passes twice with polarization gating and a large aperture thin-film polarizer. Due to the increased gain of the A5 an additional isolation with a Faraday rotator and a large aperture Pockels cell was required to avoid unwanted self lasing between A4 and A5. Furthermore, a 75 mm aperture Pockels cell was installed behind A5 in order to reduce the amplification of unwanted back reflections from the target. All these changes have led to an improved performance of the laser system. With a seed energy of 2.2 J from A4, a pulse energy of 54.16 J and a spectral bandwidth of 18 nm (FWHM) were achieved with the fifth amplifier. The near field profile of these pulses is shown in Fig. 1 b). To the best of our knowledge, this is the highest pulse energy so far achieved with a diode-pumped CPA laser system. The optimization of the near field profile, the focusing and the compression to a minimal pulse duration of 100 fs are part of ongoing work.

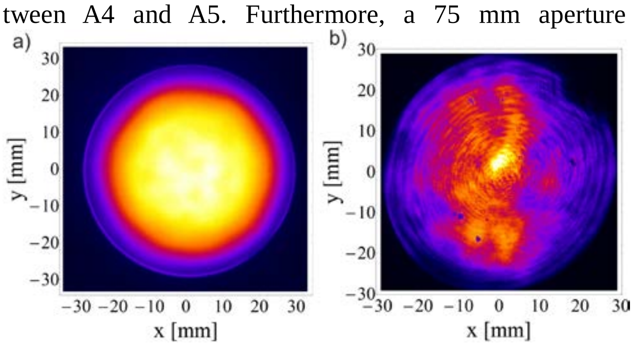

Figure 1: Measurements of the A5 amplifier. a) Pump profile with a total pump energy of 1.2 kJ. b) Near-field profile of the amplified A5 laser pulses. The Pulse energy is 54.16 J.

References

[1] M. Hornung, H. Liebetrau, A. Seidel, S. Keppler, A. Kessler, J. Körner, M. Hellwing, F. Schorcht, D. Klöpfel, A. K. Arunachalam, G. A. Becker, A. Sävert, J. Polz, J. Hein, and M. C. Kaluza, “The all-diode-pumped laser system POLARIS – an experimentalist’s tool generating ultra-high contrast pulses with high energy”, High Power Laser Science and Engineering **2**, e20 (2014).

[2] A. Kessler, M. Hornung, S. Keppler, F. Schorcht, M. Hellwing, H. Liebetrau, J. Körner, A. Sävert, M. Siebold, M. Schnepp, J. Hein, and M. C. Kaluza, “16.6 J chirped femtosecond laser pulses from a diode-pumped $Yb:CaF_2$ amplifier”, Optics Letters, Vol. 39, Issue 6, pp. 1333-1336 (2014).

[3] H. Liebetrau, M. Hornung, A. Seidel, M. Hellwing, A. Kessler, S. Keppler, F. Schorcht, J. Hein, and M. C. Kaluza, “Ultra-high contrast frontend for high peak power fs-lasers at 1030 nm“, Optics Express 22, 24776 (2014).

[#] Marco.Hornung@uni-jena.de

Reducing the pulse duration of the POLARIS-frontend to 86 fs

H. Liebetrau[*1], *M. Hornung*[1,2], *S. Keppler*[1], *A. Kessler*[1], *M. Hellwing*[1], *F. Schorcht*[2], *J. Hein*[1,2], *and M. C. Kaluza*[1,2]

[1]Institut für Optik und Quantenelektronik, FSU Jena, Germany; [2]Helmholtz-Institut Jena, Germany

Since the implementation of the cross-polarized wave generation filter [1] (XPW) in the frontend of POLARIS the width of the spectral intensity reaching the nanosecond stretcher [2] has more than doubled to 45 nm. The spectral range which can be transmitted through the stretcher was so far limited by the geometry and the sizes of the optics to a window of 32 nm (hard cut). This clip in the spectrum has a great influence on the final pulse duration and the intensity contrast in the slope of the main pulse [3], in such a way that it increases the pulse duration and also increases the intensity in the slope.

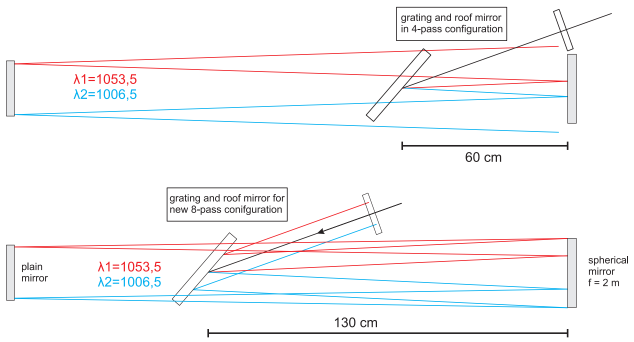

Figure 1: Change in the setup of the ns-stretcher. Two exemplary wavelength rays are shown which are not transmitted in the 4-pass setup but in the new configuration.

To enlarge the width of the transmission window the configuration of the ns-stretcher was changed from a 4-pass to an 8-pass configuration. This was realized by moving the grating, the roof mirror and the input optics by 70 cm relative to the spherical mirror of the telescope (see Fig. 1). The stretching factor of 148 ps/nm of the pulses is kept constant, by doubling the passes through the stretcher to eight. Additionally the 6" plain mirror was replaced by a one with a diameter of 200 mm.

The theoretical spectral window has now been increased to 47 nm, where the lateral beam displacement after the second pass is not taken into account. The experimental transmission window has a width of 44 nm (Fig. 2) due to the displacement and a finite beam size. The stretching factor remained constant and spectral shaping in the second amplifier A2 produced a wider spectrum resulting in a longer duration of the stretched pulses. Thus the pulses can be amplified up to 50 mJ in the second amplifier with a spectral intensity of 30 nm FWHM (see Fig. 2), supporting a Fourier transform limited (FTL) pulse of 82 fs (Fig

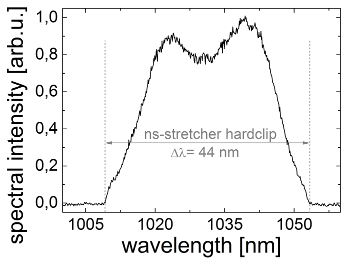

Figure 2: Spectral intensity of the A2-amplifier pulses with spectral clip from the ns-stretcher

3). These amplified pulses are then sent to the nanosecond-compressor.

The resulting pulse duration is shown in Fig. 3, depicting a pulse of 86 fs full width at half maximum (FWHM). With a 70% transmission efficiency of the compressor the final energy of these pulses is 35 mJ, making them the shortest pulses in the this energy range produced with a fully-diode pumped solid state laser so far. The broader spectrum reached within the frontend should lead to a reduction of the pulse duration of the final amplification stages as well.

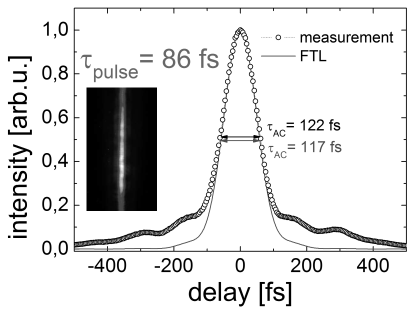

Figure 3: 2^{nd}-order pulse duration measurement of the A2 pulses and Fourier transform limit (FTL) of the spectral intensity

References

[1] H. Liebetrau, M. Hornung, A. Seidel, M. Hellwing, A. Kessler, S. Keppler, F. Schorcht, J. Hein, and M. C. Kaluza, Opt. Exp. **22**, 24776 (2014).

[2] M. Hornung, R. Bödefeld, M. Siebold, A. Kessler, M. Schnepp, R. Wachs, A. Sävert, S. Podleska, S. Keppler, J. Hein, and M. C. Kaluza, Appl. Phys. B **101**, 93 (2010).

[3] M. Kalashnikov, A. Andreev, and H. Schönnagel, Proc. SPIE **7501**, 750104 (2009).

* Hartmut.Liebetrau@uni-jena.de

Temporal characterization of the XPW contrast enhancement stage in the POLARIS frontend

H. Liebetrau[*1], *M. Hornung*[1,2], *S. Keppler*[1], *A. Kessler*[1], *M. Hellwing*[1], *F. Schorcht*[2], *J. Hein*[1,2], *and M. C. Kaluza*[1,2]

[1]Institut für Optik und Quantenelektronik, FSU Jena, Germany; [2]Helmholtz-Institut Jena, Germany

The effect of cross-polarized wave generation (XPW) proven to be an indespensable tool to enhance laser pulse parameters such as pulse duration and intensity contrast in high intensity lasers. An XPW-stage together with a picosecond-CPA was tested in 2014 [1] and fully implemented in the frontend of the POLARIS-laser [2] in 2015. During this implementation the temporal properties of this nonlinear filter where characterized from the several hundred-picosecond down to the femtosecond range.

The XPW pulse is generated inside a BaF_2-crystal from a 100 fs, 16 nm, 2 mJ laser pulse, which is provided by the frontend regenerative amplifier A1 embedded in a picosecond stretcher-compressor system [1]. The nonlinear XPW effect leads to a spectral broadening by a factor of 2.8, resulting in an extremely broad spectral intensity with a full width at half maximum of 45 nm (Fig. 1 (a)).

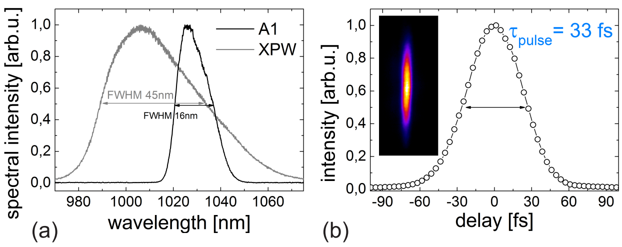

Figure 1: (a) Spectral intensities of the amplified (black) and nonlinear filtered frontend pulse (grey); (b) 2^{nd}-order autocorrelation measurement (inset) of the XPW pulses, line out taken at center

To characterize the filtered pulses in time, the residual material dispersion was eliminated by 6 reflections on a pair of dispersion compensating mirrors compressing the pulses. The 2^{nd}-order autocorrelation is shown in Fig. 1 (b) proving an extremely short pulse with a pulse duration of 33 fs. These compressed pulses are analyzed first with a *Wizzler*, which is capable of measuring the spectral phase via Self-referenced spectral interferometry (SRSI) and reconstruct the pulse shape within a time window ranging from -1.5 to 1.5 ps. The measurement in Figure 2 shows that the leading and trailing edges of the filtered pulses show no measurable signal above 10^{-4}. In comparison a theoretical gaussian pulse (grey dashed line) is shown in Fig. 2 (a), illustrating the high temporal intensity contrast of the XPW pulses.

For the characterization in the few hundred picosecond range the pulses are measured with an *Sequoia*- 3^{rd}-order

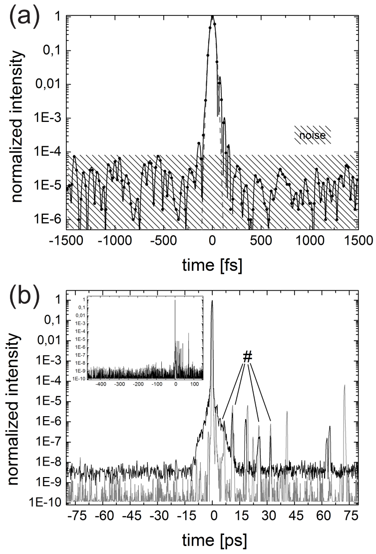

Figure 2: XPW pulses: (a) SRSI measurement (black dots) and ideal 48 fs gaussian pulse (dashed grey line); (b) 3^{rd}-order cross-correlation measurement XPW (black) and front end pulses (grey), inset full measurement range

cross-correlator. This measurement is shown in Fig. 2 (b) compared to the measurement of the amplified pulses (grey line). The slope of the main pulse is enhanced by 4 orders of magnitude in intensity contrast and several side-pulses e.g. at +62 ps are suppressed by at least that amount. Due to the extremely good cleaning properties, several pulses coming from the measurement device (#) where identified, making these cleaned pulses a useful tool for characterizing such instruments, as well.

In summary, we temporally characterized the filtered frontend pulses from a few hundred picoseconds down to the femtosecond range and demonstrated their excellent contrast.

References

[1] H. Liebetrau, M. Hornung, A. Seidel, M. Hellwing, A. Kessler, S. Keppler, F. Schorcht, J. Hein, and M. C. Kaluza, Opt. Exp. **22**, 24776 (2014).

[2] M. Hornung, H. Liebetrau, A. Seidel, S. Keppler, A. Kessler, J. Körner, M. Hellwing, F. Schorcht, D. Klöpfel, A. K. Arunachalam, G. A. Becker, A. Sävert, J. Polz, J. Hein, and M. C. Kaluza, HPLaser **2** (2014).

* Hartmut.Liebetrau@uni-jena.de

Kilowatt Average Power, Millijoule Pulse Energy, 8-channel Femtosecond Fiber CPA System

M. Kienel[1,2], M. Müller[2], A. Klenke[1,2], S. Hädrich[1,2], J. Rothhardt[1,2], J. Limpert[1,2,3], A. Tünnermann[1,2,3]

[1]Helmholtz-Institute Jena, Fröbelstieg 3, 07743 Jena, Germany;

[2]Institute of Applied Physics, Abbe Center of Photonics, Friedrich-Schiller-Universität Jena, Albert-Einstein-Str. 15, 07745 Jena, Germany;

[3]Fraunhofer Institute for Applied Optics and Precision Engineering, Albert-Einstein-Str. 7, 07745 Jena, Germany

Performance scaling of femtosecond high-power fiber-laser systems is a challenging task, since limitations are set by thermal and nonlinear effects up to optically induced damage. In terms of average power, fibers are ideal candidates due to their intrinsically good thermal management given by the advantageous aspect ratio. However, mode instabilities set an upper limit for the specific fiber setup. Although fibers provide outstanding beam quality, in terms of pulse peak-power, nonlinear pulse distortions induced by self-phase modulation limit the usefulness due to the beam confinement in small cores. Moreover, self-focusing sets the ultimate limit. Straightforward mitigation strategies such as increasing the guided beam diameter by advanced fiber designs and applying chirped-pulse amplification (CPA) helped to push the performance further over the past decade. But further increasing the mode-field diameter and the stretched pulse duration becomes challenging.

A promising approach scaling both the average power and the peak power even further is the coherent beam combination (CBC) technique [1], which can also be thought of spatial multiplexing. In this case, a laser pulse is split prior amplification onto N spatially separated amplifiers. After amplification of each pulse in its respective amplifier channel, a coherent superposition leads to a performance scaling by a factor of N, in the best case. To ensure efficient combination an active feedback loop has to be applied.

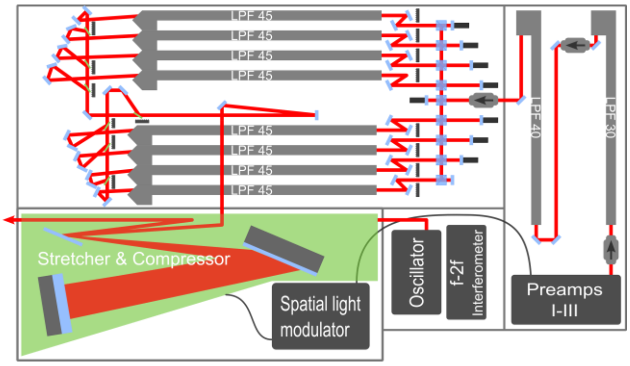

Fig. 1: Scheme of the 8-channel fiber-CPA system.

We have previously demonstrated the viability of this concept and have now realized a high-performance fiber-CPA system with 8 combined large-mode area fiber amplifiers. The corresponding experimental setup is schematically depicted in Fig. 1. In particular, the 8 amplifiers have been packaged in compact modules to allow for an overall small footprint of the system. As active feedback control the Hänsch-Couillaud technique is applied.

With this setup an average power of 1 kW and a pulse energy of 1 mJ has been achieved, which is far beyond the performance of a single fiber. An excellent combination efficiency of >95% could be demonstrated, proving the scaling opportunities of this concept with the number of parallel channels.

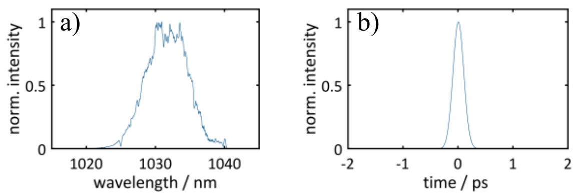

Fig. 2: a) Spectrum of the combined pulses and b) reconstructed pulse profile at 1 kW average power.

This laser system has already been employed for a variety of experiments, ranging from the creation of 200 W average power few-cycle pulses to generating 100 W average power pulses at ultra-violet wavelengths. In future it will be used for the generation of extreme ultra-violet light through the high-harmonic generation process.

A further scaling opportunity for the peak power and pulse energy is to additionally divide the pulses temporally, i.e. producing pulse trains. This approach allows for scaling the pulse peak power of the single amplifier in addition to CPA. Thus, the next step will be employing both spatial and temporal multiplexing [2] in the fiber-CPA system presented above. Additionally, work is being done to integrate the multiple amplifier channels into multicore fibers, thus allowing to increase the number of channels even further. We could already demonstrate the combination with a four-core fiber together with a compact beam splitting and combination element. We are confident, that all these steps taken will push towards TW-class fiber lasers.

References

[1] J. Limpert, A. Klenke, M. Kienel, S. Breitkopf, T. Eidam, S. Hädrich, C. Jauregui, and A. Tünnermann, IEEE JSTQE **20**, 268 (2014).

[2] M. Kienel, M. Müller, A. Klenke, T. Eidam, J. Limpert, and A. Tünnermann, Opt. Lett. **40**, 522 (2015)

* This work has been partly supported by the German Federal Ministry of Education and Research (BMBF) under contract 13N12082 “NEXUS,” contract 13N13167 “MEDUSA” and by the European Research Council under the ERC grant agreement no. [617173]. A. K. and M. K. acknowledge financial support by the Helmholtz- Institute Jena. M. M. acknowledges financial support by the Carl-Zeiss Stiftung.

† jens.limpert@uni-jena.de

Temporal Shaping of High Peak Power Pulse Trains from a Burst-Mode Laser System

Jürgen Reiter[1,2], Jörg Körner[1,2], Joachim Hein[1,2] and Malte C.Kaluza[1,2]

[1]Institute of Optics and Quantum Electronics, Friedrich-Schiller-University, Max-Wien-Platz 1, 07743 Jena, Germany;
[2]Helmholtz Institute Jena, Fröbelstieg 3, 07743 Jena, Germany

It has been shown in the past that pulsed laser systems operating in the so-called "burst mode" are a beneficial approach to generate high peak power laser pulses at high repetition rates suitable for various applications. The "burst mode" is a special operation scheme for a pulsed laser system. In this mode, the system produces pulses at a relatively high energy and repetition rate, for a short period in time, ranging from some microseconds to several tens of milliseconds. After this so-called "burst", a time period without laser operation allows for thermal relaxtion of the system. During the burst, the laser system approaches the efficiency of a continuously-pumped system, while due to the limited time of operation the cooling requirements for the components are vastly reduced in comparison to continuously-operated systems with a similar output power. So far, most high-energy burst-mode laser systems put great effort into generating a homogeneous energy distribution across the burst duration, e.g., by shaping the pump pulse. We developed a new shaping technique, which is able to produce arbitrary energy distributions within the burst by pre-shaping the seed pulse burst with a Pockels cell.

The Pockels cell is used with a fixed peak voltage and rise time for shaping the bursts. Since the laser pulse duration can be considered to be very short as compared to the Pockels cell's switching time, temporally shifting the laser pulse across the rising edge modulates its polarization. Hence, in combination with a polarizing optic, the transmitted pulse energy can be varied arbitrarily. This allows to generate bursts with a freely adjustable energy distribution and, additionally, to pre-compensate any amplitude modulations introduced by the following amplifiers. The method was tested with an ultra-short pulse burst mode laser amplifier system producing bursts of 1 ms duration with a pulse repetition rate of 1MHz and a maximum output power of 800W during the burst [2].

Furthermore, a method to predict the influence of the amplifier on a non-uniformly shaped burst was successfully tested to produce a pre-defined pulse shape after amplification [3]. This was realised by expending the theory of Will et al. [1] to predict the time dependent change in the inversion density.

Figure (2) shows a step function as an energy distribution example of the output burst after the amplification. In order to achieve such a distribution the energy distribution illustrated in Figure (1) has to be used as an input. The measurements presented were carried out using two photo diodes, one measuring light leaking through a plane mirror before the Pockels cell and one after the shaping section. The results are based on the relative height of both signals with respect to each other to compensate for pulse-to-pulse variations of the energy of the seed laser.

The developed technique can offer new possibilities in material processing and the detection of fast processes in combustion diagnostics.

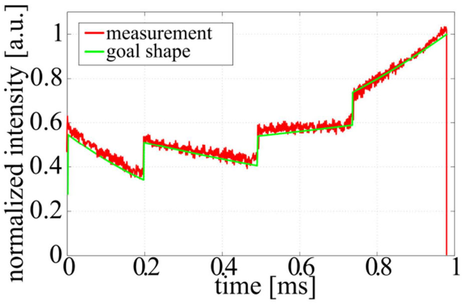

Figure 1: Input pulse train shaped to obtain a stair-shaped output.

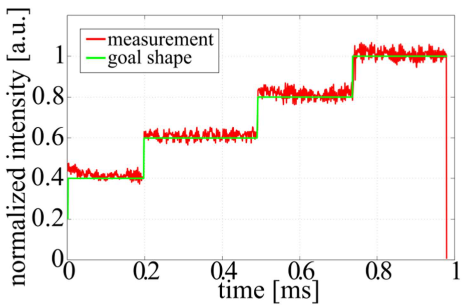

Figure 2: Resulting output pulse train after amplification of the input burst shown in Figure (1).

References

[1] Will, I.; Liero, A.; Mertins, D.; Sandner, W. Feedback-stabilized Nd:YLF amplifier system for generation of picosecond pulse trains of an exactly rectangular envelope. IEEE J. Quantum Electron. 1998, 34, 2020–2028.

[2] Körner, J.; Hein, J.; Liebetrau, H.; Seifert, R.; Klöpfel, D.; Kahle, M.; Loeser, M.; Siebold, M.; Schramm, U.; Kaluza, M.C. Efficient burst mode amplifier for ultra-short pulses based on cryogenically cooled Yb3+:CaF2. Opt. Exp. 2013, 21, 29006–29012.

[3] Körner, J.; Reiter, J.; Hein, J.; Kaluza, M.C. Temporal Shaping of High Peak Power Pulse Trains from a Burst-Mode Laser System. *Appl. Sci.* 2015, *5*, 1790-1802.

Milliwatt Average Power Narrowband High Harmonic Source

R. Klas [1,2], S. Demmler [1,2], M. Tschernajew [1,2], S. Hädrich [1,2],
J. Rothhardt [1,2], J. Limpert [1,2,3], A. Tünnermann [1,2,3],

[1]Friedrich-Schiller-Universität Jena, Abbe Center of Photonics, Institute of Applied Physics, Albert-Einstein-Straße 15, 07745 Jena, Germany
[2]Helmholtz-Institute Jena, Fröbelstieg 3, 07743 Jena, Germany
[3]Fraunhofer Institute for Applied Optics and Precision Engineering, Albert-Einstein-Straße 7, 07745 Jena, Germany

Author e-mail address: robert.klas@uni-jena.de

Table-top extreme ultraviolet light (XUV) sources based on high harmonic generation (HHG) are of interest in many applications [1] such as material studies, e.g. of magnetic properties [2], or the study of core-level transitions or highly charged ions (HCI) [3]. However, the bandwidth of the applied XUV radiation limits the energy resolution. In fact, material studies require a relative energy bandwidth in the order of 10^{-3} [4], while precision spectroscopy of HCI aims for 10^{-4} and smaller relative bandwidths, e.g. for testing fundamental theories, such as QED [3]. Furthermore, a high photon flux is desired for sufficient count rates, statistics, and signal-to-noise-ratios. Recently, it has been shown that short wavelength drivers allow for very efficient HHG in combination with a narrow energy bandwidth [1]. This is due to λ^{-6} scaling of the HHG efficiency and the better phase-matching conditions, which completely makes up for the losses in down-converting of the driving wavelength [1]. Here, we present a table-top XUV source with a record-high photon flux, based on a high average power femtosecond fiber laser and subsequent second harmonic generation (SHG) followed by HHG in a noble gas.

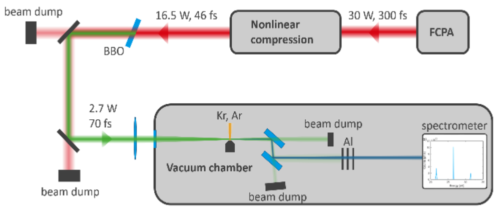

Fig.1: Generic setup for high harmonic generation with compressed and frequency doubled femtosecond pulses from a high average power fiber laser system (FCPA).

The experimental setup is shown in Fig.1. The driving laser is a two channel coherently combined fiber chirped pulse amplifier (FCPA), which delivers 1 mJ, 300 fs pulses with a central wavelength of 1030 nm and a repetition rate of 120 kHz, resulting in 120 W of average power. Afterwards, a nonlinear compression with an argon-filled hollow-core fiber compresses the pulses to a pulse length of 45 fs at 66 W of average power (0.55 mJ pulse energy). These pulses are now frequency doubled via a BBO crystal delivering 85 fs pulses at a central wavelength of 515 nm with an average power of 11 W (92 µJ pulse energy). Two dichroic mirrors separate the green from the infrared light. Subsequently HHG is realized via focussing of the green beam into a gas jet. In order to separate the green from the XUV light, two fused silica plates at Brewster's angle for 515 nm are used.

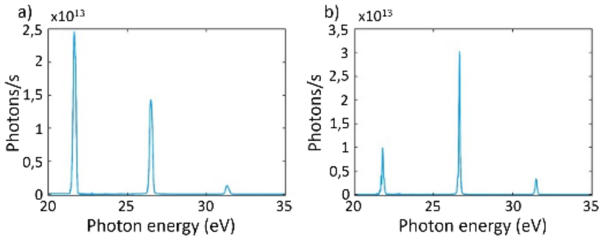

Fig. 2: XUV spectra generated with a) krypton and b) argon

A further suppression of the remaining green light is done using two additional aluminium filters. A flat-field spectrometer is used to characterize the XUV light. The photon flux of each harmonic can be calculated using the known detection efficiencies together with a propagation correction (absorption/transmission on the way to the detector) as well as spatial cutting at the grating (limited grating size) and the detector (limited detector size). This leads to 2.7 mW of average power for the harmonic at 21.6 eV when using krypton as a generating gas (Fig.2a)) with a relative energy bandwidth of $9.5\cdot10^{-3}$. When using argon as a generating gas, the energy bandwidth is further reduced to $\sim4\cdot10^{-3}$ at 21.6 eV and 31.3 eV (Fig. 2 b)). The 11th harmonic at 26.6 eV exhibits an even narrower spectral bandwidth of only $\sim3\cdot10^{-3}$ (resolution limited). This spectral narrowing is due to Fano-resonances in the photo-absorption spectrum of argon [5]. In this case the average power is still as high as 1.5 mW within this narrow line.

In conclusion we presented a narrow band high photon flux HHG source, driven by a nonlinearly compressed, frequency doubled fiber CPA system. HHG of these pulses yielded more than 2.7 mW of average power at 21.6 eV with a relative spectral width below 10^{-2} and due to a window-type Fano resonance in argon we achieved 1.5 mW at 26.6 eV with a relative spectral width of $3\cdot10^{-3}$. This is, until now, the highest average power ever reported from a HHG source in this spectral region. The unique combination of high photon flux and narrow bandwidth will foster many applications in future. It will particularly enable unique experiments on HCIs at the future FAIR facility [3].

References

[1] H. Wang et al., Nat. Commun. **6**, 7459 (2015)
[2] S. Mathias et al., PNAS 109.13, 4792-4797 (2012).
[3] J. Rothhardt et al., Phys. Scr. T166, 14030 (2015).
[4] A. Damascelli et al., Rev. Mod. Phys. 75, 473 (2003).
[5] J. Rothhardt et al., Phys. Rev. Lett. 112, 233002 (2014).

ASE deterioration by amplification saturation in high-power CPA laser systems*

S. Keppler[#,1], A. Sävert[1], J. Körner[1], M. Hornung[1,2], H. Liebetrau[1], J. Hein[1,2], and M. C. Kaluza[1,2]

[1]Institute of Optics and Quantum Electronics, FSU Jena, Germany; [2]Helmholtz-Institute Jena, Germany

Experiments on relativistic laser-plasma interactions using high-intensity laser systems with peak intensities in excess of $I_0 = 10^{21}\,\mathrm{W/cm^2}$ were strongly investigated during the last decade. Here, it has been found that the temporal intensity contrast (TIC) is one of the most crucial parameters for high-intensity laser-matter interactions. Hence, the TIC improvement and characterization is one of the most important challenges of high-power laser development.

In general, the TIC, regarding the amplified spontaneous emission (ASE), provides a constant level for high-power laser systems which are not operated in saturation [1]. However, if saturation occurs, the TIC deteriorates significantly with each amplifier. So far, the temporal intensity contrast has been characterized – for most cases – at reduced peak energy. This eventually leads to an underestimation of the on-target ASE at high peak powers.

Considering the ASE amplification, the fluence of the generated ASE (F = E/A) is orders of magnitude lower than the fluence of the main pulse. As a consequence, the ASE does not reduce the inversion significantly and the temporal characteristic of the ASE is determined by the time dependent gain of the main pulse. Assuming a Gaussian-shaped main pulse it is evident, that the rising edge of the main pulse experiences a higher gain than the main part of the main pulse due to its lower fluence. Hence, the part of the ASE which comes before the main pulse at $t < t_0$, with t_0 corresponding to the peak intensity of the main pulse, is amplified more than the main pulse itself leading to a TIC deterioration (TD).

To quantify the time-dependent TIC deterioration $\mathrm{TD}(t)$, the time-dependent gain $g(t)$ has to be compared to the total gain g_{total} of the main pulse, i.e. $\mathrm{TD}(t) = g(t)/g_{\mathrm{total}}$, for each pass of the amplification. This can be done by considering the non-linear photon transport equations for laser amplification, which were derived by Lee M. Frantz and John S. Nodvik (Eqs. (27) and (28) in [2]). Assuming a Gaussian-shaped main pulse with duration τ and a homogeneous initial inversion N_0, the time-dependent main pulse gain $g(t) = \Phi_{\mathrm{out}}(t)/\Phi_{\mathrm{in}}(t)$ can be expressed by

$$g(t) = \left\{1 - \exp\left(-\frac{1}{2}\frac{F_{\mathrm{in}}}{F_{\mathrm{sat}}}\left(1 + \mathrm{erf}\left[\frac{t}{\tau}\right]\right)\right)1 - \frac{1}{g_0}\right\}^{-1}.$$

Here, F_{in} is the seed fluence and F_{sat} is the saturation fluence of the laser material. The total gain of the main pulse can be calculated to

$$g_{total} = 1 + \frac{F_{sat}}{F_{in}}\ln\left(g_0 - (g_0 - 1)\exp\left(-\frac{F_{in}}{F_{sat}}\right)\right).$$

With each amplification pass n, the main pulse is amplified by the gain factor, $g_{\mathrm{total}}^{(n)}$, of the n^{th} pass and the inversion is reduced according to the respective extraction efficiency $\eta_{\mathrm{ex}}^{(n)}$. Hence, for the total TIC deterioration of an amplifier, the deterioration of each pass has to be taken into account. However, considering only the relevant part of the ASE at times $t < t_0$ we found that it is sufficient to consider the energy extraction of one single pass with an appropriate total extraction efficiency of the amplifier of $\eta_{\mathrm{ex}} = \sum_{n=1}^{\mathrm{passes}} \eta_{\mathrm{ex}}^{(n)}$. If further only the maximal TIC deterioration is of interest, it can be calculated to [1]

$$\mathrm{TD}(t \to -\infty) = \frac{g(t)}{g_{\mathrm{total}}} = g_0\left(1 - \frac{\ln\left(1 - \eta_{ex} + \frac{\eta_{ex}}{g_0}\right)}{\ln(1 - \eta_{\mathrm{ex}})}\right).$$

Fig. 1 shows a comparison of the calculated TIC (green and red line numerically calculated, black dashed line analytally calculated) with an extended measurement of the Jeti40 laser system over a time range of 1.5 ns. The analytical calculation shows an excellent agreement with the measurement.

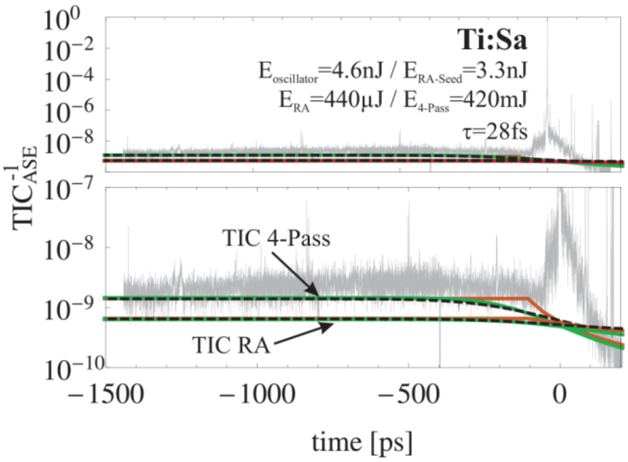

Figure 1: 3rd-order cross-correlation measurement of the TIC (gray solid line) of the JETI40 system. The measurement shows the TIC of the amplified pulse including the main amplifier. The solid lines represent a numerical simulation of the TIC assuming a Gaussian (green) and rectangular shaped (red) temporal shape of the main pulse for the measured amplifiers and the RA only. The black dashed line represents the analytical TIC calculation.

References

[1] S. Keppler *et al.* Laser & Photon. Rev. doi 10.1002/lpor.201500186 (2015).

[2] L. M. Frantz and J. S.Nodvik, J. Appl. Phys. **34**, 2346 (1963).

* Work supported by the European Commissions (EC) 7th Framework Programme (LASERLAB-EUROPE, grant no. 228334) and the Bundesministerium für Bildung und Forschung (BMBF) (03ZIK445 and 03ZIH531).

#Sebastian.Keppler@uni-jena.de

Nonlinear pulse compression of ultrafast thulium-based fiber laser systems

M. Gebhardt[1,2], C. Gaida[2], F. Sutzki[2], S. Hädrich[1,2], C. Jauregui[2], J. Limpert[#1,2,3], and A. Tünnermann[1,2,3]

[1]Helmholtz-Institute Jena, Fröbelstieg 3, 07743 Jena, Germany; [2]Institute of Applied Physics, Abbe Center of Photonics, Friedrich-Schiller-Universität Jena, Albert-Einstein-Str. 15, 07745 Jena, Germany; [3]Fraunhofer Institute for Applied Optics and Precision Engineering, Albert-Einstein-Str. 7, 07745 Jena, Germany

High-performance, ultrafast laser systems operating in the mid-infrared wavelength region are interesting sources for numerous industrial and scientific applications. A very prominent and demanding example is the study of high-field light matter interactions such as high-harmonic generation (HHG). The use of high repetition rate thulium-based fiber laser systems (TFL) emitting at around 2 µm wavelength is a very promising strategy to achieve both, high photon energies (because of the increased ponderomotive potential) and high photon flux (due to the high average power of the driving laser) in phase-matched HHG. Sources with such unique output parameters have great potential to become tomorrow's first choice for subsequent applications like nm-scale imaging [1].

Recently, the performance level of ultrafast TFLs has been significantly improved. Nowadays, these systems are capable of delivering >200 MW peak power or >150 W average power [2, 3]. However, the achievable pulse durations are typically on the order of several hundreds of femtoseconds. In order to further increase the pulse peak power of a given TFL and to shorten the pulse duration allowing for better HHG efficiency we have studied nonlinear pulse compression schemes at around 2 µm wavelength. In two separate experiments we have used a gas filled hollow-core Kagome-type photonic-crystal fiber [4] (PCF) and a solid-core fused silica fiber [5], respectively.

Kagome PCF

We have demonstrated nonlinear pulse compression of the output coming from a TFL using a gas-filled Kagome-type PCF for the first time. In this experiment, the laser delivered 34 µJ pulses with 400 fs FWHM pulse duration at a repetition rate of 100 kHz. The nonlinear pulse compression setup is schematically depicted in Fig. 1. It consisted of the laser itself, the Kagome-type PCF filled with xenon gas at 11 bar pressure as the nonlinear broadening stage and fused silica plates for subsequent temporal pulse compression. This simple setup exploits the favourable dispersion properties of fused silica in the two micron regime, which make it possible to compensate the majority of the self-phase modulation induced chirp. The compressed output pulses had an energy of 20 µJ. A significant reduction of the pulse duration can be expected when comparing the measured autocorrelation (AC) traces at the fiber input and after the SiO_2-based compressor (Fig. 2). Supported by numerical simulations we have retrieved a compressed pulse duration of less than 70 fs, which corresponds to <11 optical cycles and 200 MW of peak power. Such a source is already extremely interesting for driving high-field light matter interactions at 2 µm wavelength.

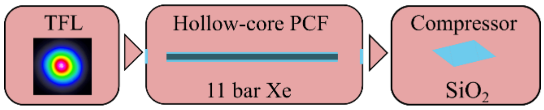

Figure 1: Schematic sketch of the experimental setup.

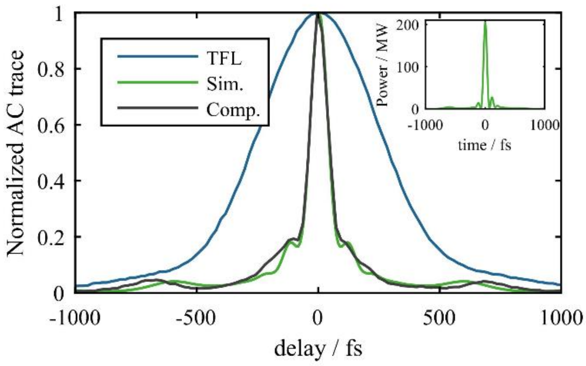

Figure 2: Measured AC traces before (blue) and after the nonlinear compression (black) as well as numerical simulation (green). Inset: Retrieved pulse profile.

Solid-core LPF

By using a solid-core fused silica large-pitch fiber (LPF) for the nonlinear pulse compression, the spectral broadening and the temporal pulse compression can be forced to happen simultaneously inside of the fiber. This leads to large compression factors and allows for addressing different, but just as interesting output parameters. Hence, we have performed a second experiment that validated the wavelength dependency of the self-focusing limit and resulted in 24 fs FWHM pulse duration, 24 MW peak and 24 W average power. The unique combination of high average power and few-cycle pulses obtained directly from a fiber makes this source appealing for subsequent applications such as intra-pulse difference frequency generation.

Outlook Our future work will concentrate on nonlinear pulse compression using gas-filled hollow capillaries. Exploiting the full potential of ultrafast TFLs a high average power few-cycle source with GW peak power at 2 µm wavelength is in reach. This will be an ideal driver for high photon flux HHG with high photon energies well within the water window.

References

[1] G. Tadesse al., UFO Conference (2015)
[2] F. Stutzki et al., Opt. Lett. 40, 9 (2015).
[3] F. Stutzki et al., Opt. Lett. 39, 4671 (2014).
[4] M. Gebhardt et al., Opt. Lett. 40, 2770 (2015)
[5] C. Gaida et al., Opt. Lett. 40, 5160 (2015)

#jens.limpert@uni-jena.de

Upgrade of the PHELIX pre-amplifier towards higher repetition rates *

U. Eisenbarth† [1], *S. Götte*[1], *S. Kunzer*[1], *D. Reemts*[1], *B. Zielbauer*[1], *and V. Bagnoud*[1]
[1]GSI, Darmstadt, Germany

In the past year, significant progress has been achieved at the PHELIX laser facility on the way towards higher pulse repetition rates. Based on detailed studies on the characterization of a flashlamp-based amplifier head an improved pre-amplifier system has been designed. These studies represent an important milestone for the first stage of a system upgrade towards higher performance.

The PHELIX Pre-Amplifier is a flashlamp-based Nd:glass laser amplifier system with a typical pulse output energy of up to 10 J and a repetition rate of one shot every 3 minutes. This limitation mainly arises from thermal wavefront deformations such as defocus, astigmatism and higher order aberrations as well as birefringence effects. Nowadays several experiments such as X-ray generation or laser particle acceleration demand higher shot rates allowing more systematic studies on the investigation of the acceleration processes as well as improvements of the used targets.

In order to increase the repetition rate, the 45 mm amplifier head as well as a new pulsed power system driving the flashlamps have been developed in a separate test setup. New Nd:glass laser materials exhibiting higher heat conductivity coefficients have been tested with respect to wavefront aberrations and gain while operated at repetition rates up to one shot every 15 s.

If the waiting time between two shots is shorter than the typical time constants for cool-down a pile-up behavior can be observed. As it turns out, the overall wavefront aberration (peak to valley value) over many shots however does not increase exceeding all limits but approaches a steady state, whose absolute value is determined by the repetition rate (see figure 1). Due to this steady state, stable operation can be achieved employing adaptive optics in order to compensate for these aberrations. A more detailed wavefront analysis shows that the defocus aberration contributes to more than than 80 % to the overall wavefront error. Fortunately this error can easily be compensated using a motorized lens in the optical setup. The remaining aberrations are compensated using a deformable mirror. Both, the wavefront measurement as well as the active compensation have been significantly improved in the test setup.

Another effect during operation with increasing repetition rates is birefringence which also arises from thermal gradients in the active laser material. This effect leads to local depolarization of the laser beam passing the laser rod.

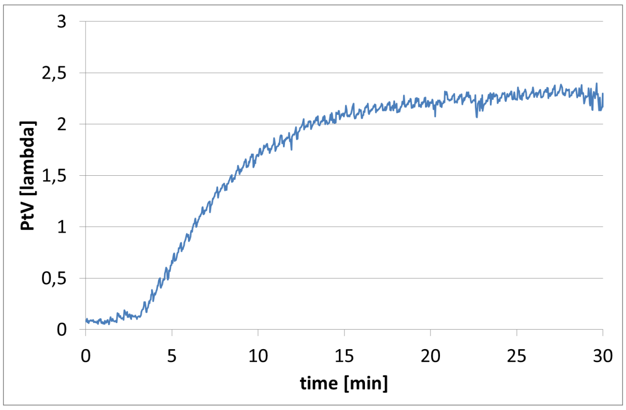

Figure 1: Evolution of the laser wavefront aberration (PtV) over time. The repetition rate was one shot every 25 s.

In combination with polarization optics this would result in a significant loss of output energy. In order to overcome this limitation, the amplifier head is operated in a double-pass configuration in combination with a Faraday rotator.

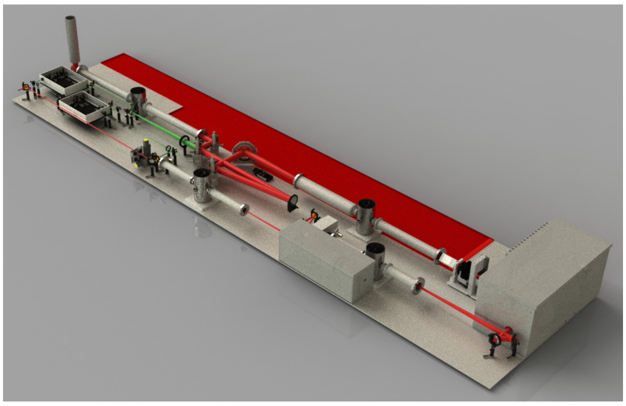

Figure 2: View of the planned Pre-Amplifier upgrade

Based on the above tests and improvements a new Pre-Amplifier system has been designed (figure 2) delivering pulses with output energies up to 20 J at a repetition rate of one shot every 25 s. The integration of the new PHELIX Pre-Amplifier setup is planned for summer 2016. This upgrade and the experiences gathered also represent an important step forward for the planned 100 J APPA laser system at the FAIR project.

* This report is also published in the GSI Scientific Report 2015
† u.eisenbarth@gsi.de

Determination of the temporal pulse shape of a seeded free-electron laser at FERMI*

H. Höppner[1]*, M. J. Prandolini*[†2]*, R. Riedel*[2]*, S. Toleikis*[1]*, F. Tavella*[3]*, and FERMI Collarboration*[4]

[1]DESY, Hamburg, Germany; [2]Helmholtz-Institut Jena, Jena, Germany; [3]SLAC, Menlo Park (CA), USA; [4]Elettra-Sincrotrone Trieste, Trieste, Italy

A detailed measurement campaign was carried out to determine the pulse duration – in particular complex pulse sturcutres – of the XUV externally seeded free-electron laser FERMI (Trieste, Italy). The single-shot, optical-XUV cross-correlation method was used to determine the XUV pulse shape [1].

Introduction

The goal of FELs in general is to provide intense and ultrashort light pulses. The FEL pulse duration defines the rate of deposited energy on the sample. Therefore an accurate knowledge of the pulse duration is an essential pre-requisite for the end-user. In this work, we present a dedicated set of experiments, based on cross correlation techniques, to investigate the pulse duration of the seeded source FERMI in a wide wavelength range and for different machine setups. Complete details of these measurements are described in [2]. In this summary, we demonstrate the possibilities of the application of this method to a multi-pulse structure.

Experimental method and results

In this approach, the FEL pulse is used to excite transient electrons into the conduction band of a dielectric material (Si3N4, SiO2, diamond) or semiconductor (GaAs, Si). The wavefront of the FEL is tilted with respect to the target; thus the integrated FEL fluence is encoded spatially and temporally into the surface of the target. The subsequent temporal evolution of the excited transient electrons is monitored by a probing laser with a wavefront parallel to the target. For more details see [1].

A central element of this experiment was an external compact single-stage non-collinear optical parametric amplification (NOPA). Since the available pump-probe laser at FERMI is limited to 100 fs, the NOPA is used to generate shorter optical probe pulses in the range of 30 fs, in order to improve the temporal resolution of the experiment.

For this experiment the dispersive section (R_{56}) of the electron acelerator was detuned to a value of 36 μm in order to produce multiple pulses. Fig. 1 shows a measurement of the cross-correlation data. From the depth and relative long duration of the cross-correlation signal, compared to 100% transmission, and with the previously eastimated plasma decay parameter, it is confirmed that this FEL pulse must have a longer pulse duration. In order to model this cross-correlation data, we made assumptions based on the corresponding measured spectrum (not shown). This spectrum shows at least three spectral modes, indicating a complex temporal structure. Therefore we modeled the cross-correlation data with a main pulse of 50 fs followed by satellite pulses separated by $t_{sep} \sim 75$ fs. The time separation of the pulses was estimated, assuming FT-limited pulses. Using these assumptions, a modeled FEL intensity profile is shown in Fig. 1. The intensity ratio between main pulse and satellite pulses is 3.33:1.67:1. The estimated pulse duration of the satellite pulses from simulation is $\sim 70-80$ fs.

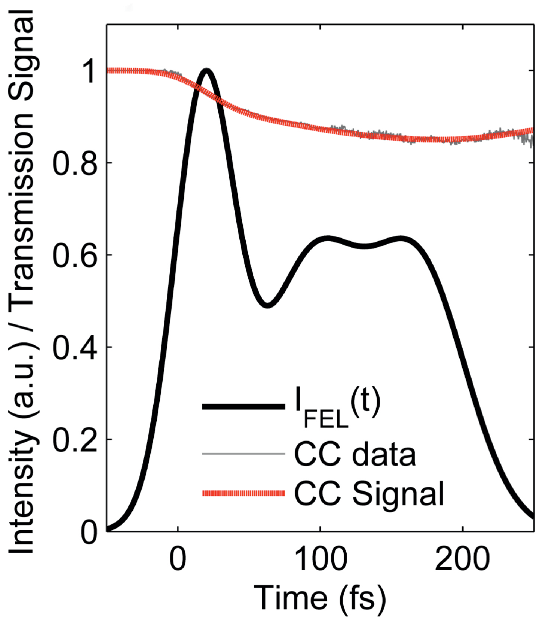

Figure 1: Pulse duration measurement with a detuned parameter: single-shot cross-correlation data points together with its retrieved curve fit and the retrieved FEL temporal pulse structure at 26.17 nm.

References

[1] R. Riedel et al. Nat. Comm. **4** 1731 (2013)

[2] P. Finetti, H. Höppner, et al. "Pulse duration measurement of a seeded free-electron laser: the case of FERMI" to be submitted to *Phys. Rev. Accel. Beams* (2016)

* Work supported by HI Jena/DESY.

† mark.prandolini@desy.de

Design and simulation of a possible seeded HGHG setup at FLASH2*

T. Tanikawa[1], *B. Faatz*[1], *and M.J. Prandolini*[† 2]
[1]DESY, Hamburg, Germany; [2]HI-Jena, Jena, Germany

After construction of a high repetition rate (100 kHz), tunable (720–900 nm), optical parametric chirped-pulse amplifier (OPCPA) with pulse energies up to 1.12 mJ and a pulse duration of 30 fs [1], design and simulations were carried out of a seeded high-gain harmonic generation (HGHG) setup at FLASH2.

Introduction

Free-electron lasers (FEL) based on large scale linear electron accelerators are sources of highly intense extreme ultraviolet (EUV) and X-ray radiation. FELs can be "seeded" by shot noise radiated from an electron beam as it passes through an undulator. This process is called self-amplified spontaneous emission (SASE). As a result, SASE pulses suffer from fluctuations in pulse energy, pulse duration, spectral and temporal coherence, and arrival time. These parameters can be greatly improved by seeding the FEL with an external seeding laser. There are several methods to seed a FEL; one promising approach is high-gain harmonic generation (HGHG). In this case, the seeding laser wavelength is a sub-harmonic of the final undulator radiation. We have designed and simulated a possible HGHG setup for FLASH2 (Fig. 1).

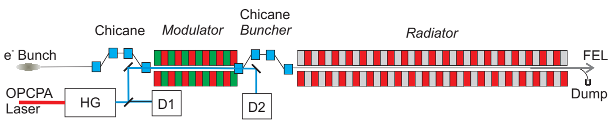

Figure 1: A schematic of a possible HGHG setup at FLASH2. The harmonic generator (HG) creates third harmonics of the tunable OPCPA beam (720–900 nm) [1]. The first chicane creates space to bring in the seeding laser into the modulator. The HGHG process then takes place in the modulator, buncher and radiator. D1 and D2 are laser and radiation diagnostics.

Results

The HGHG process is simulated with the three dimensional code SIMPLEX (Ver. 2.0.2). The main parameters used in the simulations are given in [1]. The seed laser is assumed to be Fourier-limited with pulse duration of 30 fs. Electron beam and undulator parameters are given by FLASH2 parameters. Because the K-parameter of the FLASH2 undulator has a maximum value of 2 rms, the maximum wavelength at a beam energy of 700 MeV is 42 nm. Simulations were performed covering seed wavelengths 240–300 nm, generated by using the THG of the tunable OPCPA [1]. Therefore to reach wavelengths below 40 nm, the radiator was tuned to the 7th and 9th HGHG. Still higher harmonics were not chosen, because sufficient FEL power is not generated.

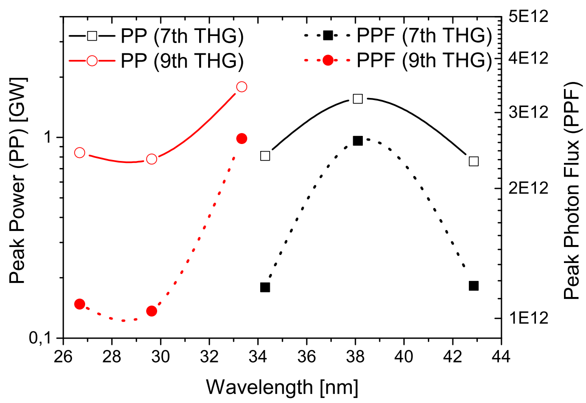

Figure 2: A summary of all simulations of the 7th and 9th HGHG using the THG of the OPCPA at 720, 800 and 900 nm. The dependence of peak power (left) and peak photon flux (right, in units of photons/pulse/0.1% bandwidth) on wavelength.

A summary of output parameters – the peak power and peak photon flux against FEL wavelength – is given in Fig. 2. Finally, simulations were performed in order to determine the influence of seeding laser energy fluctuations on the final FEL shot-to-shot energy fluctuations. Assuming the seeding laser has a energy fluctuation of 4.2% rms at 267 nm [1], the output fluctuations of the 7th and 9th HGHG would be 0.27% rms and 0.64% rms (results not shown) at around the optimal seed energy, respectively.

References

[1] H. Höppner, A. Hage, T. Tanikawa, M. Schulz, R. Riedel, U. Teubner, M. J. Prandolini, B. Faatz, and F. Tavella, New J. Phys. **17** (2015) 053020

* Work supported by HI Jena/DESY.
† mark.prandolini@desy.de

Stimulated Raman Backscattering at PHELIX*

B. Landgraf[1,2], *F. Gärtner*[3,4], *D. Kartashov*[2], *A. Hoffmann*[1], *Z. Samsonova*[1,2], *G. Vieux*[5], *G. McKendrick*[5], *D. Jaroszynski*[5], *J. Jacoby*[4], *T. Kühl*[1,3], *and C. Spielmann*[1,2]

[1]Helmholtz Institute Jena, Jena, Germany; [2]Institute of Optics and Quantum Electronics, Abbe Center of Photonics, Friedrich-Schiller University Jena, Jena, Germany; [3]GSI, Darmstadt, Germany; [4]Institute for Applied Physics, Plasmaphysics, Goethe-University Frankfurt/Main, Frankfurt/Main, Germany; [5]University of Strahclyde, Glasgow, United Kingdom

Introduction

Stimulated Raman Backscattering (SRBS) is a promising way to upgrade existing high intensity systems beyond the Petawatt(PW) level [1]. To overcome scaling limitations in state of the art chirped pulse laser amplifiers the intensity has to be increased after passing the last solid state device. SRBS describes a three wave interaction in laser plasmas in which a plasma wave is generated due to the ponderomotive force of a beatwave originating from two counter-propagating frequency shifted laser pulses. The frequency difference is crucial because it defines the optimal plasma frequency.

Methods

In the experiment the 25 cm diameter beam of PHELIX was split into two 100 cm^2 quadratical, vertically aligned beams. The pulse duration of both beams is independently controlled by a grating compressor assembled by the PHELIX laser team. The pump pulse duration is 31 ps. The energy ratio of both beams is variable and can span several orders of magnitude with a maximum energy up to 50J per beam. Additionally the temporal overlap of both beams can be varied with an integrated delay stage. Both beams can be separated spatially in the target chamber and then focused at the end of two beamlines. The seed beamline is used to redshift the fundamental laser beam as described in [2]. Both beams are focused by f/80 into a gaseous target and typical pulse properties are measured.

Results and Discussion

We measured amplification of the backscattered pulse with a spectral width of 50 nm corresponding to 20 times the original spectral width. From spectrally resolved measurements as shown in Fig. 1 we deduced a pulse energy of a few 100 μJ corresponding to a conversion efficiency of 1%. A study of the scaling possibilities was carried out and a case for moderate pump pulse energy was presented. Limiting factors of high energy pulses were identified and will be but published soon. We have also identified, always present, critical requirements regarding laser quality and stability. Despite the currently low measured intensity conversion of 20%, wer are optimistic that further optimization is possible to at least conserving the peak intensity allowing experiments within the ultrashort pulse regime with PHELIX.

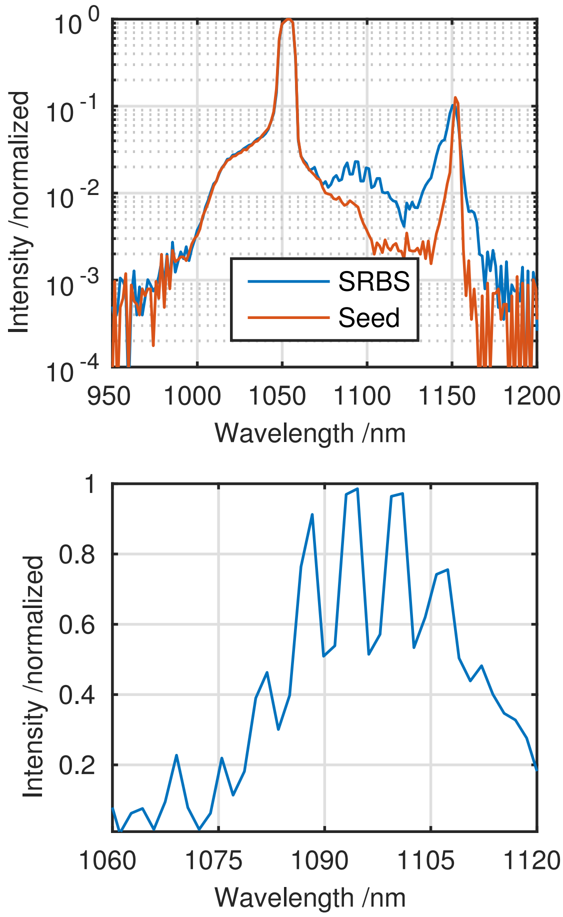

Figure 1: SRBS signal and comparison to the plasma transmission of the seed pulse.

References

[1] V. M. Malkin, G. Shvets, and N. J. Fisch. "Fast compression of laser beams to highly overcritical powers." Physical review letters 82.22 (1999): 4448.

[2] B. Landgraf, et al. "Generation of multi-millijoule red-shifted pulses for seeding stimulated Raman backscattering amplifiers" Optics Express 23, (2015): 7400–7406.

* Work supported by GSI(PHELIX), GSI(HIJ), HGShire/European Regional Development Fund (EFRE)/state of Thuringia (TMBWK) under Grant No. B 715-08008/TR, U Strathclyde

Laser Particle Acceleration

Optical Probing of High-Intensity Laser-Droplet Interactions*

G. A. Becker[1], M. B. Schwab[1], R. Lötzsch[1], H-P. Schlenvoigt[3], M. Rehwald[3], D. Klöpfel[2], J. Polz[1], A. Sävert[1], U. Schramm[3], and M. C. Kaluza [1,2]

[1]Institut für Optik und Quantenelektronik, Friedrich-Schiller-Universität Jena, Germany; [2]Helmholtz-Institut Jena, Germany; [3]Institut für Strahlenphysik, Helmholtz-Zentrum Dresden-Rossendorf, Germany

Since the first observation of laser-driven proton acceleration in 2000 many further experiments have been performed to better understand the accelerating process. Unfortunately, most experiments rely on the detection of the accelerated particles and on PIC simulations instead of direct investigation of the laser-plasma interaction.

Our approach to acquire a deeper understanding of the laser-target interaction is, in addition to ion and X-ray diagnostics, to use the few-cycle optical probe beam on the JETI 40 laser [1]. The main problem with probing typical foil targets is the difficulty in mounting the foil in a way conducive to probing both the front and back side of the foil at the same time. Targets which overcome this problem are water droplets, since a jet of water droplets needs no mechanical mounts that impedes transverse optical probing schemes. Therefore, it is possible to record information about the plasma from both the front side of a droplet, where the laser hits, as well as from the back side of a droplet, from which the accelerated ions should be generated.

Nonetheless, there are difficulties with using an optical probe to image the laser-droplet interaction. As the laser pulse interacts with the droplet, or more precisely with the plasma that is formed on the front side of the droplet, the generated plasma scatters both the laser's bandwidth as well as up- and down-converted laser frequencies. This scattered light is so intense and so broadband that it will saturate any spectrally unfiltered probing images making the observation of the interaction region nearly impossible as seen in figure 1a.

There are several ways to reduce the scattered light recorded in the probe's imaging system. First is to use the second harmonic of the main JETI 40 laser pulse centered at 400 nm as the driver pulse. Conversion of the laser light in the plasma tends preferentially to shorter wavelengths, suppressing the scattered light above 400 nm. Second is to spectrally filter the few-cycle probe using a filter with high transmission in the range 710 ± 20 nm and an optical density of 6 for all other relevant wavelengths. And finally, a high quality, broadband polarizer can be used to suppress the depolarized scattered light from the plasma while allowing high transmission of the probe when aligned to the polarizer's transmission axis. With these modifications to the probe beam system it was possible to record high quality shadowgrams (Fig. 1b – f) as well as interferograms.

By changing the temporal delay between the main pulse and the few-cycle probe pulse we could observe the evolution of the laser-plasma interaction both before and after the main pulse's arrival. The ion acceleration happens typically on the femtosecond timescale in which the droplet's expansion has not yet started (Fig. 1b). Delaying the probe's arrival even further one sees the hydrodynamic expansion of the droplet occurring (Fig. 1c – f) on the picosecond to nanosecond timescale. For well aligned shots, the droplet begins to expand symmetrically and remains opaque as its density is above the critical plasma density for the probe centered at 710 nm. Additionally, the surfaces of the neighboring droplets which face the expanding droplet are also ionized and begin to expand. In figure 1e and 1f one sees the expanding droplet interacting with the neighboring droplets and in figure 1f the plasma density decreases below the critical density and what remains of the droplet becomes transparent to the probe. Although the hydrodynamic expansion is not directly related to the ion acceleration process, one can, from the quality of the expansions symmetry and extension, deduce how well the droplet was hit by the main pulse, which in turn can be correlated to the measured signals relating to particle energy, beam shape and X-ray emission.

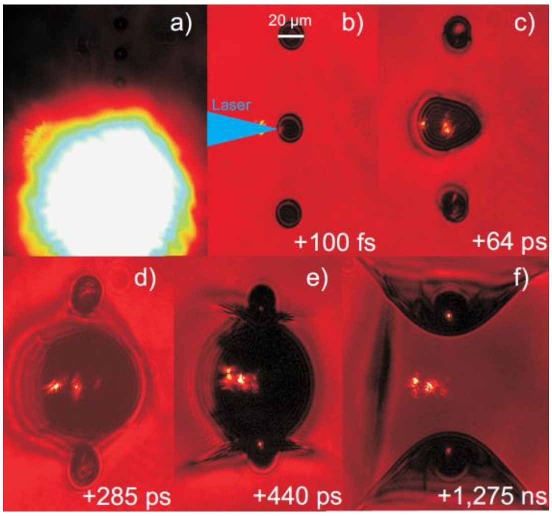

Figure 1: Shadowgrams of laser-droplet interaction. a) Picture from a former experiment (J. Polz et al. 2011). b) – f) Hydrodynamic expansion of the targeted droplet.

References

[1] M. B. Schwab et al., "Few-cycle optical probe-pulse for investigation of relativistic laser-plasma interactions", Appl. Phys. Lett. 103, 191118 (2013).

*Work is funded in part by onCOOPtics

Observation of the plasma lens effect using LWFA electron bunches

D. Hollatz[1], *S. Kuschel*[1,2], *M. Kaluza*[1,2], *and M. Zepf*[1,2]
[1]Friedrich-Schiller-Universität Jena; [2]Helmholtz-Institut Jena

Simulations

The first part of the work was to perform many simulations about the plasma lens effect to get a knowledge base. The setup is shown in Fig 1. An electronbunch of

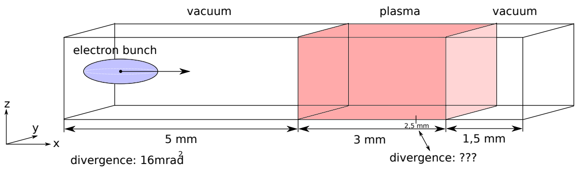

Figure 1: Setup of the simulations.

given spatial and momentum distribution travels through a plasma. After 2.5mm the divergence might have changed. This change in divergence depends on the density of the plasma and on the bunch properties. Some results of this simulations are shown in Fig 2. Here one can see the divergence (y-axis) after 2.5mm for different plasma densities (x-axis). Different lines are showing the change in behaviour while changing the bunch length (coloured lines). Some results are that there is an optimal plasma density for

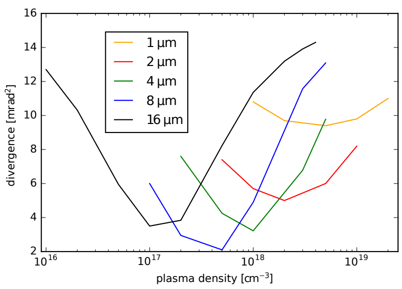

Figure 2: Selected results of the simulations.

maximum divergence reduction and this plasma density depends on the bunch length as shown in Fig 2.

Experiment

The second part of the work was an experiment for observing the plasma lens effect. The experimental setup is shown in Fig 3. The JETI laser pulse is focussed into the LWFA gas cell, accelerates electrons, diverges after that and finally ionizes the second gas jet. The LWFA electrons are travelling through the plasma and the plasma lens effect can occur which is measured via the beam profile on the scintillating screen. The plasma density is measured with

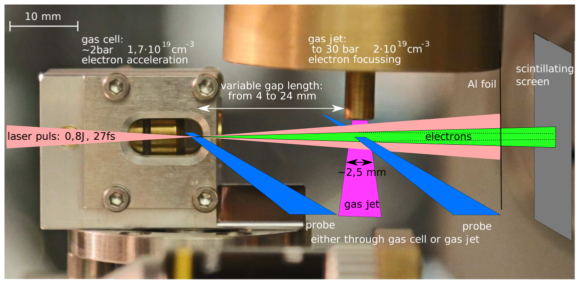

Figure 3: Target for LWFA (gas cell) and for the plasma lens (gas jet) in close-up-view. Probe beam and scintillating screen (not drawn to scale) for diagnosis.

a $6fs$ probe beam and the electron energy with an electron spectrometer. Some results of this experiment are shown in Fig 4. One important result is, that the plasma lens effect

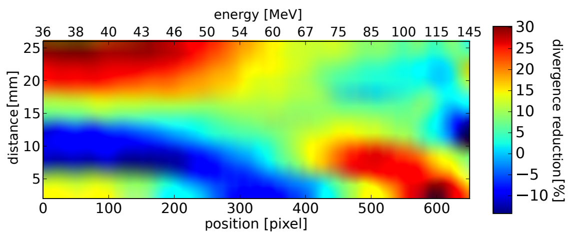

Figure 4: The divergence reduction (colorscale) of the electron bunch due to the plasma lens effect is shown depending on the electron energy (x-axis) and the distance between the gas cell and the gas jet (y-axis).

is different for electrons with different energies so that the divergence of some electrons is not decreased but even increased. Another observation is that the distance between the gas cell and the plasma lens determines the energy of the electrons which can be focussed best as shown in Fig 4.

References

[1] P. Chen et al: *Plasma lens experiment at the final focus test beam*. Nucl. Instr. & Meth. A410 pp. 407-417, (1998)

[2] J. B. Rosenzweig & P. Chen: *Beam optics of a self-focusing plasma lens*: Phys. Rev. D 39, 2039 (1989)

[3] D. H. Whittum et al: *PLASMA SUPPRESSION OF BEAMSTRAHLUNG*, Pt. Acc. Vol. 34, pp. 89-104 (1990)

The author gratefully acknowledge the computing time granted by the John von Neumann Institute for Computing (NIC) and provided on the supercomputer JUROPA at Jülich Supercomputing Centre (JSC).

Laser Wakefield Acceleration: Investigating Pointing Stability

M. B. Schwab[1], A. Sävert[1,2], S. Kuschel[1,2], D. Hollatz[1,2], M. Zepf[1,2,3], M. C. Kaluza[1,2]
[1]Institute of Optics and Quantum Electronics, Jena, Germany; [2]Helmholtz Institute, Jena, Germany; [3]Department of Physics and Astronomy, Queens University, Belfast, UK

Introduction

The JETI 40 laser system at the Institute of Optics and Quantum Electronics and the Helmholtz-Institute Jena is used to study the laser-plasma interactions driving Laser Wakefield Acceleration (LWFA). Ultra-short electron (e') bunches are created by focusing the JETI 40 laser to relativistic intensities of ca. 5×10^{18} W/cm² into a gas jet or gas cell forming an e'-plasma with e'-density between 5×10^{18} to 5×10^{19} cm^{-3}. The peak intensity of the laser drives a plasma wave into which plasma electrons are injected and accelerated to relativistic velocities. Two injection mechanisms, self-injection [**1-3**] and ionization injection [**4**], have been investigated using the JETI 40's few-cycle probe beam system (fc-probe) [**5**].

Experimental Results

With each shot of the laser into the gas cell the e'-bunch's transverse profile was recorded with a plastic scintillator and images of the plasma wave are imaged using the fc-probe. This data allows changes in the electron bunch and plasma wave to be correlated. Both helium gas and a 90:10 He:N_2 mixture were used in a gas cell to investigate self- and ionization injection, respectively.

Divergence	**1/e Diameter (mrad)**	**Over N Shots**
HeN_2	15.5 ± 5.5	130
He	21.8 ± 26.5	30
HeN_2	11.2 ± 2.2	Best 15
He	6.1 ± 2.1	Best 15
Pointing	**X-axis (mrad)**	**Y-axis (mrad)**
HeN_2	± 5.2	± 8.4
He	± 34.9	± 29.4
Charge	**% Charge in 1/e bunch area**	
HeN_2	5.7 ± 1.9	
He	0.4 ± 0.3	

Table 1: Measured divergence, pointing and charge density of transverse e'-beam profiles. Pointing is given as a range in which 90% of shots were measured.

On average (see **Tbl. 1**), e'-bunches created via ionization injection (He:N_2) displayed a smaller transverse divergence, better pointing, and higher charge density compared to self-injection (pure He). The potential for optimizing the self-injected e'-bunches can be seen when comparing the best 15 shots of each data set. Here, the 1/e divergence for self-injected electrons reduced by more than a factor of 3; however, the amount of charge inside the 1/e diameter remains smaller compared to ionization injection. This low charge density in the self-injection case is another indicator that this mechanism using a gas cell was far from being optimized, considering the wealth of publications showing highly charged, well collimated bunches via self-injection.

Fig. 1 shows averaged, centroid-overlapped e'-bunch profiles. The solid lines represent the average 1/e full divergence, dashed lines show the average 1/e full divergence for the best 15 shots, and dotted lines show inside which area 90% of all shots fell. Here, one sees the reduction in pointing stability between bunches created via ionization and self-injection (dashed lines).

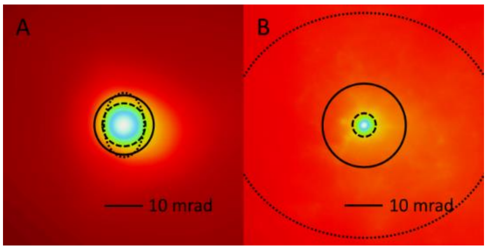

Figure 1: Transverse e'-beam profiles for (A) ionization injection and (B) self-injection.

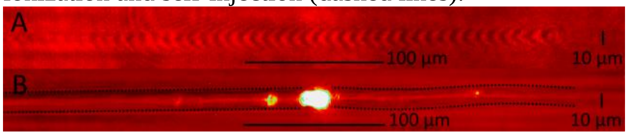

Figure 2: Shadowgraphic images representative of (A) ionization injection and (B) self-injection. Dotted lines added to show modulation of plasma channel. Driver laser propagates from left to right.

Fig. 2 shows example shadowgrams. In (A), a long train of plasma wave oscillations with no wiggling in the vertical direction. This is how the plasma wave appeared in several thousand shots with ionization injection. Image (B) shows the plasma channel for the self-injection case. The large white spot is indicative of wavebreaking radiation, after which the plasma channel shows a clear vertical wiggling motion. It is suspected that transverse injection into the plasma wakefield can seed this motion, effecting the pointing stability of the e'-bunches [**6**].

Conclusion

The analysis of the LWFA experiments on the JETI 40 laser is still ongoing. It is clear that the fc-probe is a unique tool for investigating laser-plasma dynamics. The ability to directly observe the laser-driven plasma waves and correlate this information with other experimental parameters has already begun producing new insights into LWFA mechanisms [**7**]. The understanding of what leads to the observed transverse modulation of the plasma channel will be beneficial building more stable LWFA.

References

[1] S. P. D. Mangles et al. Nature **431**, 535 (2004).
[2] C. G. R. Geddes et al. Nature **431**, 538 (2004).
[3] J. Faure et al. Nature **431**, 541 (2004).
[4] C. McGuffey et al. PRL **104**, 025004 (2010).
[5] M. B. Schwab et al. APL. **103**, 191118 (2013).
[6] M. B. Schwab et al. In Preparation (2016).
[7] A. Sävert et al. PRL. **115**, 055002 (2015).

High-energy-density electron beam from interaction of two successive laser pulses with subcritical-density plasma*

Jingwei Wang#, M. Zepf, and S. Rykovanov
Helmholtz Institute Jena, Jena 07743, Germany

Two-pulse scheme

We propose a scheme to produce a high-energy-density (HED) electron beam by enhancing the trapping and acceleration of the subcritical-density plasma (SCDP) electrons with a second laser pulse that propagates in the thin wake channel of the first laser pulse. The accelerated electrons are well bunched and have high charge and energy densities. They are useful for enhancing the space-charge field behind a solid-density foil in target normal sheath acceleration (TNSA) of ions, bremsstrahlung sources, etc.

Long capillary and SCDP

In the simulations we see that the propagation range of the first laser pulse in the SCDP is very limited because of the strong laser plasma interactions. The second laser pulse can propagate a much longer distance in the well-formed wake channel created by the first pulse, and creates its own quasi-cavity and wake channel. A large number of accelerated electrons are then trapped in the wakefield of the second laser pulse for a long time and are thus further accelerated. Eventually a thin HED electron beam is formed along the axis, as shown in Fig. 1(f).

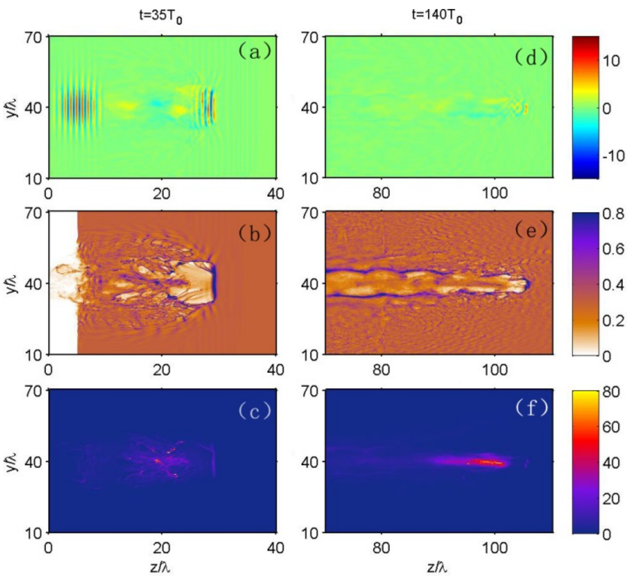

Figure 1: (a) and (d) Laser electric field, (b) and (e) electron density, (c) and (f) electron energy density at time $35T_0$ and $140T_0$.

The electron acceleration process consists of two stages. In the first ($t<100T_0$), the dominant acceleration mechanism is betatron resonance acceleration with the help of the self-generated quasi-static electric field and magnetic field in the channel [1,2]. In the second acceleration stage the electrons are accelerated by the wakefield when the still intense second pulse enters the pristine plasma. Most of the gain comes from the first stage, and the spectral peak of the final electron bunch can reach 230 MeV, as shown in Fig. 2(a).

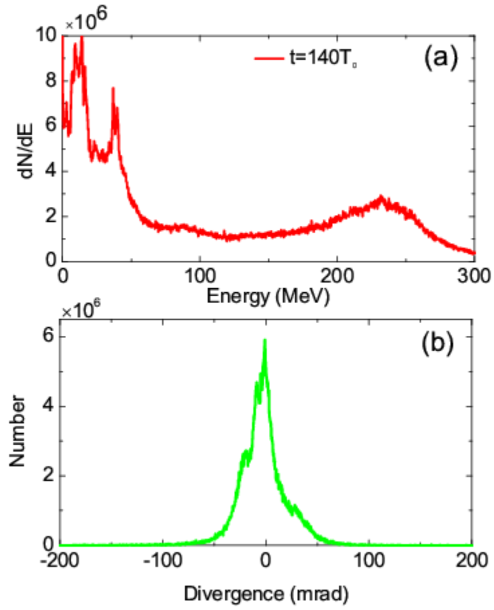

Figure 2: (a) The electron energy spectrum. (b) The electron beam angular spectrum.

Beam extraction

We terminate the SCDP at 100λ to extract the HED beam. The divergence of the ejected electron bunch is 13 mrad as shown in Fig. 2(b). Such tight lateral squeezing can be attributed to the second wake, which is much narrower than the first given that the second laser pulse propagates in a practically tailor-fitted narrow channel. The charge of the bunch can be estimated to be 3 nC. The density of the out-streaming electrons has a peak value of 0.3 critical density. The peak value of the electron density is more than 2×10^{15} J/m^3, as contrast to the peak energy density of 10^{14} J/m^3 from typical wakefield acceleration.

References

[1] J. W. Wang *et al.*, High-energy-density electron beam from interaction of two successive laser pulses with subcritical-density plasma, Phys. Rev. Accel. Beams 19, 021301 (2016).
[2] A. Pukhov *et al.*, Particle acceleration in relativistic laser channels, Phys. Plasmas 6, 2847 (1999).

* Work supported by Helmholtz Association (Young Investigator's Group No. VH-NG-103)
# J.Wang@gsi.de

Optimized laser ion acceleration at the PHELIX laser facility *

F. Wagner †[1,2], *C. Brabetz*[1], *U. Eisenbart*[1], *B. Zielbauer*[1], *and V. Bagnoud*[1,2]
[1]GSI, Darmstadt, Germany; [2]Helmholtz Institut Jena, Germany

Laser driven ion acceleration is one of the main applications of the PHELIX short pulse system. Since the commissioning of the PHELIX laser in 2008 several experiments have been undertaken, aiming at optimized properties of laser-accelerated ion beams e.g. beam collimation, spectral shape and maximum energy. Besides specific developments of sophisticated target compositions and geometries, the laser system has been continually improved.

One important achievement in recent years has been the implementation of an ultrafast optical parametric amplifier (uOPA) which enables a temporal contrast level better than 10 orders of magnitude up to an instant of $100\,\mathrm{ps}$ before the peak intensity [1,2]. Thanks to this ultra-high contrast the use of micrometer and sub-micrometer thick targets for laser ion acceleration experiments has become possible. It is well known that the use of such thin targets along with a sufficiently high temporal contrast of the laser pulse is particularly favorable for ion acceleration via the target normal sheath acceleration (TNSA) mechanism and could lead to enhanced cutoff energies. Furthermore, for a certain match of laser and target conditions alternative acceleration mechanisms could come into play, e.g. the laser breakout afterburner (BOA) mechanism [3].

The feasibility of applying sub-micrometer thick targets at PHELIX for ion acceleration has been studied in several experiments in 2013 and 2014. Fig. 1 showns a TNSA spectrum obtained from the interaction of the PHELIX pulse with a $700\,\mathrm{nm}$ thick target (shot 7451). The spectrum was measured using radiochromic film in stack configuration as we described in more detail in [3]. High particle numbers between 10^9 and 10^{12} protons per MeV for energies above $5\,\mathrm{MeV}$ as well as the relatively high cutoff energy of $38\,\mathrm{MeV}$ confirmed the achieved temporal contrast.

During that experiment, the maximum achievable ion energy was limited due to on-shot aberrations that reduced the intensity on the target. In 2015 we undertook a dedicated internal beamtime to improve the beam quality of the fully amplified PHELIX pulse. Three active elements were used to reduce aberrations: a lens which was switched between a position for alignment and one for full energy shots to compensate for defocus aberration, a mirror after the main amplifier that was actively bent to compensate for astigmatism and a deformable mirror to reduce remaining aberrations. The beam quality was monitored using a Shack-Hartmann wavefront sensor. In addition we mapped the far field after the main amplifier during a full energy shot with a newly commissionned 16-bit CMOS camera (Hamamatsu model C11440-22CU).

Three representative far field images are shown in Fig. 2. Using these images the maximum on-target intensity could be estimated to be 5×10^{20}, 2×10^{20} and $5 \times 10^{19} W/cm^2$ for the cases **a**, **b** and **c**, respectively. In conclusion a much higher maximum intensity is achieved when the full active control of the on-shot aberrations is applied. This was also confirmed by the proton yield. A typical spectrum obtained from a sub-micrometer thick target is shown in Fig. 1 (shot 11831). Particle numbers and the cutoff energy have improved significantly. In Particular, the cutoff energy of $85\,\mathrm{MeV}$ is a new world record for laser ion acceleration via the TNSA mechanism.

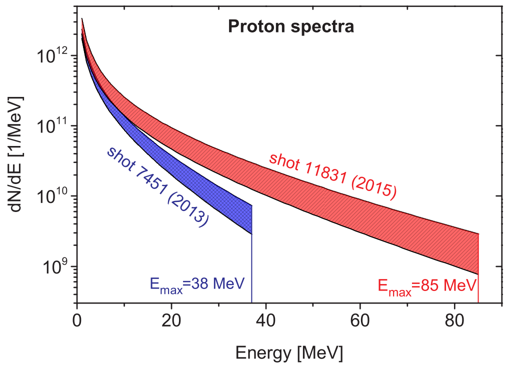

Figure 1: Spectra of protons accelerated via the TNSA mechanism from a shot on a $700\,\mathrm{nm}$ thick target after the implementation of the uOPA in 2013 (shot 7451) and from a shot on a $900\,\mathrm{nm}$ thick target using active control of the on-shot aberrations in 2015 (shot 11831).

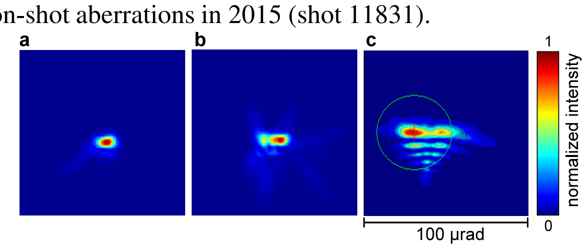

Figure 2: Far field images of the PHELIX pulse for **a**: the cold system, **b**: full active aberration control (lens, bent mirror and deformable mirror) and **c**: reduced aberration control (just lens)

References

[1] F. Wagner et. al., Appl. Phys. B **116**, 2013

[2] F. Wagner et. al., Opt. Expr. **22**, 2014

[3] F. Wagner et. al., Phys. Plasmas **22**, 2015

[4] F. Wagner et. al., submitted to Phys. Rev. Lett. 2016

* This report is also published in the GSI Scientific Report 2015
† f.wagner@gsi.de

Laser-driven proton acceleration with solid hydrogen targets

J.Polz,[1] A.P. L. Robinson,[2] A. Kalinin,[3] G. A. Becker,[1] R. A. Costa Fraga,[3] M. Hellwing,[1] M. Hornung,[4] S. Keppler,[1] A. Kessler,[4] D. Klöpfel,[4] H. Liebetrau,[1] F. Schorcht,[4] J. Hein,[1, 4] M. Zepf,[1, 4, 5] R. E. Grisenti,[3, 6] and M. C. Kaluza[1, 4]

[1]Institut für Optik und Quantenelektronik, 07743 Jena, Germany; [2]Central Laser Facility, Rutherford-Appleton Laboratory, Chilton, Oxon., OX11 0QX, UK; [3]Institut für Kernphysik, Goethe-Universität, 60438 Frankfurt, Germany; [4]Helmholtz-Institut Jena, 07743 Jena, Germany; [5]Department of Physics and Astronomy, Queen's University Belfast, Belfast BT7 1NN, UK; [6]GSI - Helmholtzzentrum für Schwerionenforschung, Planckstr. 1, 64291 Darmstadt, Germany

Introduction

For more than a decade laser-proton acceleration was based on the acceleration of protons from contamination layers on foil targets or from the target substrate itself (e.g. [1]). An energy transfer to heavier ions and therefore a reduction of the conversion efficiency from laser energy into protons is inevitable [2]. To overcome this problem, a target based on solid hydrogen suitable for laser-plasma-interaction experiments has been developed [3] and successfully implemented.

Experimental Setup and Results

The experiment was performed at the POLARIS laser facility, which delivered pulses of 2.5 J energy and 217 fs duration during this experiment. The pulses were focused by an f/2.5 off-axis parabolic mirror to a focal spot size of 8.4 µm^2. 25.9% of the laser energy were encircled in this area resulting in an averaged intensity of 3.5×10^{19} W/cm^2.

The cryogenic source [3] was generating liquid hydrogen jets with a diameter of 10 µm. When injected into vacuum the hydrogen further cooled down due to evaporation, leading to solidification before the liquid stream could break up into droplets, hence forming a filament of solid hydrogen with the same diameter as the nozzle. The laser was incident onto the filament under normal direction. The generated protons propagated towards a Thomson parabola spectrometer. Here the energy spectrum of the protons was recorded (cf. Fig. 1).

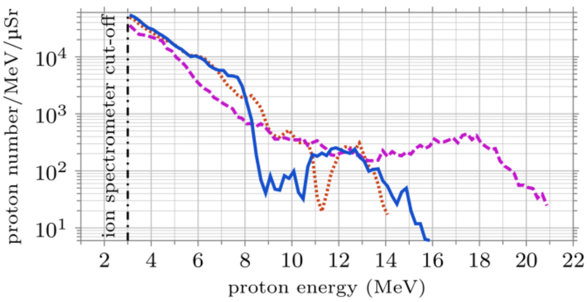

Figure 1: exemplary proton spectra

During the experimental campaign 2197 shots on filaments of hydrogen of 99.999% purity have been conducted. In 30.5% of our recorded spectra the low energy part of the spectrum showed an exponential decay as expected by TNSA, but the high energy part exhibited clear non-thermal features. We identified the origin of this behaviour with the help of 2D PIC simulations as collisionless shock acceleration in the gas corona surrounding the filament. This corona is generated due to the high vapour pressure of hydrogen (i.e. 71.9 mbar at 13.947 K, triple point).

In Fig. 2, the plots of the proton density and the corresponding electric field from the simulation of a 10.5 µm solid hydrogen filament of density 40 n_c (n_c – critical electron density) surrounded by a corona of 2 µm length and 0.08 n_c density is shown at three different time steps.

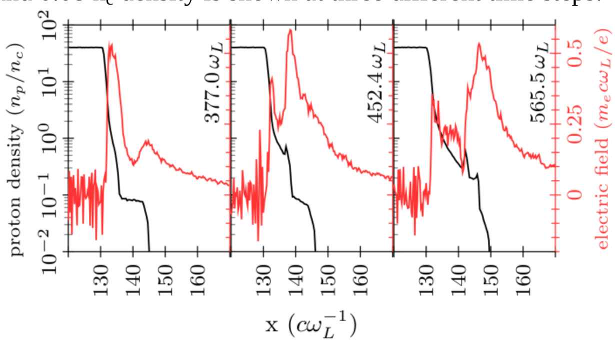

Figure 2: Proton density distribution and corresponding electric field as seen in 2D PIC simulations

The spike in the electric field corresponding to the filament-corona interface at 377.0 ω_L generates a collisionless electrostatic shock, propagating into the corona (cf. change in proton density and corresponding spike in electric field in snapshots at 452.4 ω_L and 565.5 ω_L). In the case of a uniform and constant drive, such electrostatic shock would result in monoenergetic proton spectra. However, since the drive in our case is neither strictly constant nor uniform and the protons undergo further acceleration by TNSA, this effect results in a production of a distinct cleft in the proton spectra. The proton spectra obtained from the simulation are similar as those shown in figure 1. For simulations lacking a corona surrounding the target, the spectrum changed to exponential decaying without modifications, as expected by plain TNSA. In addition to these spectral modulations, a significantly higher conversion efficiency was observed. Data is still under analysis.

References

[1] R. A. Snavely *et al.*, Phys. Rev. Lett. **85**, 2945 (2000)
[2] M. E. Foord *et al.*, High Energy Density Physics **3**, 365 (2007).
[3] R. C.-Fraga *et al*,. Rev. Sci. Instr. **83**, 025102 (2012).

Photon and Particle Spectroscopy

XUV coherence tomography with laser-based sources*

S. Fuchs† [1,2], *M. Wünsche* [1,2], *J.J. Abel*[1], *J. Bernert*[1], *J. Biedermann*[1], *M. Möller*[1,2], *C. Rödel*[1,2], *and G.G. Paulus*[1,2]

[1]University, Jena, Germany; [2]Helmholtz Institute, Jena, Germany

Optical coherence tomography (OCT) is a well-established method to retrieve three-dimensional, cross-sectional images of biological samples in a non-invasive way using near-infrared radiation. The axial resolution of OCT with broadband visible and near-infrared sources typically reaches axial (depth) resolutions in the order of a few micrometers. We developed soft-X-ray coherence tomography (XCT), which takes advantage of the fact that the coherence length can be significantly reduced if broadband extreme UV (XUV) and soft X-ray (SXR) radiation is used. XCT can display its full capabilities when used in the spectral transmission windows of the sample materials. For instance, the silicon transmission window (30-99 eV) corresponds to a coherence length of about 12 nm, thus suggesting applications for semiconductor inspection. In the water window at 280-530 eV, a coherence length as short as 3 nm can be achieved and highlights possible applications of XCT for life sciences.

Since 2013 the Project is supported by the German Federal Ministry for Education (BMBF) within the VIP (Validierung des Innovationspotentials) program. Our setup utilizes a variant of a Fourier-domain OCT setup that completely avoids a beamsplitter. Broadband XUV light is focused on the surface of the sample. The reflected spectrum is measured with a grating spectrometer consisting of a gold transmission grating and a toroidal mirror (spectrometer-based OCT). The top layer reflection assumes the role of a reference beam. A Fourier transform including dispersion correction of the reflected spectrum needs to be computed for retrieving the structural information. A 3D-image can be captured by scanning the focus over the sample. A proof-of-principle experiment has been performed at synchrotron sources successfully and has been published now [1].

Since XCT exploits the spectral broadness of the light source to achieve axial resolution it can be regarded as a perfect application for laser-driven high-harmonic generation sources due to their intrinsic broad bandwidths. In fact, the bandwidth of HHG would have disadvantages for other imaging methods such as confocal microscopy or coherent diffraction imaging. In addition, HHG enables XCT to become a table top nanometer imaging technique. Thus we developed a suitable HHG source in the energy range of the silicon transmission window (30-99eV) with sufficient flux by using laser pulses with an energy of 1.8mW, a pulse duration of 50fs, and a wavelength of 1300nm driven by an OPA. In 2015 we could show that XCT works with laser-based sources for the first time. We were able to achieve three-dimensional tomographic images of structured samples. Due to the spectral filtering with thin aluminum foils, which is needed for HHG sources, the broadness of the spectrum is limited by the filter's absorption edge and thus the axial resolution of the method is about 20 nm in the silicon transmission window. We improved the lateral resolution by an order of magnitude in comparison to the synchrotron measurements down to 10μm. A laser-driven XCT scan is shown in figure 1. 1900 single measurements were taken in an area of about 900x500μm. The measurement time was 9 hours, which is only a factor of three slower than a comparable synchrotron scan. Next steps are further improvements in lateral resolution and enabling material-sensitive contrast to reconstruct the compounds the layers consist of.

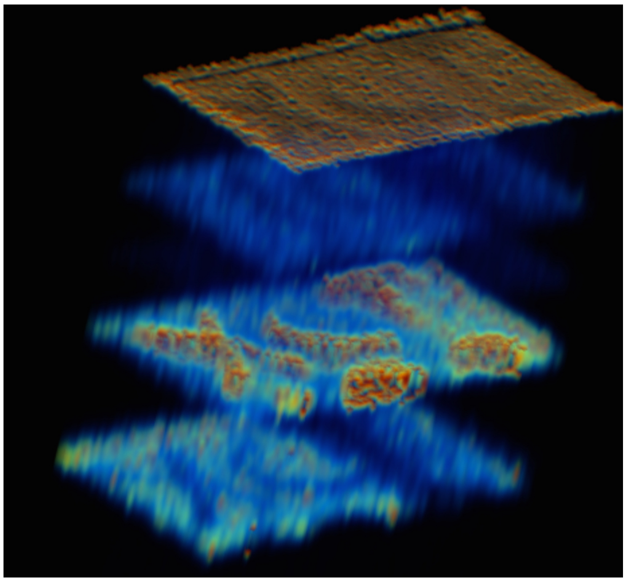

Figure 1: Threedimensional image taken with laser-based XCT. The lateral dimension is 900 x 500μm. The axial dimension is 300nm. The sample consists of buried 5nm thick gold structures embedded in silicon. The structure is clearly visible with a lateral resolution of about 15μm.

* Work supported by BMBF VIP-Project "X-CoherenT", HI Jena, and DFG TR18 A7

† silvio.fuchs@uni-jena.de

References

[1] Fuchs, S. *et al.* , "Nanometer resolution optical coherence tomography using broad bandwidth XUV and soft x-ray radiation", Scientific Reports 6, p. 20658 (2016)

Extreme ultraviolet digital in-line holography using a high harmonic source

M. Zürch[*,1,2,3]*, and C. Spielmann*[1,3]

[1]IOQ, FSU Jena, Germany; [2]University of California, Berkeley, CA 94720, U.S.A.; [3]HI Jena, Germany

Large scale facilities such as FELs and synchrotrons are used since a decade as sources to provide insight into matter and dynamics at the nanoscale. The short wavelength in the extreme ultraviolet (XUV) and soft x-Rays and high photon flux are key for resolving nanoscopic structures. A powerful alternative on the lab scale are High Harmonic Generation (HHG) sources, which are now routinely employed for various imaging applications, for instance by means of coherent diffraction imaging (CDI). Recent progress within the Helmholtz Institute demonstrated reflection geometry imaging for surface studies [1], identification and classification of cancer cells [2] and transmission imaging down to the wavelength level [3].

However, a major drawback of coherent diffraction imaging is the need to retrieve the phase of the measured diffraction pattern by means of iterative algorithms which are prone to fail with slightest inhomogeneities or noise on the captured data.

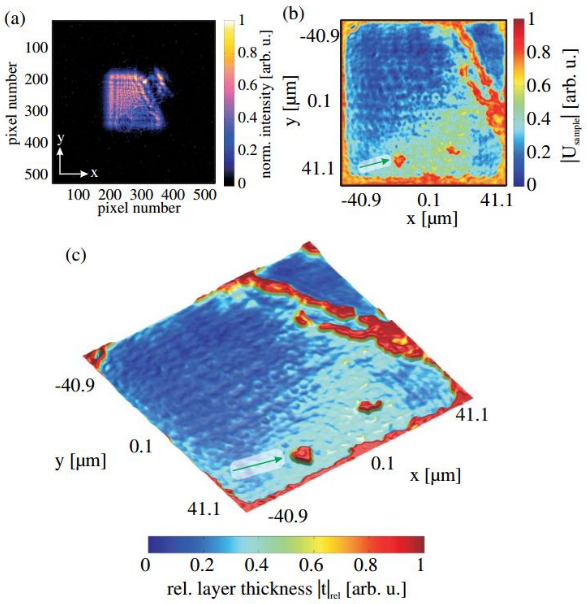

Figure 1: (a) Hologram measured at 38nm wavelength. (b) The retrieved object shows a silicon nitride membrane on which different objects were dispersed. Further solvent remains visible. (c) 3D information gathered by this holographic technique show features on the surface of the membrane in full detail. Layers of few nanometer thickness can be identified. Taken from [4]

Holography is an imaging technique that overcomes the need for near-perfect diffraction data by interfering the light diffracted by the object with a known reference wave.

* michael.zuerch@uni-jena.de

In a recent experiment a HHG source driven by an ultrafast titanium-sapphire laser was employed for digital in-line holography experiments. By means of a toroidal mirror and a grating a single harmonic line at 38nm wavelength was selected by a one micron pinhole. The pinhole subsequently generates a spherical wave that acts as illumination and reference wave at the same time, making up an in-line holography scheme (Fig. 1a).

As test object ultrathin silicon nitride membranes on which polystyrene beads were dispersed were imaged. Solvent remains formed additional structures that could be resolved in great detail (Fig. 1b). An optimized algorithm was developed to reconstruct the measured holograms allowing for near real-time twin-image-free reconstruction of the raw data. Further, the reconstruction showed robust behaviour against noise and imperfection of the measured hologram. We could demonstrate a spatial resolution of about one micron, limited by the size of the reference pinhole, and a field-of-view of 100 by 100 micron. Mapping the absorption into a three-dimensional map of the sample, the surface and swelling of the membrane was imaged in high detail (Fig. 1c). Despite not quantified, we estimate the resolution in z-direction to be a few nanometers. Full details of this experiment and the reconstruction procedure are reported elsewhere [4].

Digital in-line holography in the XUV is a good candidate for further studies that employ high temporal resolution. While it is experimentally challenging to achieve spatial resolutions comparable to those routinely achieved by CDI, the robustness and real-time reconstruction along with the availability of the phase-locked laser are the clear advantages of the demonstrated technique. High-resolution morphology determination in combination with phase-contrast imaging for thin-film characterization and applications arising thereof are further in reach.

References

[1] M. Zuerch, C. Kern, and C. Spielmann, “XUV coherent diffraction imaging in reflection geometry with low numerical aperture”, Opt. Express 21 (2013), pp. 21131-21147

[2] M. Zürch, et al., “Cancer cell classification with coherent diffraction imaging using an extreme ultraviolet radiation source”, J. Med. Imag. 1 (2014), 031008

[3] M. Zuerch, J. Rothhardt, et al., “Real-time and Subwavelength Ultrafast Coherent Diffraction Imaging in the Extreme Ultraviolet”, Sci. Rep. 4 (2014), 7356

[4] M. Zürch, and C. Spielmann, “Extreme ultraviolet digital in-line holography using a tabletop source”, Appl. Opt. 54 (2015), 5992

Coincidence ion imaging of gas-phase molecules with a high repetition rate XUV high harmonic source

J. Rothhardt[1,2], S. Hädrich[1,2], Y.Shamir[2], M. Tschernajew[1,2], R. Klas[1,2], A. Hoffmann[2], G. K. Tadesse[1,2], A.Klenke[1,2], T. Gottschall[2], T. Eidam[2], J. Limpert[1,2,3], A. Tünnermann[1,2,3]

[1]Helmholtz Institute Jena, Fröbelstieg 3, 07743 Jena, Germany
[2]Institute of Applied Physics, Abbe Center of Photonics, Friedrich-Schiller-University Jena, Albert-Einstein-Straße 15, 07745 Jena, Germany
[3]Fraunhofer Institute for Applied Optics and Precision Engineering, Albert-Einstein-Straße 7, 07745 Jena. Germany

R. Boll[4], C.Bomme[4], H. Dachraoui[4], B. Erk[4], M. Di Fraia[7], D. A. Horke[5], T. Kierspel[5], T. Mullins[5], A. Przystawik[4], E. Savelyev[4], J. Wiese[5], T. Laarmann[4,8], J. Küpper[5,6,7], D.Rolles[4,8]

[4]Deutsches Elektronen-Synchrotron DESY, Notkestrasse 85, 22607 Hamburg, Germany
[5]Center for Free-Electron-Laser Science (CFEL), DESY, Notkestrasse 85, 22607 Hamburg, Germany
[6]Department of Physics, University of Hamburg, Luruper Chaussee 149, 22761 Hamburg, Germany
[7]Hamburg Center for Ultrafast Imaging (CUI), University of Hamburg, Luruper Chaussee 149, 22761 Hamburg, Germany
[8]J. R. Macdonald Laboratory, Department of Physics, Kansas State University, Manhattan, Kansas 66506, USA

Ultrashort-pulse sources of XUV and X-ray photons enable studies of matter on atomic (picometer) length and (femtosecond) time scales. As such, they constitute an indispensable tool for many areas of modern science. Ultrafast molecular imaging experiments aim at understanding and controlling fundamental processes in photochemical reactions in space and time [1]. A particularly powerful method for such studies is the coincident momentum imaging technique [2], which yields multi-dimensional data sets that can provide channel-resolved and kinematically complete measurements that contain a wealth of information and allow studies in the molecular reference frame [3]. However, it requires less than one ionization event per XUV / X-ray pulse in the probed sample to unambiguously correlate the detected ionization fragments. Therefore, the acquisition of sufficient statistics is only feasible with high-repetition-rate pump-probe sources, ideally with a multi-kHz repetition rate. Moreover, the x-ray pulses must be synchronized to optical pump pulses with femtosecond precision, which is difficult at FEL facilities due to the long beam paths through these machines and the intrinsic arrival time jitter [4].

Here, we present coincidence experiments on iodomethane (CH_3I) that were conducted with a 50–100 kHz repetition rate table-top XUV source. This XUV source was enabled by a state-of-the-art chirped-pulse-amplification fiber-laser system that incorporates coherent combination of two main amplifiers [5] and post-compression. It delivers 0.6 mJ pulses, at ~ 1.03 µm wavelength with a duration of 35 fs at repetition rates up to 100 kHz, which are employed for high-harmonic generation (HHG). Particular optimization of the photon flux of the 57th harmonic yielded up to $6.8 \cdot 10^{10}$ photons/s at a repetition rate of 50 kHz, which represents the highest photon flux so far reported from any HHG source in this spectral range.

This allowed for the first successful demonstration of a coincidence measurement on inner-shell ionized gas-phase molecules on a table-top.

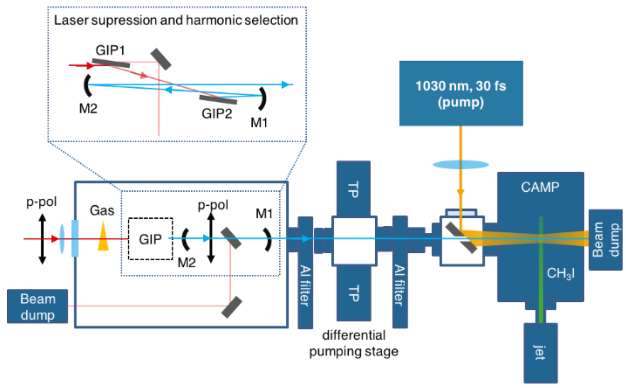

Fig. 1. Top view on the experimental setup used for high harmonic generation. The inset shows a more detailed side-view of the separation of the harmonics from the fundamental driving laser, selection of a single harmonic and focusing of the harmonic into the experiment. (GIP – grazing incidence plates, M1/2 – XUV mirrors at 68.6 eV, TP – turbo pumps, CAMP – CFEL-ASG Multi Purpose end station [6]).

The experimental setup is schematically shown in Fig. 1. The laser beam enters the experiment from the left and is focused onto an argon gas-jet for HHG. The generated XUV photons are separated from the driving infrared laser beam via grazing incidence plates, which transmit the IR

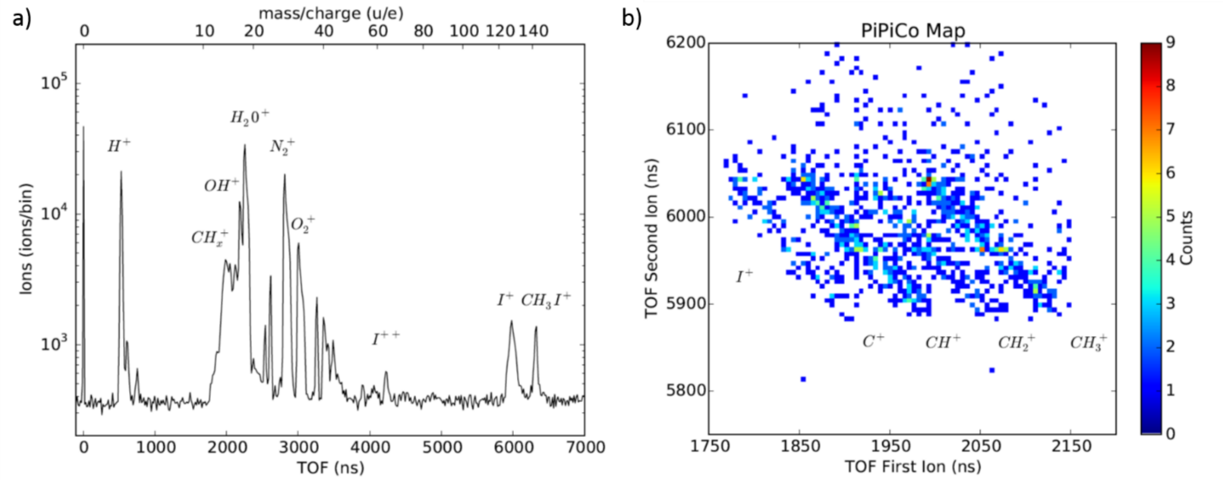

Fig. 2. Ion time-of-flight mass spectrum recorded at 68.6 eV photon energy. The CH3I+ parent ion as well as several ionic fragments can be seen along with several ions resulting from the ionization of the residual background gas in the chamber. b) Ion-ion coincidence spectrum of CH_3I zoomed in on the region containing the coincidences between CHx^+ (x = 0, …, 3) and I^+ fragments.

but reflect the XUV light. Two multi-layer mirrors are employed to collimate and refocus the XUV beam onto the molecular jet. Several aluminium filters and a differential pumping stage ensure a sufficient vacuum in the experimental chamber.

The coincidence experiment was performed in the CAMP instrument [6]. The current setup consists of a doubly skimmed supersonic molecular beam (nozzle diameter: 30 µm, skimmer diameters: 200 and 400 µm, distance nozzle to interaction region: roughly 70 cm and a double-sided velocity map imaging (VMI) spectrometer equipped with two microchannel plate (MCP) detectors with position-sensitive delay-line anodes.

We recorded electron-ion-ion coincidence data for the photoionization of CH_3I molecules by the HHG pulses. At a photon energy of 68.6 eV, the cross sections for both valence and inner-shell ionization at this photon energy are roughly equal [62]. Thus, the CH_3I molecules can either be valence ionized, resulting predominantly in singly charged CH_3I^+ ions, or a I(4d) inner-shell electron can be removed, which leads to a doubly or triply charged final state after the inner-shell vacancy relaxes via Auger decay. The majority of these doubly or triply charged cations then break up into charged fragments as seen in the ion time-of-flight mass spectrum shown in Fig. 2 (a). A plot of the ion-ion coincidences between CHx^+ (x = 0, 1, 2, 3) fragments and I^+ fragments is shown in Fig. 2 (b). Due to momentum conservation, these coincidence events, which resulted from a (quasi-) two-body fragmentation — the neutral or charged H^+ fragments that may also be emitted carry very little momentum due to their light mass — can be clearly identified by diagonal lines in the photoion-photoion coincidence (PIPICO) spectrum. Note that these results were obtained from a 20-hour long measurement during which the laser system, the high harmonic generation, and the coincidence apparatus were operated constantly and without interruption. The required measurement times will be significantly reduced by further increasing the photon flux of the XUV source and by increasing the density of the molecular beam. Thus, pump-probe experiments will be feasible on few-10 fs time scales. Since HHG sources can also provide attosecond pulses at high repetition rates [7], such experiments are expected to access attosecond time scales in future.

References

[1] A. Rudenko and D. Rolles, J. Electron Spectros. Relat. Phenomena **204**, 228 (2015).

[2] B. Erk, R. Boll, S. Trippel, D. Anielski, L. Foucar, B. Rudek, S. W. Epp, R. Coffee, S. Carron, S. Schorb, K. R. Ferguson, M. Swiggers, J. D. Bozek, M. Simon, T. Marchenko, J. Kupper, I. Schlichting, J. Ullrich, C. Bostedt, D. Rolles, and A. Rudenko, Science **345**, 288 (2014).

[3] J. Ullrich, R. Moshammer, A. Dorn, R. D rner, L. P. H. Schmidt, H. Schmidt-Böcking, R. Doerner, and H. Schmidt-Boecking, Reading **66**, 1463 (2003).

[4] T. Ishikawa et al., Nat. Photonics **6**, 540 (2012).

[5] A. Klenke, S. Breitkopf, M. Kienel, T. Gottschall, T. Eidam, S. Hädrich, J. Rothhardt, J. Limpert, and A. Tünnermann, Opt. Lett. **38**, 2283 (2013)

[6] L. Strüder, Nucl. Instruments Methods Phys. Res. Sect. A Accel. Spectrometers, Detect. Assoc. Equip. **614**, 483 (2010)

[7] M. Krebs, S. Hädrich, S. Demmler, J. Rothhardt, A. Zair, L. Chipperfield, J. Limpert, and A. Tünnermann, Nat Photon **7**, 555 (2013)

More details on the presented experiments can be found at arXiv:1602.03703.

Design and construction of a wide-spectral-range XUV spectrometer and first observation of SASE radiation at FLASH2*

T. Tanikawa[1], *A. Hage*[1,2], *M. Kuhlmann*[1], *B. Faatz*[1], *F. Tavella*[3], *and M. J. Prandolini*[†4]

[1]DESY, Hamburg, Germany; [2]Queen's University, United Kingdom; [3]SLAC, Menlo Park (CA), USA;
[4]Helmholtz-Institut Jena, Jena, Germany

The Free-electron LASer in Hamburg (FLASH) has been extended with a new undulator line FLASH2 in 2014. A compact grazing-incident wide-spectral-range spectrometer based on spherical-varied-line-spacing (SVLS) gratings in the extreme ultraviolet (XUV) region was constructed to optimize and characterize the free-electron laser (FEL) performance at FLASH2. The first light using self-amplified spontaneous emission from FLASH2 was observed by the spectrometer during a simultaneous operation of both undulator lines – FLASH1 and FLASH2.

Introduction

The FLASH facility started user operation at DESY in 2005, and currently provides extreme ultraviolet (XUV) photon pulses within a wavelength range from 4.2 to 52 nm. These high coherence pulses, with typical peak power of up to 3 GW and pulse durations of 10-200 fs, open up exciting new opportunities and applications, such as studies on ultrafast reaction dynamics and multiphoton processes within a femtosecond time scale. In 2014, the newly constructed undulator line FLASH2, using the same electron beam accelerator as the existing undulator line FLASH1, successfully achieved a first lasing using self-amplified spontaneous emission (SASE) (Fig. 1).

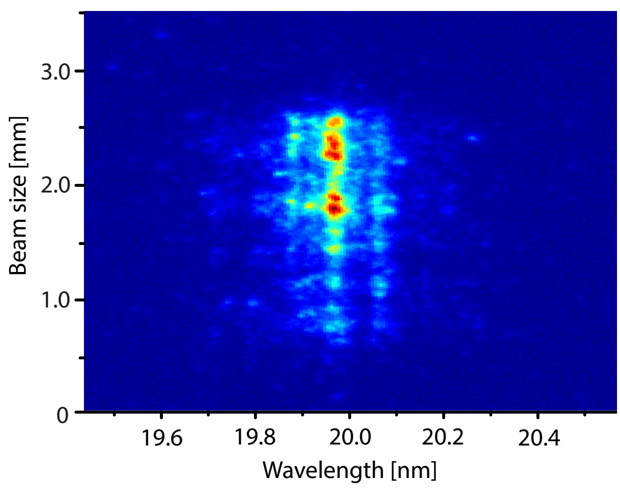

Figure 1: A typical spectral profile of SASE radiation from FLASH2, measured at the wavelength of 20 nm.

The compact wide-spectral-range XUV spectrometer

This spectrometer was designed as a compact, flexible, general purpose spectrometer covering a spectral range from 1 to 62 nm with a potential resolving power from 1050 to 14400 depending on the wavelength and the signal intensity [1]. In addition, it can be used for SWORD measurements, as a seeding laser diagnostic tool and it will be available for FEL users in the future. The spectrometer was extensively characterized including AFM to measure the quality of the grating surface. Wavelength calibration was carried out at the monochromatic beamline PG2 at FLASH1 and the measured resolution was compared to simulations. In this first application – commissioning phase for first lasing at FLASH2 – the resolving power was limited by the required slit size to achieve a sufficient intensity on the camera, because no focusing optics were installed during this phase.

First SASE observation from FLASH2

The SASE signal was measured shot-by-shot with the compact wide-spectral-range XUV spectrometer. The measurement was carried out at the wavelength of 20 nm. Since the first photon beamline at FLASH2 is currently under construction, there were no focusing optics for the spectrometer at the photon diagnostic section. Therefore, in order to get sufficient intensity onto the camera, the slit width of 330 μm was chosen for this experiment, resulting in an expected resolving power of 406, which corresponds to a resolution of 0.05 nm at the wavelength of 20 nm. A typical measured spectral profile is shown in Fig. 1. The measured total SASE bandwidth of 0.124 nm at a wavelength of 20 nm agrees well with 3D numerical simulations using GENESIS (0.114 nm). GENESIS also predicts a single SASE-spike bandwidth of 0.008 nm at this wavelength, which is beyond the resolution of the spectrometer in this experimental configuration. In the future, by focusing of the FEL radiation at the spectrometer as well as closing the slit to less than 50 μm, this spectrometer can resolve all spectral SASE spikes.

References

[1] T. Tanikawa, et al., "First observation of SASE radiation using the compact wide-spectral-range XUV spectrometer at FLASH2", submitted to *Nucl. Instrum. Meth. A* (2016)

* Work supported by HI Jena/DESY.
† mark.prandolini@desy.de

Strong sub-luminal propagation of x-ray pulses

K.S. Schulze[1,2], I. Uschmann[1,2], R. Loetzsch[1,2], B. Marx[2], R. Röhlsberger[3], K.P. Heeg[4], J. Evers[4], J. Haber[3], D. Schumacher[3], E. Förster[1,2], and G.G. Paulus[1,2]

[1]Helmholtz Institute Jena, Germany; [2]Friedrich-Schiller-Universität Jena, Germany; [3]Deutsches Elektronen Synchrotron DESY, Germany; [4]Max-Planck-Institut für Kernphysik, Heidelberg, Germany.

The advent of the laser, more than 50 years ago, has enabled the control of light-matter interaction and opened a new field with a whole slew of remarkable effects: quantum optics. One of these is the deceleration of light, which is discussed as a possibility for the realization of switches in optical networks. On the other hand, x-rays have a multitude of applications due to its small wavelength. Combining both give new insights into light-matter interaction. An important fact is the possibility of x-rays to interact with the nucleus, which allows quantum optics with nuclear transitions. Thus, the recent success in combining x-ray polarimetry with resonant nuclear scattering paved the way for quantum optics with x-rays.

High-purity x-ray polarimetry for nuclear resonant scattering

The main issue in nuclear resonant scattering at synchrotrons is the selection of scattered photons from a background, which is orders of magnitude higher, since the bandwidths of the resonances are in the neV or µeV range. We used a trick for this selection. Photons that are scattered resonantly can change their polarization depending on the orientation of the initial polarization to a magnetization of the sample. With the help of an x-ray polarimeter, these scattered photons can be selected, whereas the photons, which are not scattered resonantly, can be suppressed by more than eight orders of magnitude. This high suppression could only be realized by a high-purity polarimeter, which we developed together with the University of Jena in the last years [1]. The careful preparation of channel-cut crystals, which was specially designed for the nuclear transition of the Mössbauer isotope ^{57}Fe, was the main key for realizing such a high purity. The use of asymmetric (840)-reflections inside the channel-cut crystals allows both: a high polarization purity and a relative large angular acceptance for x-ray beams that are focused with Beryllium lenses. Since the polarimetric method dramatically supresses the background, pure spectra of the resonantly scattered photons can be obtained. The success of the method has already led to the discovery of spontaneously generated coherences [2].

Sub-luminal propagation of x-rays

In a recent experiment, we observed a strong reduction of the group velocity of x-rays, which interacted with ^{57}Fe nuclei [3]. This experiment was carried out within a collaboration between DESY Hamburg, the Max Planck Institute for Nuclear Physics Heidelberg, the University Jena and the Helmholtz Institute Jena. Besides the high-purity polarimeter, the setup consists of two samples, which contains the Mössbauer isotope ^{57}Fe: one sample, which acts as bandpass, and a second one, which provides a steep dispersion of the refractive index over the full energetic range of the x-ray pulses. The latter is realized by a thin-film cavity with embedded ^{57}Fe. Plotting the photons, that passes the setup, over their traveling time and energy, one can observe a strong delay of the photons close to the nuclear resonance of the embedded ^{57}Fe (Fig. 1). In the future, this "slow" light can amplify the light-matter interaction, so that non-linear effects in the x-ray range will be accessible.

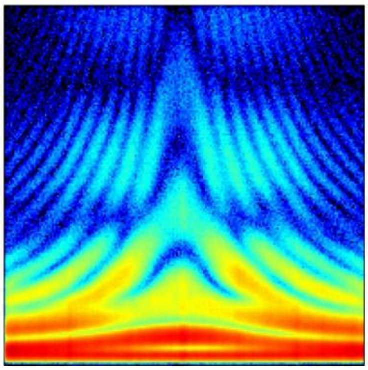

Figure 1: Propagation of x-ray pulses inside a sample enriched with the iron isotope 57. The vertical direction shows a temporal beat pattern, whereas the horizontal direction displays the deviation of the photon energy from the nuclear resonance of iron-57. Close to the resonance (in the middle), the x-ray pulses are strongly delayed.

References

[1] B. Marx, I. Uschmann, S. Höfer, R. Lötzsch, O. Wehrhan, E. Förster, M. Kaluza, T. Stöhlker, H. Gies, C. Detlefs, T. Roth, J. Härtwig, and G.G. Paulus, "Determination of high-purity polarization state of X-rays", Optics Communications 284: 915-918, 2011.

[2] K. P. Heeg, H.-C. Wille, K. Schlage, T. Guryeva, D. Schumacher, I. Uschmann, K. S. Schulze, B. Marx, T. Kämpfer, G. G. Paulus, R. Röhlsberger, and J. Evers, "Vacuum-Assisted Generation and Control of Atomic Coherences at X-Ray Energies", PRL 111, 073601, 2013

[3] K. P. Heeg, J. Haber, D. Schumacher, L. Bocklage, H.-C. Wille, K. S. Schulze, R. Loetzsch, I. Uschmann, G. G. Paulus, R. Rüffer, R. Röhlsberger, and J. Evers, "Tunable sub-luminal propagation of narrow-band x-ray pulses", PRL 114: 203601, 2015

Linear polarization measurement in elastic hard x-ray scattering*

K.-H. Blumenhagen†[1,2,3], *S. Fritzsche*[1,2], *T. Gassner*[1,2,3], *A. Gumberidze*[3,4], *R. Märtin*[1,3], *N. Schell*[5], *D. Seipt*[1], *U. Spillmann*[3], *A. Surzhykov*[1], *S. Trotsenko*[1,3], *G. Weber*[1,3], *V. A. Yerokhin*[1,6], *and Th. Stöhlker*[1,2,3]

[1]HI-Jena, Germany; [2]University of Jena, Germany; [3]GSI, Darmstadt, Germany; [4]EMMI, Darmstadt, Germany; [5]HZG, Geesthacht, Germany; [6]Peter the Great St. Petersburg Polytechnic University, Russia

The elastic scattering of photons from atoms has been studied experimentally. While previous studies on elastic scattering covered a broad range of photon energies and target materials [1, 2], they mostly considered unpolarized photon beams in the hard x-ray regime. A few experiments, where the photon polarization was taken into account [3], were limited to the following scenarios (excluding magnetic scattering [4], where one uses oriented targets): (1) Measuring the elastic scattering differential cross section when the incident photon beam is partially linearly polarized. (2) Measuring the linear polarization of the elastically scattered beam when the incident beam is unpolarized. Both these types of experiment suffered from low statistics due to technological shortcomings: Low-intensity polarized x-ray sources on the one hand and inefficient x-ray polarimeters on the other. These problems could be reduced with the advent of novel technologies, so a new type of elastic scattering experiment became feasible, which is presented in this report: Measuring the linear polarization of the scattered beam, when the incident beam is highly linearly polarized. To observe relativistic effects, a scenario with strong electromagnetic fields was chosen, namely the scattering of 175 keV hard x-rays from a high-Z target (gold). An intense, highly linearly polarized photon beam at that energy was provided by the High Energy Materials Science Beamline P07 [5] at the third-generation synchrotron radiation source PETRA III at DESY, Hamburg. The polarization of the scattered beam was analyzed with a dedicated solid state strip Compton polarimeter [6] at three scattering angles θ in the polarization plane of the incident beam (coplanar geometry). For this, the Compton polarimetry technique [7] was applied, which involves a measurement of the φ_C-distribution, where φ_C is the azimuthal scattering angle of Compton scattering events inside the polarimeter. Fitting the φ_C-distribution allows to extract the polarization of the beam incident on the polarimeter surface. In the present work, a non-analytical fit function based on Monte Carlo simulations was employed. The reason for this procedure (instead of using the analytical Klein-Nishina Compton scattering cross section) was to include detector effects. An example of a φ_C-distribution together with the corresponding fit is shown in figure 1 (a). Preliminary results for the polarization of the elastically scattered beam are presented in figure 1 (b).

* Work supported by HGS-HIRe / Helmholtz Alliance (HA216/EMMI) / DESY and HZG support at beamline P07. This report is also part of the GSI Scientific Report 2015 DOI:10.15120/GR-2016-1

† k.-h.blumenhagen@gsi.de

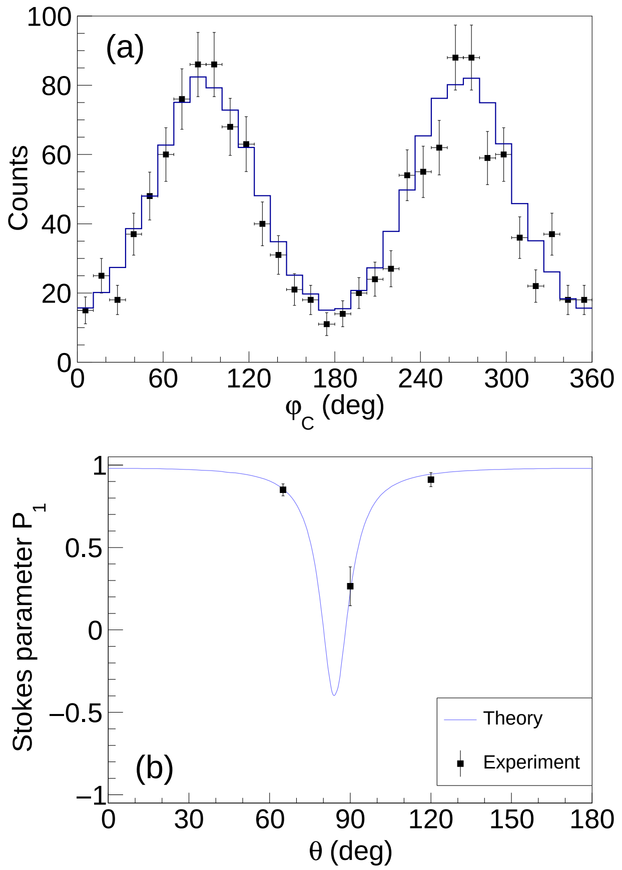

Figure 1: Preliminary results: (a) φ_C-distribution with fit from Monte Carlo generated spectra at $\theta = 65°$. (b) Stokes parameter P_1 of the elastically scattered photon beam. Theory from [8] which is based on [9, 10].

References

[1] P. P. Kane et al., Phys. Rep. 140, 75-159 (1986).

[2] D. A. Bradley et al., Radiat. Phys. Chem. 56, 125-150 (1999).

[3] S. C. Roy et al., Phys. Rev. A 34, 1178-1187 (1986).

[4] M. Cooper and W. Stirling, Radiat. Phys. Chem. 56 85–99 (1999)

[5] N. Schell et al., Mater. Sci. Forum 772, 57-61 (2014).

[6] D. Protic et al., IEEE Trans. Nucl. Sci. 53, 3181-3185 (2005).

[7] F. Lei et al. Space Sci. Rev. 82 309–388 (1997).

[8] A. Surzhykov et al., private communication (2014).

[9] A. Surzhykov et al., Phys. Rev. A 88 062515 (2013).

[10] A. Surzhykov et al., J. Phys. B 48 144015 (2015).

Refractive index measurements at γ-ray energies up to above 1 MeV for materials with different charge numbers Z

M. M. Günther[1,2,#] *,M. Jentschel* [3], *A. Pollitt* [3], *P. G. Thierolf* [4], *M. Zepf* [2], *W. Ziegler*[2]
[1]GSI, Darmstadt, Germany; [2]Helmholtz-Institut Jena, Jena, Germany; [3]Institut Laue-Langevin, Grenoble, France; [4]Ludwig Maximilians Universität, Garching, Germany

The knowledge of the refractive properties of materials plays an important role in many optical applications. Recent investigations of the refractive index of several materials were done up to 133 keV [1]. A next step is the application of refractive optics in the γ-ray energy range. However, the refractive behaviour of materials at such high photon energies isn't well known. The experimental access in this regime is very difficult due to the tiny decrement of the refraction index from n=1. Sophisticated instrumentation is necessary to investigate the refractive behaviour. First and only experiments on Silicon [2] were performed using the γ–spectrometer GAMS5 at the Institut Laue-Langevin (ILL) in Grenoble (France)[3]. The result was surprising because a sign change in the real part of the refraction index was observed about 700 keV which couldn't be explained. In 2015 we measured for the first time the index of refraction of compound and elemental materials with different Z at γ energies up to above 1 MeV. The experiment was performed at the new GAMS6 γ-spectrometer during the commissioning at the ILL. We used an improved experimental systematics which eliminates systematic errors, unknown occurred in experiments at GAMS5. The set up is shown in Figure 1.

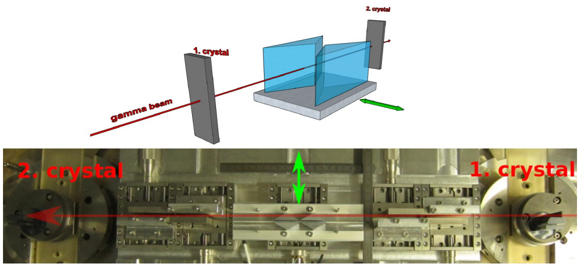

Figure 1: Principle of the experimental set up at GAMS6.

GAMS6 is operated under vacuum which eliminates errors concerning temporal drifts in the optical heterodyne Michelson interferometer used for high resolution angle measurements. The drifts occur due to earth atmospheric variabilities in temperature, pressure and humidity. A spectrometric method was used for the measurement of the angular deviation of a γ beam after the propagation through a prism. The expected deviation angle is in the range of about 10^{-8} radian because refraction is very weak. GAMS6 consisting of two flat perfect Si crystals. The first crystal defines the γ energy band by Bragg diffraction and collimates the beam. The second crystal acts as an angle analyser by rocking around the vertical axis. The rotation angle is controlled by an optical interferometer. The angular resolution is about 10^{-9} radian. An active vibration control system leads to an accuracy in angle measurement of 1/300 interferometer fringe (1 Fringe=$50*10^{-9}$ radian). After propagation of the beam through the two crystals the angular intensity profile is measured by a HPGe detector. The center of the rocking curve presents the angular position of the γ beam. The γ beam is generated by neutron capture processes of an in-pile Gd_2O_3 target close to the nuclear fission reactor core. The γ emission rate is about 10^{16} γ/s. The γ beam is collimated with the result of a 2 mm small beam at GAMS6 with a flux of more then 10^9 γ/s. We used Si, Ge, SiO_2, and fused silica hollow prisms each with a prism angle of 120 degree. The hollow prisms are filled with fluid Hg. Groups of prisms of the same material but opposite prism angle on the right and the left side are placed on the prism mount within the beam between the spectrometer crystals (see Figure 1). By moving the prism right and left within the beam, the prism pairs refract the beam in opposite directions. This allows on the one hand to measure smaller refractive effects and on the other hand to use lower prism angles, which reduces the attenuation.

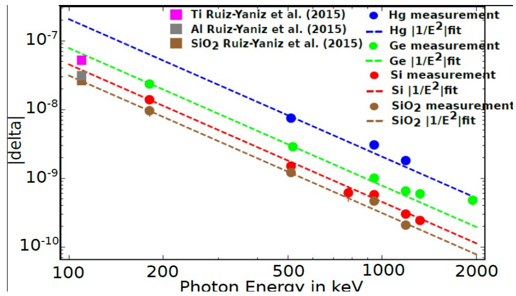

Figure 2: Preliminary results of recent experiment. Real part δ of complex refraction index as function of γ energy.

The preliminary results can be summarized as follows and will be described in more detail in [4]: We found and eliminate systematic errors occurred at GAMS5 refractive index measurements. No sign change of the real part of the refraction index was measured for all used materials with the result of a refraction index n<1. For energies below 1 MeV we see a $1/E^2$ dependency of the dispersion curves (Figure 2). At energies above 1 MeV in case of the high Z materials we observed a trend in the slope of the dispersion curves which is weaker than $1/E^2$. This trend is not expected in classical scattering theory and has to be investigated in more detail in further experimental campaigns, where measurements of high Z materials at γ energies above 1 MeV will be performed.

References

[1] M. Ruiz-Yaniz et al., Phys. Rev A **91**, 033803 (2015)
[2] D. Habs, M.M. Günther et al., Phys. Rev. Lett. **108**, 184802 (2012)
[3] E.G. Kessler Jr. et al., NIM A **457**, pp. 187-202 (2001)
[4] M.M. Günther et al., publication in preparation (2016)

m.guenther@gsi.de

Combining x-ray spectroscopy and imaging of laser-heated Titanium at the POLARIS Laser Facility

R. Loetzsch[1,2], T. Kämpfer[1,2], K. Zeil[3], , G. Becker[1,2], S. Kraft[3], H-P. Schlenvoigt[3]

F. Brack[3], I. Uschmann[1,2], U. Schramm[3], M. C. Kaluza[1,2] , E. Förster[1,2],

[1] Helmholtz-Institut Jena, Fröbelstieg 3, D-07743 Jena, Germany; [2] Institut für Optik und Quantenelektronik, Friedrich-Schiller-Universität Jena, Max-Wien-Platz 1, D-07743 Jena, Germany;

[3] Helmholtz-Zentrum Dresden-Rossendorf, Bautzner Landstraße 400, D-01328 Dresden

The interaction of a sub-picosecond, high-intensity laser pulse with a solid target produces high-density plasma on its surface, which is accompanied by the acceleration of electrons to relativistic velocities and heating of the bulk material. The spectroscopic analysis of the K-shell emission of the target, in combination with spatial resolution, is a powerful tool to characterize properties of such highly coupled plasmas in the “warm dense matter” (WDM) regime such as bulk electron temperature and temperature gradients [1]. Furthermore, the transport of the relativistic electrons leads to strong electric and magnetic fields, especially at the interfaces of thin foils. In particular, protons and other ion species are accelerated to MeV energies at the rear side of a thin target due to the so-called ‘target normal sheet acceleration’ mechanism (TNSA). This process is strongly influenced by the target design. For instance, the reduction of the lateral dimensions of the target could lead to a significant enhancement of the TNSA proton energies [2]. Spectroscopic analysis of the X-ray rear side emission provides insight into important properties at the rear surface such as temperature [3]. The aim of the project is to correlate the measurement of the plasma emission to proton emission, and thus gaining a deeper understanding of the underlying processes.

In the reported experiments, the frequency doubled POLARIS laser heated titanium foils with lateral dimensions down to 50 µm. The proton emission was measured with a Thomson parabola. The X-Ray instrumentation included both a K_α imager based on a toroidally bent GaAs crystal, as well as a spectrometer with 1-dimensional spatial resolution. The imager has a magnification of 2.7, a bandwidth of 11 eV and allows for spatial resolution of ~10 µm. The spectrometer is also based on a toroidal GaAs crystal and allows imaging of the Titanium $K_{\alpha1}$ and $K_{\alpha2}$ emission with very high spectral resolution (~10000) and a one-dimensional spatial resolution of 7.5 µm. Both crystals were aligned to image onto different parts of the same in-vacuum CCD camera.

Two typical ‘single-shot’ emission spectra and K_α-images of a 2 µm thick foil and 1µm thick Ti discs with diameter of 100 and 200 µm, illuminated at relativistic intensities, are shown in Figure 1. The images show an inhomogeneous K_α-emission: a homogeneous, but weak emission of the whole disk and a much stronger emission around the interaction point. The 1D-resolved spectra show a small emitting region over the whole spectral range, and extended line emission, which is strongly blue-shifted with respect to the cold $K_{\alpha1}$ and $K_{\alpha2}$ lines (indicated by vertical lines in figure 1) for the disc targets. From this line shift, temperatures of several tens of eV could be deduced by comparison with detailed line shape calculations [4]. This blue shift, and thus bulk temperature, is strongly enhanced for the smaller targets, indicating a more efficient heating of the target by refluxing electrons for size reduced targets. Furthermore, in contrast to foil targets, the blue shift does not vary spatially, showing a homogeneous heating of the targets. The inhomogeneous K_α-images could thus be attributed to strong continuum emission confined to the interaction region, where the hot electron fraction is produced.

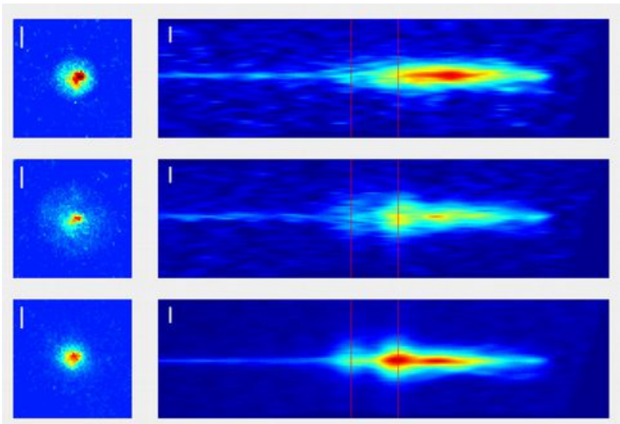

Figure 1: Single-shot K_α image (left) and emission spectrum (right) of a foil target (lower row), a 200 µm large (middle row) and a 100 µm large (lower row) Titanium disk, recorded at the POLARIS laser. (The foil emission is shown in a different colour scale than the disc targets.) The emission spectrum has increasing photon energy from left to right and spatial resolution in the vertical direction. The red vertical lines mark the positions of the cold $K_{\alpha1}$ and $K_{\alpha2}$ lines. The scale bars represent 50 µm.

References

[1] U. Zastrau, et al, Phys. Rev. E 81 (2010), 026406 1-4
[2] S. Buffechoux, et al., PRL 105 (2010), 015005
[3] F.Perez, et al., PRL 104 (2010), 085001
[4] E. Stambulchik, *et al.*, J. Phys. A 42 (2009), 214056

High efficient X-ray optics for spectroscopy of highly charged ions

R. Loetzsch[1,2], B.Grabiger[2], I. Uschmann[1,2] E. Förster[1,2],

[1] Helmholtz-Institut Jena, Fröbelstieg 3, D-07743 Jena, Germany; [2] Institut für Optik und Quantenelektronik, Friedrich-Schiller-Universität Jena, Max-Wien-Platz 1, D-07743 Jena, Germany;

Precision x-ray spectroscopy of highly charged ions at traps and storage rings provides for a unique tests of relativistic and quantum electrodynamical effects in strong electromagnetic fields. The spectral resolution of such experiments is limited to date by the spectral resolution of semiconductor detectors. There are two pathways under investigation to overcome these limits: first by the use of crystal spectrometers [1] and second the use of detectors with higher spectral resolution. Such high-resolution detectors could be microcalorimeter. With these detectors, very high energy resolution in the order of a few eV in the energy range up to 100 keV could be obtained. [2] The drawback is the limited solid angle and thus detection efficiency, which limits the use of these detectors for spectroscopy of weak transitions. To increase the detection efficiency of these devices, collecting X-ray optics can be used. The potential of such crystal optics is investigated. This includes the evaluation of different crystal-optical schemes by simulations and the development of crystal machining techniques, to obtain the desired crystal reflection properties.

Such an optic should have an bandwidth of ~100 eV, should be usable in an wide energy range of some keV in the energy range between 5 and 50 keV, concentrate the reflected photons to a mm sized spot and meet some geometrical constrains emerging from the bulky vacuum systems of both the source and the detector.

Highest collection efficiency of the optic is obtained by maximising the solid angle covered by the optic. In the diffraction direction, this implies the use of mosaic crystals, while the crystal is bent to a full ring in the perpendicular direction. The crystal quality must meet stringent requirements: on the one hand the integrated reflectivity must be as large as possible, on the other hand, the width of the reflection curve must not be too large to avoid aberrations of the optic. The possible crystal materials are pyrolythic graphite (HOPG or HAPG) and lithiumfluoride (LiF). The former is available as large, very flexible sheets with high reflectivity and small reflection curve width, but is expensive. The latter has to be treated by flexing, grinding, heat or pressure to obtain the desired reflection properties, but is cheaper.

In a first step of the project, we thoroughly investigated the concept of such an optic by raytracing simulations to predict optimal geometry and constrain the requirements on the crystal quality. This lead to the design of an optic, optimized for the energy range between 7 and 12.5 keV. The optic comprises a toroidal shape with 53 and 720 mm bending radii, respectively, and is made from 100 µmthick highly annealed pyrolythic graphite (HAPG) crystals on a diamond turned aluminium mould. We extensively tested the optic in terms of reflection properties of the crystal, reflection homogeneity, focus size and collection efficiency in a wide energy range (see figure 1). [3]

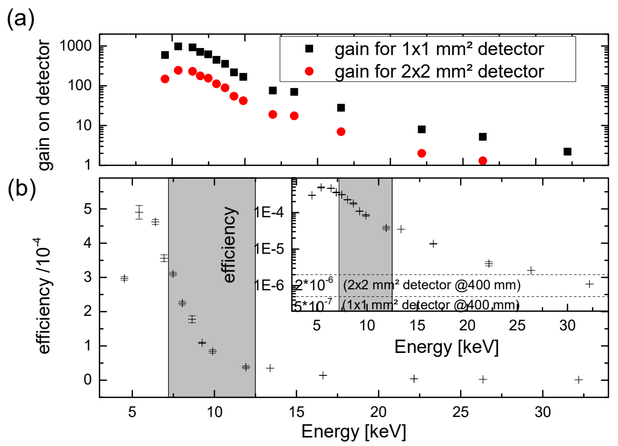

Figure 1: (b) Measured collection efficiency of the optic. The inset shows the same on a logarithmic scale. The solid angle of a 1 by 1 and a 2 by 2 mm detector, respectively, at a distance of 400mm from the source is also shown for comparison. The grey areas mark the designated energy range of the optic. (a) shows the increase of photon flux on the detector as compared to no optic.

The focus of the optic is well below 1 mm in the whole energy range, fitting to the size of microcalorimetric detectors. The gain of photon flux by using the optic is in the range between 670 (170) and 70 (16) for the 1×1 and 2×2mm detector, respectively, in the energy range between 7 and 12 keV. This shows clearly the potential of such an optic in the investigation of weak transitions.

In a further step, we want to increase the efficiency of such an optic at higher photon energies, where LiF crystals could become superior to graphite. A first LiF optic was build, which has very promising collection efficiency of $3*10^{-5}$ at 20 keV, but still rather large aberrations. These aberrations will be reduced in future by optimizing the optical scheme.

References

[1] H. Beyer, et al, Spectr. Acta Part B: 59 (2004), 1535
[2] V. Andrianov, et al., Journal. of Low Temperature.Physics 151, 1049 (2008)
[3] R. Loetzsch, I. Uschmann, E.Förster, and G.G. Paulus, to be submitted.

X-ray emission from nanostructured surfaces irradiated by intense ultrashort laser pulses

Z. Samsonova[1,2], E. Förster[1,2], R. Hollinger[1], S. Höfer[2], D. Kartashov[1], T. Kämpfer[1], D. Khaghani[3], P. Neumayer[3], C. Ronning[4], O. Rosmej[3], R. Röder[4], C. Spielmann[1,2,#], Th. Stöhlker[1,2,3], L. Trefflich[4] , I. Uschmann[1,2],

[1] Institute for Optics and Quantum Electronics, FSU Jena, Germany; [2]Helmholtz Institute Jena, Germany; [3] GSI Darmstadt, Germany; [4] Institute for Solid State Physics, FSU Jena, Germany

In this report we present results in experimental investigation of interaction of nanostructured solid targets with moderate energy and intensity ultrashort laser pulses (several mJ and ~10^{17} W/cm^2) and relativistically intense, high energy laser pulses.

Experiments were performed with two morphologically different types of samples. The first type, the "grass" samples, is a disordered array of single crystalline nanowires with diameters of ≈150 nm, average spacing of about 200 nm and lengths of several microns, arranged vertically on a sputtered <100 μm thick ZnO:Al layer deposited on a 500 μm silicon wafer (Fig.1a). The second type, the "spaghetti" sample, represents a pile of nanowires with the parameters close to the grass-sample, but chaotically arranged along the surface (Fig.1b). For comparison, a polished 300 μm thick crystalline ZnO plate was used as a reference target.

Experiments in moderate intensity regime were conducted at a 1 kHz, 804 nm wavelength femtosecond laser system delivering 55 fs pulses with up to 3.5 mJ energy and operating in a single shot mode. The beam was focused by an off-axis parabolic mirror under 41° angle on the target surface providing the peak intensity of about 10^{17} W/cm^2. The target was placed in a vacuum chamber pumped down to 10^{-4} mbar. Spectral diagnostic of the emission was conducted in air after the emission was passing through a 50 μm thick kapton window.

Spectra of the generated X-ray emission were measured with two bent crystal spectrometers based on toroidal SiO_2 10-1 and cylindrical LiF 220 crystals, using cooled back-illuminated X-ray CCD cameras as detectors. To detect higher energy quanta, Timepix detector capable measuring photon energies up to 1 MeV was used.

The X-ray spectra of emission detected by the Timepix detector are presented in Fig.1. The measured hard X-ray spectrum reaches the border of the detector sensitivity and a flux enhancement of more than one order of magnitude in the region above 100 keV is registered. The efficiency

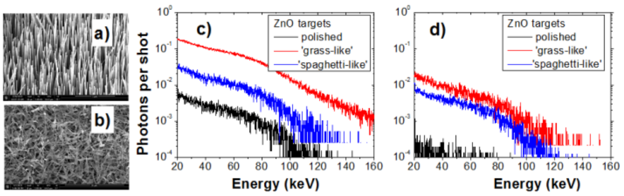

Fig.1: SEM images of the a) "grass" and b) "spaghetti" sample. Hard X-ray spectra from the polished, "grass" and "spaghetti" samples for c) p-polarized and d) s-polarized laser beam.

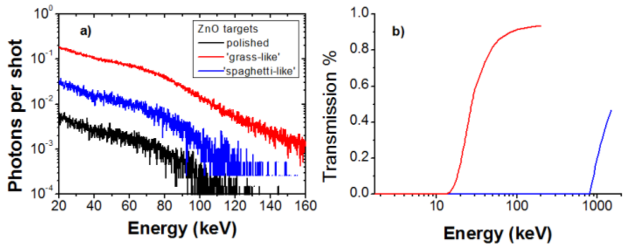

Fig.2: a) Hot counts detected by XCCD camera from the polished, "grass" and "spaghetti" samples for p-polarized laser beam. The energy scale does not correspond to reality because the detector is not calibrated for measuring energetic electrons. b) Transmission of a 3 mm thick Al plate for X-ray and electrons.

depends on laser polarization (Fig.1c,d), suggesting that the Brunel mechanism of electron heating might be involved. The CCD detector in the high-resolution spectrometer near the output window has detected not only Kα and Kβ lines (not shown) but also large amount of hot counts. By placing a 3mm thick Al plate in front of the kapton window we verified that these counts resemble flux of relativistic electrons (Fig.2), which is more than two orders of magnitude higher for nanostructured targets than for the polished sample.

Experiments for relativistic regime of interaction were conducted using 45 fs, 130 mJ laser pulses at 400 nm wavelength. The beam was focused by an off-axis parabolic mirror close to normal incidence on a target providing the peak intensity of 2.7×10^{19} W/cm^2. The observed characteristic transition lines in the spectral energy region 8.7-9.0 keV demonstrate generation of highly charged ionic states of Zn up to He-like Zn^{+28} from both nanostructured and polished samples (Fig.3). Remarkably, the observed K_α emission from Zn^{+28} generated in nanostructured target has almost the same intensity as the K_α emission from neutral Zn, pointing on the possibility to achieve very high density of highly charged plasma.

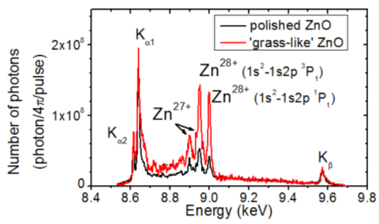

Fig.3: Calibrated spectra of X-ray emission obtained from a "grass like" (red solid line) and polished (black dashed line) targets.

Many-electron projectile stripping cross section studies at the ESR gas target*

G. Weber[1,2], *M. O. Herdrich*[2,3], *R. D. DuBois*[4], *P.-M. Hillenbrand*[1,5], *S. Sanjari*[1,7], *D. F. A. Winters*[1], *N. Petridis*[1,6], *and Th. Stöhlker*[1,2,3]

[1]GSI, Darmstadt, Germany; [2]HI-Jena, Germany; [3]IOQ, Univ. Jena, Germany; [4]Missouri S&T, Rolla, MO, USA; [5]IAMP, Univ. Giessen, Germany; [6]IKF, Univ. Frankfurt, Germany; [7]EMMI, Darmstadt, Germany

Charge-changing processes, i. e. loss or capture of electrons, occurring in ion-atom and ion-ion collisions belong to the most basic interactions in all types of plasmas. Moreover, in accelerators interactions between projectile ions and the residual gas can lead to a change of the projectile charge state. In the presence of dispersive ion optical elements, the trajectories of up- or down-charged ions do not match the one of the reference charge state, resulting in a successive defocussing and, as a consequence, loss of beam intensity. Moreover, ions impinging on the beam line walls give rise to several unwanted effects, such as increased radiation levels and significant degraded vacuum conditions due to ion-impact induced desorption. For the FAIR project, in order to reach highest beam intensities, while minimizing the limitations induced by space charge, and avoiding losses in stripper targets, the use of low- to medium-charged, many-electron ions is planned [1]. However, in the relevant energy region from 10 MeV/u up to a few GeV/u the number of bound electrons of these ions is far above that of the corresponding equilibrium charge state, making projectile stripping, sometimes also referred to as electron loss, the dominant beam loss process. Thus, for the planning of future accelerators and ion beam experiments, precise knowledge of the stripping cross sections of many-electron projectiles is necessary. As the theoretical treatment of such many-body atomic physics problems is quite challenging, experimental benchmarks are needed to test the various predictions of different theory models [2].

Recently, two electron loss studies covering beam energies up to 50 MeV/u for U^{28+} ions was presented [3,4]. We now report on a follow-up experiment using again U^{73+} projectiles which was performed at a higher beam energy of 150 MeV/u at the ESR gas target and covering a broad range of the target atomic number Z. After injecting the beam into the ESR the ions were stored and electron cooling was applied. After a few seconds, when stable beam conditions were reached, the shutter of the internal gas target was opened and a gas jet being perpendicular to the ion beam axis was formed inside the interaction chamber of the ESR. Up- or down-charged ions produced in interactions with the target were subsequently lost due to collisions with the beam line walls or dedicated scrapers after passing the bending magnets. N_2, Ar, Kr, and Xe were used as target gases with densities between a few times 10^9 and a few times 10^{11} particles/cm^3. The beam lifetime, which is dominated by the electron loss cross section (i. e. projectile ionization), was deduced from measuring the ion beam intensity as a function of time using a DC current transformer (DCCT) and the integrated Schottky signal of the new resonant pickup.

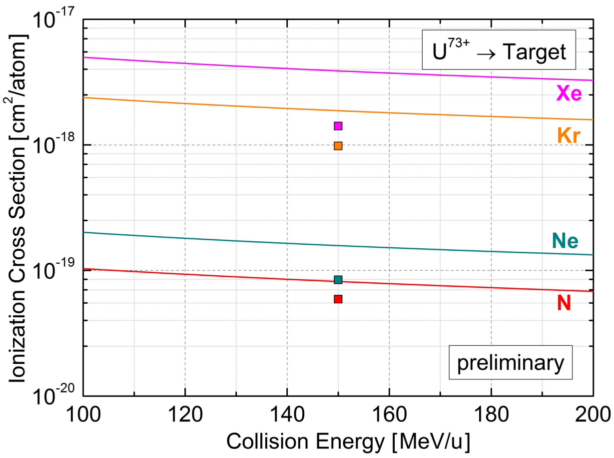

Figure 1: Preliminary: Compilation of the total electron-loss cross section for U^{73+} ions in collisions with various target gases.

A detailed analysis of the obtained data in order to extract the projectile electron loss cross section for the various target gases has been performed. Preliminary results are shown in Fig. 1 together with theoretical predictions by V. P. Shevelko et al. [5]. As already found in previous studies, the electron loss in collisions with heavy targets is significantly overestimated by theory. This issue will be discussed in detail in an upcoming publication.

References

[1] FAIR - Baseline Technical Report (2006)

[2] V. P. Shevelko et al., *Electron Loss and Capture Processes in Collisions of Heavy Many-Electron Ions with Neutral Atoms*, in: Atomic Processes in Basic and Applied Physics **68**, 125-152, Springer (2012)

[3] G. Weber et al., Phys. Rev. ST AB **12**, 084201 (2009)

[4] G. Weber et al., Phys. Rev. ST AB **18**, 034403 (2015)

[5] V. P. Shevelko, private communication (2015)

* Work supported by the Alliance Program of the Helmholtz Association (HA216/EMMI) and by HIC-for-FAIR through HGS-HIRe and Helmholtz-CAS Joint Research Group HCJRG-108. This report is also part of the GSI Scientific Report 2015 DOI:10.15120/GR-2016-1

Strong field ionization of the He^{+}-ion

P. Wustelt[1,2]*, M.Möller*[1,2]*, T. Rathje*[1,2]*, A.M. Sayler*[1,2]*, S. Trotsenko*[1]*, T. Stöhlker*[1,2]*, and G.G. Paulus*[1,2]
[1]Helmholtz Institute Jena, Germany; [2]Institute of Optics and Quantum Electronics, Jena, Germany

Ionization of atoms by intensive laser pulses is essential for all strong-field phenomena like above-threshold ionization, high harmonic generation, laser-based electron or ion acceleration. There exists several theoretical approaches to gain insight in these phenomena. Since the required intensities for the investigation of these processes exceed the order of PW/cm^2, perturbation theory for the treatment of atomic processes is not possible.

The most desirable theoretical approach is the numerical ab-initio solution of the time-dependent Schrödinger equation (TDSE). Despite of the rapid increase in computing power during the last decade the full integration of the TDSE demands enormous computational resources for intensities high enough to ionize ions and for mid-IR wavelengths. One therefore has to restrict oneself to classical or semi-classical methods. In the simplest case, the classical equations of motion are integrated in order to gain insight in the involved processes. However, it is necessary to prove and validate the different methods among themselves and in comparison to highly accurate measurements.

The most fundamental benchmark systems in the theoretical description of matter are single electron systems, in particular the hydrogen atom. In order to be able to use very high intensities without premature ionization, the use of hydrogen-like ions, in the simplest case the single charged He atom, is advantageous. We have performed a series of experiments where the strong-field ionization of the He^{+}-ion in linearly and elliptically polarized laser fields is probed by measuring the momentum distribution (see Fig.1).

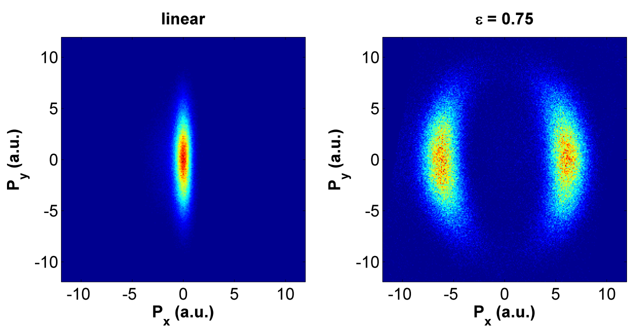

Figure 1: Measured ion momentum distribution of He^{2+}: with linearly polarized laser fields (left) and with elliptically polarized laser fields (right).

Experimentally, the recently developed ion beam apparatus is used together with a high-power high-repetition rate laser system that delivers 10-mJ, 35-fs laser pulses. The ion beam is produced by a duoplasmatron ion source, a radio frequency ion source or an EBIT (electron beam ion trap). The ion beam is accelerated to several keV and guided through a series of Einzel lenses, a Wien filter, deflectors and pinholes. After the laser matter interaction, the full three dimensional momentum distribution of the resulting fragments are measured with a position- and time-sensitive detector.

Status of the project: The momentum and charge state distributions of ions resulting from the ionization of singly charged Xenon, Neon and Helium are studied as a function of intensity and ellipticity of the laser pulses. Peak intensities up to $6{\cdot}10^{16}$ W/cm^2 allow the observation of highly charged ions up to Xe^{8+}, Ne^{5+} and He^{2+}. In Fig.2 the measured intensity dependence of the momentum spectra of the He^{2+}-ion is shown. At very high intensities a distinct saturation behavior of the momentum can be observed, which is explained by depletion of the ground state of the single charged Helium ion. This implies that the saturation intensity of He^{+} was reached in the experiment [1]. The results are compared to predictions from different theoretical methods of tunneling theory. Calibration of these theories in comparison with the measurements based the on single-active-electron dynamics plays an important role in the understanding of ionization in multi electron systems.

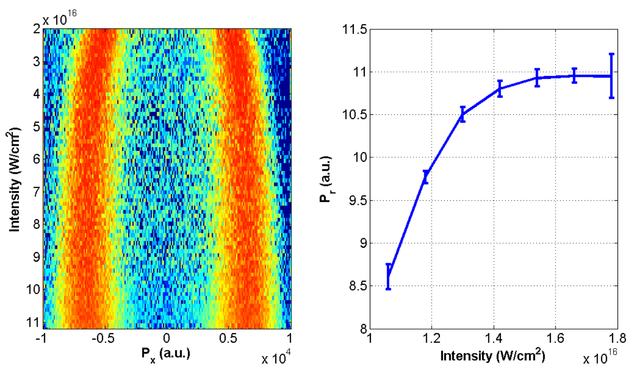

Figure 2: Intensity dependence of the momentum parallel to the minor polarization axis (left) and fit result for the mean radial momentum in ellipticity corrected polar coordinates (right) for different intensities.

References

[1] P. Wustelt, M. Möller, T. Rathje, A. M. Sayler, T. Stöhlker, and G. G. Paulus, *Phys. Rev. A* **91**, 031401(R) (2015)

Cryogenic Current Comparator for Storage Rings and Accelerators*

J. Golm [1,2], R. Geithner[1,4], R. Neubert[2], V. Tympel[2], F. Kurian[1,3], T. Sieber[3], M. Schwickert[3], P. Seidel[2], and T. Stöhlker[1,3,4]

[1]Helmholtz-Institute Jena, Jena, Germany; [2] Institute of Solid State Physics FSU, Jena, Germany
[3]GSI, Darmstadt, Germany; [4] Institute for Optics and Quantum Electronics FSU, Jena, Germany

The First Cryogenic Current Comparator (CCC) for a non-destructive highly sensitive monitoring of nA-beams was developed in the 90s. In recent years this system was optimized for lowest possible noise-limited current resolution in combination with a high system bandwidth of about 200 kHz. This improved CCC consists of commercial state-of-the-art SQUID components, niobium shielding and a toroidal niobium pick-up coil with nanocrystalline NANOPERM® core material [1].

The existing CCC has been installed and tested in the Antiproton Decelerator (AD) at CERN in cooperation with GSI, HIJ and Friedrich-Schiller-University Jena, to measure the low-intensity coasting beam. Modifications were required for this implementation in order to adapt the AD beam parameters. The signal slew rate during AD injection exceeds the slew rate of CCC-system because the current suddenly jumps from 0 to $\approx 12\ \mu$A. To solve this problem a low pass filter was inserted between the pick-up coil and the primary coil of the matching transformer [2].

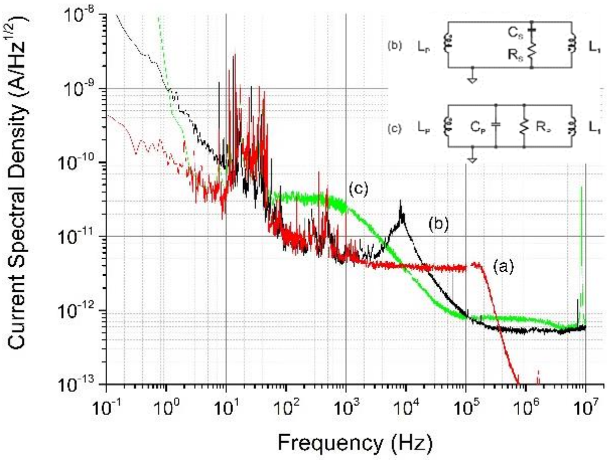

Figure 1: Current noise of the CCC in the original configuration without filtering in the input circuit (a), with serial connection of R_S and C_S (b), and with parallel connection of R_P and C_P (c) between the pick-up coil L_P = 104 µH and the primary coil L_1 = 104 µH of the matching transformer.

The different tested setups and the corresponding noise spectra are shown in Figure 1. From the first serial setup of resistor and capacitance follows an additional noise contribution around the resonant peak. This is the reason why a parallel connection of resistor and capacitance was chosen for the final setup at AD. The setup is more stable and fulfils the required bandwidth of 1000 Hz but it also yields an additional noise contribution [2].

Figure 2 shows a beam commissioning cycle measured successfully with the CCC. It is important to find the machine parameters where the particles can travel through the ring without interaction. Particles which hit the wall are lost for the beam. During the measurement shown here the beam got entirely lost during the first cooling plateau (time span ~45 – 80 s). This moment is clearly visible in the measurement and confirms that the CCC can be an important tool for beam measurements [3].

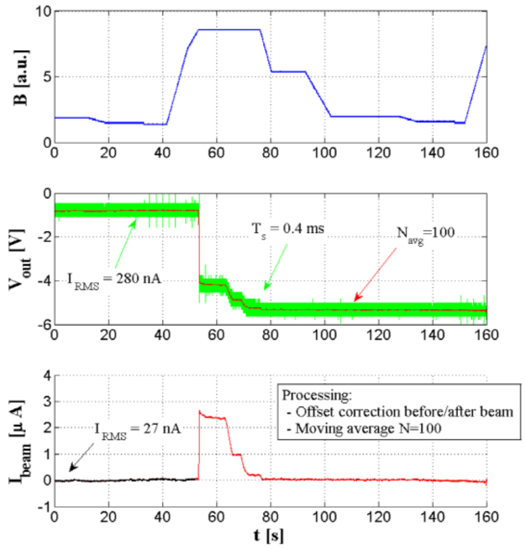

Figure 2: Top Plot: Magnetic Cycle of AD Dipoles in arbitrary Units. Middle plot: SQUID/FLL raw signal of beam current (in green), and same signal filtered with a moving average (in red). Bottom plot: calibrated beam current measurement after filtering and baseline recovery (before beam injection and after beam extraction) [3].

Within the FAIR project (Facility for Antiproton and Ion Research) an improved SQUID-based CCC is intended to be used as diagnosis device for ion beams. In July 2015 a three-year BMBF joint project (development, sensor optimization and test of cryogenic current comparators for use on novel ion sources, accelerator systems and storage rings) with Friedrich Schiller University Jena, GSI Darmstadt, Leibniz Institute of Photonic Technology Jena and TU Darmstadt started.

References

[1] R. Geithner et al., Phys. Scr. T166 014057, (2015)
[2] R. Geithner et al., Proc. IBIC 2015, Melbourne, Australia. MOPB013, (2015).
[3] M. Fernandes et al., Proc. IBIC 2015, Melbourne, Australia. WEPF04, (2015).

* Report also published in annual reports of [2,4]

S-EBIT facility: Status Report*

S. Trotsenko[1,2], N. Bauer[2], W. Chen[2], J. Menssen[1,2,3], G. Vorobjev[2], D. Racano[2], A. Gumberidze[2,4], C. Kozhuharov[2], S. Purushothaman[2], F. Herfurth[2], R. Schuch[6], and Th. Stöhlker[1,2,4,5]

[1]Helmholtz-Institut Jena, D-07743 Jena, Germany; [2]GSI Helmholtzzentrum für Schwerionenforschung, D-64291 Darmstadt, Germany; [3]Hochschule Rhein Main, University of Applied Sciences, D-65428 Rüsselsheim, Germany; [4]ExtreMe Matter Institute EMMI, D-64291 Darmstadt, Germany; [5]Friedrich-Schiller-Universität Jena, D-07743 Jena, Germany; [6]Department of Physics, Stockholm University, SE-10691 Stockholm, Sweden

One of the goals of Helmholtz Institute Jena with respect to the Facility for Antiproton and Ion Research is to provide highly-charged, low-energy ions by using the S-EBIT facility currently being installed at GSI [1]. This is of particular importance during the FAIR construction related shutdown period of the GSI accelerator complex, when little to no beam time can be provided. During this period the S-EBIT shall facilitate research and development works for SPARC experiments at FAIR. This accelerator-independent source of HCI will not only provide ions necessary for R&D of HITRAP [2] experimental stations but also serve as a standalone device for research and R&D activities (e.g. development of x-ray spectrometers, calorimeter detectors, x-ray optics etc. [3]). Furthermore, the combination of S-EBIT with the available laser infrastructure e.g. JETI200 will be a unique platform for the study of highly charged ions subject to intense laser radiation [4] as it is planned at a later stage once the S-EBIT facility has been moved to Jena.

Currently, for the S-EBIT facility, two independent setups are being built: EBIT-I and EBIT-II. The first one, represents an EBIT with electron energies of up to 40keV (and ~150mA), and thus in combination with the 3T magnet it will be able to efficiently produce highly-charged ions with the charge state of up to Th^{80+}. In the case of the second EBIT, main efforts are concentrated on constructing the system able to provide electrons with highest possible energy, up to 260keV, and few hundreds mA, which in combination with 4T magnet shall produce high-Z HCI, up to bare uranium. Both EBITs will not only serve as sources of HCI but also work in a standalone operation.

The construction of the EBIT-I has been accomplished. A brand-new vacuum interlock system has been built in order to enable the EBIT to be connected to the GSI vacuum system, which would be necessary for the experiments that require extraction of the produced ions towards the HITRAP experiments. The vacuum and cryogenic tests of the system have been successfully carried out. The superconducting magnet was powered up with 60A, thus providing the magnetic field in the trap region of 3T. The high-voltage line has been built up and the first test of the system has been performed, where the voltage of 20kV (limited by the HV-supply) has been applied to the drift tubes. The supplies for the electron gun (cathode filament, bucking magnet, anode- and focus-electrode) as well as for the electron collector parts have been tested. The work on conditioning the e-gun is currently on-going; so far it has been possible to reach 3mA electron current.

The EBIT-II was equipped with the new superconducting magnet, designed to provide magnetic fields of up to 4T as well as the newly constructed drift tubes. The new shielding to separate the 4K SC-magnet from the room temperature EBIT chamber has been manufactured hosting the temperature sinking couplings for the SC-magnet current leads. The first vacuum and cryogenic tests were successfully carried out. The current leads of the SC-magnet have been optimized to minimize heat load of the system. The preparation for the first magnet test is ongoing. A new bucking coil for the electron gun has been manufactured. The new high-voltage feedthrough system for ramping the trap is currently being constructed. The vacuum system is being modified for coupling with the GSI (HITRAP) beamline.

References

[1] R. Schuch et al., JINST5, C12018 (2010)
[2] F. Herfurth et al., Phys. Scr. T166, 014065 (2015)
[3] D. Hengstler et al., Phys. Scr. T166, 014054 (2015)
[4] M. Vogel et al., Nucl. Instr. Meth. B 285, 65 (2012)

*Also a part of the GSI Scientific Report 2015, DOI:10.15120/GR-2016-1

Status of the HILITE Penning trap experiment*

M. Vogel[1], *N. Stallkamp*[1,4], *S. Ringleb*[3], *W. Quint*[1,2], *G. Paulus*[3], *and Th. Stöhlker*[1,3,4]
[1]GSI, Darmstadt; [2]Ruprecht Karls-Universität Heidelberg; [3]Universität Jena; [4]Helmholtz-Institut Jena

We are currently devising a dedicated Penning trap setup for the preparation of ion targets irradiated with high-intensity laser light, and the study of subsequent reactions. Of particular interest is the detailed investigation of multiphoton-ionisation by highly intense laser light. The central function of the setup is to provide control of the confined particles species, its density, localization and optimized overlap with the laser light. Also, the non-destructive detection of reaction products is a central property. Details on the physics case have been given in [1].

We have brought forward the functionality of the setup by building the Penning trap [2], its mounting to the cryostat, the thermal shielding and a pulsed drift tube for deceleration of externally produced ions. Measurements have shown that the required temperatures of 4 K at the trap and 45 K at the thermal shielding are indeed reached. We have performed simulations showing that ions from external sources can be decelerated in our setup from energies up to 5 keV per charge and captured in the trap with high efficiency. The components of the deceleration system have been built, together with a destructive ion detection system for testing the setup functionality, and the components for incoupling of the laser and dumping of the residual laser pulse [3]. Also, we have designed and built a non-destructive ion detection system by signal pick-up in the Penning trap with a radio-frequency resonator as seen in figure 2.

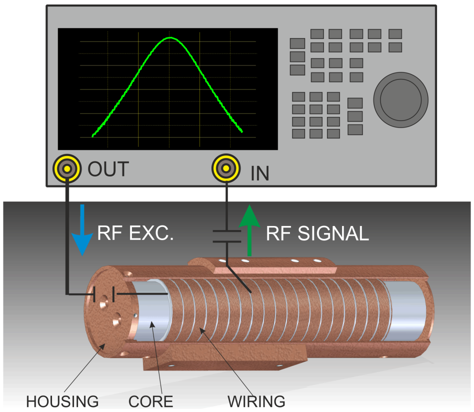

Figure 1: Schematic of the resonator.

We have equipped the system with a cryostat that allows the cooling of probes in the centre of the magnetic field to a temperature of 4 Kelvin, see the schematic in figure 1. The magnet is capable of producing well-defined field strengths of up to 6 Tesla. We have installed a control system based on LabView which allows to scan the field strength at a given rate. We have used this to measure the behaviour of a superconducting resonator in strong magnetic fields. The measurements have given valuable information on the dependence of the resonator signal on the magnetic field strength, see figure 3, which is of interest to a multitude of Penning trap experiments which feature such resonators.

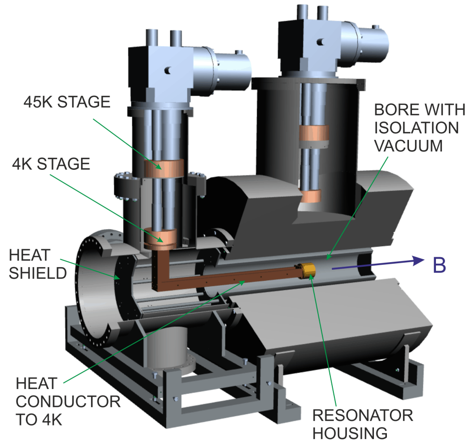

Figure 2: Resonator located in the centre of the magnet

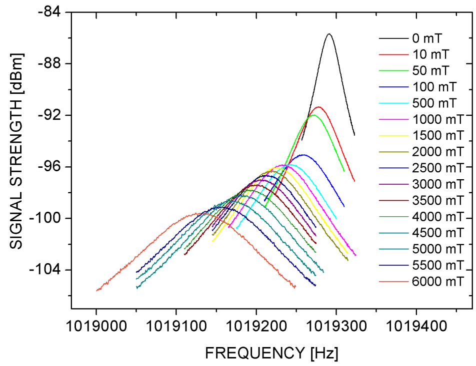

Figure 3: Resonator signal vs. magnetic field strength.

References

[1] M. Vogel, W. Quint, Th. Stöhlker and G.G. Paulus, Nucl. Inst. Meth. B **285**, 65 (2012)

[2] S. Kumar, M. Vogel, W. Quint, S. Ringleb, Th. Stöhlker, C.P. Safvan, Journal of Physics Conference Series **635** (2015) 092070

[3] S. Ringleb, M. Vogel, S. Kumar, W. Quint, G. Paulus, Th. Stöhlker, Journal of Physics Conference Series **635** (2015) 092124

*This report is also part of the GSI Scientific Report 2015 DOI:10.15120/GR-2016-1

Preparing first experimental installations at CRYRING@ESR*

M. Lestinsky[† 1], *A. Bräuning-Demian*[1], *F. Herfurth*[1], *S. Schippers*[2], *R. Schuch*[3], *Th. Stöhlker*[1,4], *and the SPARC collaboration*[1]

[1]GSI, Darmstadt, Germany; [2]JLU Gießen, Germany; [3]Stockholm University, Sweden; [4]HI Jena, Germany

CRYRING@ESR is a new heavy ion storage ring facility at GSI/FAIR and is presently under construction [1-4]. The former Swedish CRYRING is presently refitted and adapted to its new location. Commissioning of ring operation will soon start. CRYRING@ESR will be able to store all classes of ions available at ESR but at much lower ion energies. Moreover, it features excellent vacuum conditions for the storage of the highest charge states. CRYRING was conceived as a synchrotron, thus stored ions may be de- and accelerated internally to energies between ~ 0.05 and 15 MeV/u. The research collaborations SPARC, FLAIR, and NuSTAR have formulated extensive research programmes for this facility [5]. Ion-storage at low energies is ideally suited for precision spectroscopy and thus allows one, e.g., to test non-perturbative strong field QED terms, or to study transient quasi-molecular systems. Furthermore, at the border between atomic and nuclear physics, nuclear size effects, hyperfine interactions or exotic couplings between the electronic shell and the nucleus of an ion may be explored. In nuclear physics, storage of bare nuclei at low energies permits to determine fragment distributions unmasked by atomic physics. Under these conditions, e.g., nuclear reactions at the Coulomb barrier or the nucleosynthesis of heavy elements in the Gamow window of the p-process may be analyzed.

The construction is rapidly advancing, see Figure 1 for an impression of the present project status. In particular, all ring sections have been installed and the precision alignment of ion-optically active elements is currently underway. Media installations have been completed. A small ion source and a RFQ accelerator were installed as a local injector system for independent test operation of CRYRING@ESR. This injector has been commissioned and a H_2^+ beam could be accelerated to 300 keV/u [6].

In order to prepare a first generation of experiments at CRYRING@ESR, the German APPA R&D collaboration has applied for and received substantial funding within the BMBF Verbundforschung scheme [7]. An accompanying TDR for planned experimental instrumentation was drafted in parallel and has been accepted recently [8]. This instrumentation comprises various installations for a wide range of atomic physics experiments: Electron-ion collision spectroscopy with high-resolution at the electron cooler or at a high-density transverse electron target for high energies, laser spectroscopy, as well as energy-resolved determination of target radiation from the visible to the vacuum ultraviolet (VUV) regime. A number of experimental infrastructure measures were addressed as well: Particle detector mounts, and a precision voltage divider for an accurate determination of the ion velocity under cooling conditions. The current BMBF funding period runs from 2015–2018 and fits to the present timeline for the FAIR construction, which foresees a major shutdown of the GSI accelerator infrastructure after summer 2016 until early 2018. In this situation, the local injector at CRYRING@ESR is extremely valuable, as it allows for testing and optimizing of the new experimental infrastructure. This will be decisive for ensuring that the experiments at CRYRING@ESR will be ready when the GSI accelerator facility resumes operation.

Figure 1: The CRYRING construction area in Dec. 2015.

References

[1] http://www.gsi.de/cryring/

[2] H. Danared, et al., "Technical Design Report: LSR - Low-energy Storage Ring", 2011, Manne-Siegbahn-Laboratory, Stockholm University

[3] M. Lestinsky, et al., "CRYRING@ESR: A study group report", 2012, GSI Darmstadt

[4] M. Lestinsky, et al., "CRYRING@ESR: Present Status and Future Research", 2015, Phys. Scr. T166, p. 014075

[5] M. Lestinsky, et al., "Physics book: CRYRING@ESR", in preparation.

[6] F. Herfurth, et al., "The status of the CRYRING@ESR project", GSI annual report 2015, GSI Darmstadt, in print.

[7] http://appa-rd.fair-center.eu

[8] Z. Andelkovic, et al. and the SPARC collaboration, "Technical Design Report: Experimental Instrumentation of CRYRING@ESR", 2015, FAIR Darmstadt

* CRYRING@ESR is supported by GSI, HI Jena, Stockholm Univ., Jagiellonian Univ. Kraków, and BMBF Verbundforschung under various contracts.

† m.lestinsky@gsi.de

Geometrical characterization of a position-sensitive germanium detector *

T. Gassner[1,2,3], *H.F. Beyer*[3], *and U. Spillmann*[3]
[1]Helmholtz Institute Jena, Germany; [2]IOQ Jena, Germany; [3]GSI, Darmstadt, Germany

The FOCAL experiment is an ambitious x-ray crystal spectrometer project aiming for an accurate determination of the 1s Lamb shift in highly charged heavy ions, like hydrogen-like (H-like) gold Au^{79+} [1, 2]. The ions are provided by the accelerator chain of the GSI Helmholtz Centre and stored in the experiment storage ring ESR. In the ESR the ion beam can be overlapped with a supersonic gas-jet target, acting as a quasi-free electron source for the ions which may capture target electrons into an excited state during a collisional process. In the de-excitation of the ions numerous x rays are emitted and may be detected by the position sensitive semiconductor detectors of the observing FOCAL spectrometer. Since the measurement principle of a crystal spectrometer is of geometrical nature, all relevant dimensions having an influence on the final result have to be accurately specified. One of the last remaining unknowns of the assembly is the actual position of the semiconductor crystal inside the housing of the position sensitive x-ray detector [3]. For its determination a dedicated measurement campaign has been conducted at the European Synchrotron Radiation Facility ESRF in Grenoble, France, where an intense and narrow x-ray beam can be provided. The measurement made use of the fact that the anode of the semiconductor crystal is segmented into 48 vertical strips, where each strip acts as an independent x-ray detector. In the experimental hutch the detector was mounted on a horizontally movable platform facing directly the x-ray beam coming from the synchrotron. In fine steps the detector was moved horizontally while at the same time the count rate of an arbitrarily chosen vertical strip was recorded. The count rate was zero if the x-ray beam missed the selected strip (see red data points in figure 1). As soon as the beam started to intersect with the strip, the count rate increased until the whole footprint of the beam was inside the strip dimensions. The count rate did not change while the beam was moved completely inside the strip leading to a plateau like region. After reaching the opposing boundary of the strip the count rate started to fall again until the beam completely left the strip. To determine the centre of the peaking distribution a model function was fitted onto the data points. Since both, the response function of a strip as well as the x-ray beam profile, are well described by a rectangular function, the convolution of two rectangular functions, which is a trapezoidal function, was used as fitting model (blue curve in figure 1). To relate the local coordinate system of the x-ray beam position with the outer fiducial mark, also used during the original assembly procedure, a sheet of photosensitive paper, which darkens when being irradiated, had been attached to the detector front. After being irradiated for a while an optical telescope with cross hairs was justified onto the dark spot and the distance to the fiducial mark was measured be moving the detector with the aid of the platform and noting the covered distance. This optical alignment procedure was afflicted with an uncertainty of approximately 0.3 mm, which is the only limiting factor for this kind of position determination. With this measurement the last remaining geometrical unknown of the FOCAL assembly could be determined, resulting in a completely defined system for precision x-ray spectroscopic investigations.

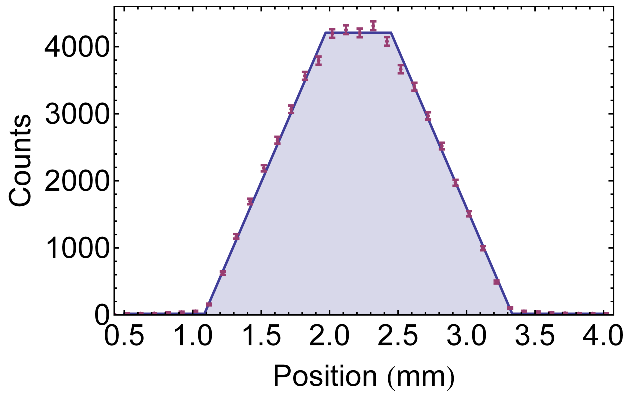

Figure 1: *Red points:* Number of triggered x-ray events in an arbitrary strip of the segmented x-ray detector as a function of position. *Blue curve:* Best fit of a trapezoidal function onto the data points, used to extract the barycentre.

References

[1] H.F. Beyer *et al.*, *Crystal optics for precision x-ray spectroscopy on highly charged ions - conception and proof*, Journal of Physics B: Atomic, Molecular and Optical Physics **48**, p. 144010 (2015)

[2] H.F. Beyer *et al.*, *Crystal optics for hard-X-ray spectroscopy of highly charged ions*, Spectrochimica Acta Part B: Atomic Spectroscopy **64**, p. 736 – 743 (2009)

[3] D. Protić *et al.*, *Two-dimensional microstrip Germanium detector for the spectroscopy of hard X-ray transitions*, IEEE Trans. Nucl. Sci. **52**, p. 319 (2005)

* This report is also part of the GSI Scientific Report 2015 DOI:10.15120/GR-2016-1

The FOCAL crystal spectrometer project

T. Gassner[1,2,3]*, H.F. Beyer*[3]*, and the FOCAL Collaboration*
[1]Helmholtz Institute Jena, Germany; [2]IOQ Jena, Germany; [3]GSI, Darmstadt, Germany

In 1947 Lamb and Retherford conducted an experiment in which they demonstrated that the measured spectrum of the hydrogen atom deviated from theoretical calculations within the framework of relativistic quantum mechanics [1]. This discrepancy in the level energy is nowadays called *Lamb shift* and could only be described by the newly developed quantum electrodynamics (QED) [2]. Modern calculations have shown that the Lamb shift ΔE_{LS} for hydrogen-like ions scale like

$$\Delta E_{\mathrm{LS}} \propto \frac{(Z\alpha)^4}{n^3} F(Z\alpha) \qquad (1)$$

with the nuclear charge Z, the principal quantum number n, the fine structure constant α and a slow varying function of the nuclear charge $F(Z\alpha)$ [3]. Due to the strong dependence of the Lamb shift on the nuclear charge Z it would be desirable to test the predictions of QED in the regime of very strong electric fields like in the case of hydrogen-like gold Au^{78+}.

After several experiments on the 1s Lamb shift, conducted with conventional semiconductor detectors [4], the twin crystal spectrometer FOCAL has been developed [5,6] which is the result of a well balanced trade-off between a high resolving power and detection efficiency. An acceptable efficiency is needed to operate the crystal spectrometer at an ion storage ring with a luminosity which is low compared to other high intensity x-ray sources like synchrotrons or nuclear reactors.

In 2012 a production beam time with the, for the first time fully equipped, FOCAL spectrometer has been conducted at the experiment storage ring ESR at the GSI Helmholtz Centre in Darmstadt, Germany. For the experiment completely ionized gold ions Au^{79+} where produced by the heavy ion synchrotron SIS18 and have been stored for investigation in the ESR at a velocity about half of the speed of light. In the ring the beam was overlapped with a supersonic gas jet leading to collisions between the gas atoms and the stored ions. During a collision it could happen that an ion captures an electron from the gas atom into an excited state which then decays to the ground state by emitting x-ray photons. These photons have been recorded with the FOCAL spectrometer and after three weeks of interruption free beam-on-target operation the spectrum shown in figure 1 could be produced. It features various transitions from excited states to the $1\,s_{1/2}$ ground state as recorded by the position sensitive x-ray detector. The for this experiment most important line is the Lyman-α_1 $2\,p_{3/2} \rightarrow 1\,s_{1/2}$ transition which can be used to conclude on the $1s$ Lamb shift of hydrogen like gold.

In a first analysis the reached precision of the Lyman-α_1 transition energy is well below 3 eV for the uncertainty introduced by the statistics only. However, the uncertainties introduced by several systematic effects [7,8] still pose a challenge to be overcome.

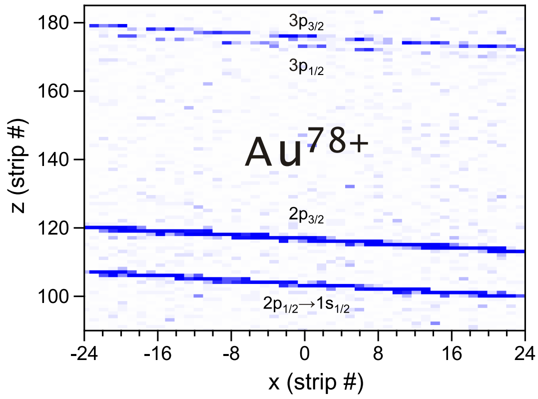

Figure 1: X-ray spectrum of hydrogen-like gold as recorded by a position sensitive detector after being dispersed by the FOCAL crystal. The lines correspond to the Lyman-α and β transitions of excited Au^{78+}.

References

[1] W. Lamb *et al.*, *Fine Structure of the Hydrogen Atom by a Microwave Method*, Phys. Rev. **72**, p. 241-243 (1947)

[2] F. Dyson, *The Radiation Theories of Tomonaga, Schwinger, and Feynman*, Phys. Rev., Am. Phys. Soc. **75**, p. 486 (1949)

[3] V. A. Yerokhin and V. M. Shabaev, *Lamb Shift of n = 1 and n = 2 States of Hydrogen-like Atoms, $1 \leq Z \leq 110$*, Journal of Physical and Chemical Reference Data **44**, p. 033103 (2015)

[4] A. Gumberidze *et al.*, *Quantum Electrodynamics in Strong Electric Fields: The Ground-State Lamb Shift in Hydrogen-like Uranium*, Phys. Rev. Lett. **94**, p. 223001 (2005) and references therein.

[5] H. Beyer *et al.*, *Crystal optics for hard-X-ray spectroscopy of highly charged ions*, Spectrochim. Acta B **64**, p. 736 (2009)

[6] H. Beyer *et al.*, *Crystal optics for precision x-ray spectroscopy on highly charged ions - conception and proof*, Journal of Physics B **48**, p. 144010 (2015)

[7] T. Gassner *et al.*, *Spatial Characterisation of the Internal Gas Target at the ESR for the FOCAL Experiment*, GSI annual report 2014, DOI:10.15120/GR-2015-1

[8] T. Gassner *et al.*, *Geometrical characterization of a position-sensitive germanium detector*, GSI annual report 2015, DOI:10.15120/GR-2016-1

A new high voltage measurement system for the ESR Electron cooler*

Johannes Ullmann[1,2], *Christopher Geppert*[1], *Jörg Krämer*[1], *Johann Meisner*[3], *Rodolfo M. Sánchez*[4], *Matthias Schmidt*[3], *Markus Steck*[4], *Thomas Stöhlker*[2,4], *Wilfried Nörtershäuser*[1]

[1] Institut für Kernphysik, Technische Universität Darmstadt, [2] Helmholtz Institute Jena, [3] Physikalisch-Technische Bundesanstalt, Braunschweig, [4] GSI Helmholtzzentrum für Schwerionenforschung, Darmstadt

In storage rings like the ESR, ions are stored at relativistic velocities. Laser spectroscopy experiments like the LIBELLE[1] experiment need to account for the large Doppler shift of the Laser wavelength in the laboratory frame to the co-moving frame of the ions. This requires a precise knowledge of the ions' velocity. The most precise method for such a velocity determination is a measurement of the electron cooler voltage [1]. A requirement for electron cooling to take place is a low relative velocity of ions and electrons. In equilibrium, which is reached after few seconds of cooling time, the velocities of both beams can be assumed equal. The electrons' velocity is mainly determined by the acceleration potential between the cathode in the electron gun and the grounded drift tubes wherein electrons and ions are superimposed. To obtain the true velocity of the ions, a correction of space charge effects in the electron beam needs to be performed via analytical [2] or experimental methods [3].

The uncertainty of the electron accelerating voltage was large in the past due to insufficient calibration devices for voltages exceeding 130 kV, and remained as the main systematic uncertainty in the previous beamtime [1]. Various failures and damages of the high voltage generator made a precise calibration *ex post* unfeasible. In collaboration with the high-voltage metrology working group of PTB[2], a direct measurement of the electron acceleration potential was possible to an accuracy of 10^{-5} [4] during the complete beam time on hydrogen- and lithium-like bismuth (LIBELLE experiment) in 2014. An additional measurement of residual frequencies in the d.c. high voltage using a ripple probe developed at PTB revealed a very clean high voltage.

Besides the anticipated leap in accuracy, the voltage measurement turned out to be an invaluable diagnosis tool. Instabilities of the ion beam that emerged during beamtime could be identified to originate from a floating drift tube inside the electron cooler, and could be clearly distinguished from instabilities of the high-voltage power supply that also arouse during beam time. The *in situ* measurement allowed to take all voltage fluctuations into account during the analysis. Therefore, a dedicated high voltage measurement system has been acquired for future precision experiments at the ESR. The setup consists of a modular high voltage divider HVS-250 manufactured by Ohm Labs, Inc., specified to a relative accuracy of 100 ppm and a precise digital voltage meter. The readout will be performed with a model 34465A Digital Multimeter by Keysight Technologies, Inc. with a precision of 30 ppm, connected to data acquisition and analysis via Ethernet over optical fiber-based communication.

The divider consists of five identical stages comprising a resistance of 50 MΩ each. The device was calibrated at PTB for voltages up to 250 kV. The divider at first did not meet the specification due to the heating of the internal resistors. The relatively small overall resistance of the divider leads to a power consumption of up to 270 W at a voltage of 250 kV. This was cured by the installation of more powerful fans in the base plate to remove the heat and keep the resistors near ambient temperature, as shown in fig 1. The new high voltage divider will be installed at the ESR during the second quarter of 2016 and will be available for beam time usage.

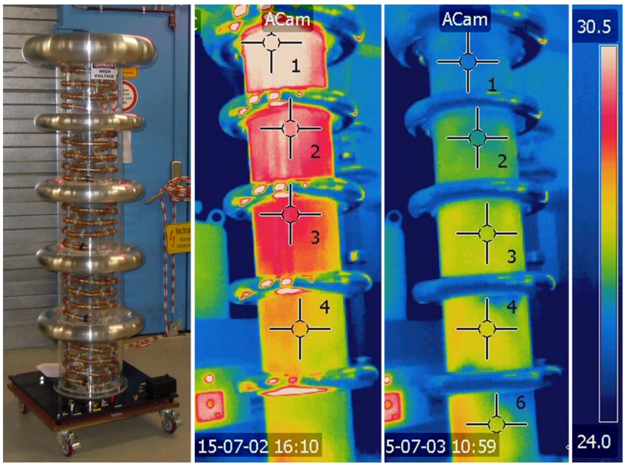

Figure 1: From left: The new Voltage divider HVS-250; infrared image of divider temperature without and with improved cooling at 250 kV. The temperature scale on the right side is shown in °C.

References

[1] M. Lochmann. Ph.D. thesis, Universität Mainz (2013).

[2] H. Winter. Dissertation, Techn. Universität Darmstadt (1999).

[3] J. Ullmann et al. *Journal of Physics B*, **48** (2015), 144022.

[4] J. Hallstrom et al. *IEEE Trans. Instrum. Meas.*, **63** (2014), 2264.

* Work supported by HIC4FAIR, HGS-HIRe, BMBF contract Nos. 05P12PMFAE and 05P12RDFA4.

[1] **Li**thium **l**ike **B**ismuth **E**xperiment with **L**aser **L**ight at **E**SR

[2] Physikalisch Technische Bundesanstalt Braunschweig, the German national metrology institute

An improved Si(Li)-Compton Polarimeter for the SPARC Collaboration

U. Spillmann[1], K.H. Blumenhagen[2,3], T. Krings[4], R. Märtin[2], M. Vockert[2,3], G. Weber[2], and Th. Stöhlker[1,2,3], the SPARC collaboration

[1]GSI, Darmstadt, Germany; [2]HI Jena, Germany; [3]IOQ, Friedrich Schiller Universität Jena, Germany; [4]Semikon Detector GmbH, Jülich, Germany.

The study of particle and photon polarization phenomena occurring in the interaction of fast ion and electron beams with matter is of particular relevance for the understanding of cosmic and laboratory plasmas where high temperatures, high atomic charge-states and high field strengths prevail. In addition, polarization-sensitive studies of radiative processes in highly-charged, heavy ions may provide detailed insights in both relativistic particle dynamics as well as QED effects and other atomic structure properties at extreme electromagnetic field strengths [1]. Moreover, x-ray polarimetry was proposed as a tool for diagnosis of spin-polarized ion beams [2]. Owing to the recent progress in x-ray detector technology, accurate measurements of the linear polarization for hard x-ray photons as well as the determination of the polarization orientation have become possible [3,4,5,6].

Figure 1: The Si(Li)-Compton Polarimeter

To strengthen the instrumentation portfolio in line with the scientific program of SPARC [7] a dedicated Si(Li)-Compton polarimeter was designed and build at Semikon Detector GmbH (see figure 1). It is based on a planar double-sided strip detector (Li-drifted silicon bulk) with a thickness of 9.2 mm. The strip structure was defined with 32 strips on each side with a pitch of 1mm and a length of 32 mm. To achieve a good energy resolution not only the detector crystal itself has a working temperature close to 110 K but also the input stages of the preamplifiers are cooled. Laboratory tests demonstrated a spectroscopic resolution of ~850 eV (p^+-side) and ~1300 eV (HV-side) at a γ-ray energy of 60 keV (Am-241). To demonstrate the homogenous spectroscopic performance the spectra of all strips of the p^+-side irradiated with an Am-241 source are presented in figure 2. The improved resolution of the system compared to our present ones [8] gives us enhanced possibilities for studying atomic transitions at lower energies and lower Z-systems as well as other systems where polarisation transfer can be observed.

To gain best physics performance also at higher x-/γ-ray energies the design of the system foresees a possible upgrade to a telescope system (Compton telescope) by installing a second planar detector (HPGe) behind the Si(Li)-detector. The mechanical design chosen, allows an arbitrary orientation of the detector without loss of LN_2.

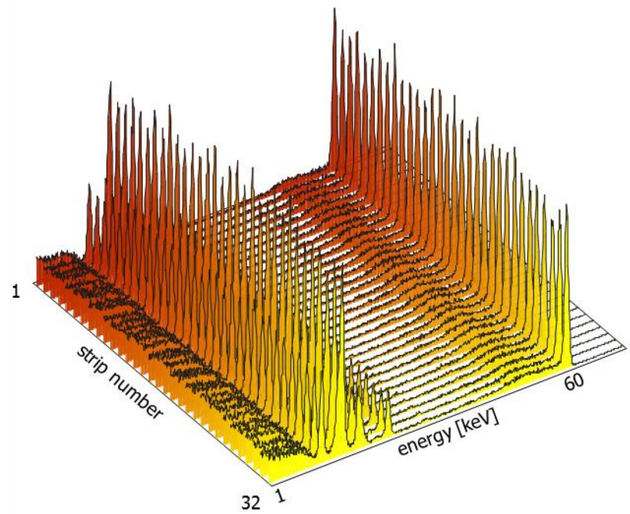

Figure 2: Energy spectra of the x-ray emission of Am-241 detected by the strip structure of the p^+-side of the detector.

References

[1] Th. Stöhlker et al., The European Physical Journal Special Topics **169**, 5 (2009)

[2] A. Bondarevskaya A et al., Physics Reports **507**, 1 (2011)

[3] S. Tashenov et al., Phys. Rev. Lett. **97**, 223202 (2006)

[4] G. Weber et al., Phys. Rev. Lett. **105**, 243002 (2010)

[5] R. Märtin et al., Phys. Rev. Lett. **108**, 26480 (2012)

[6] K.-H. Blumenhagen et al., submitted to Phys. Rev. Lett. (2016)

[7] Technical Report of the SPARC collaboration http://www.gsi.de/fair/experiments/sparc/index_e.html

[8] G. Weber et al., JINST **5**, C07010 (2010)

This report is also part of the GSI Scientific Report 2015
DOI:10.15120/GR-2016-1

Theory

Tunable polarization plasma channel undulator*

S. G. Rykovanov†[1], *J. Wang*[1], *V. Yu. Kharin*[1], *B. Lei*[1], *C.B. Schroeder*[2], *C.G.R. Geddes*[2], *E. Esarey*[2], *and W.P. Leemans*[2]

[1]Helmholtz Institute Jena, Germany; [2]Lawrence Berkeley National Laboratory, USA

Synchrotron radiation produced by the electrons travelling in the magnetic undulators is essential for our understanding of the microcosm. Presently, the lower limit to the undulator period λ_u for magnetic undulators is on the order of 1 cm. Reducing λ_u is highly beneficial as it will decrease the required electron energy for the same specified radiation wavelength. Undulators with periods on the order of a millimeter, are, therefore, of great interest.

Recently, a novel type of the plasma undulator was proposed [1]. It has been shown that the electrons injected into the wakefield created by the laser pulse undergoing centroid oscillations inside a parabolic plasma channel, wiggle with the characteristic wavelength of $\lambda_u = 2\pi Z_R$, where Z_R is the Rayleigh length of the laser pulse.

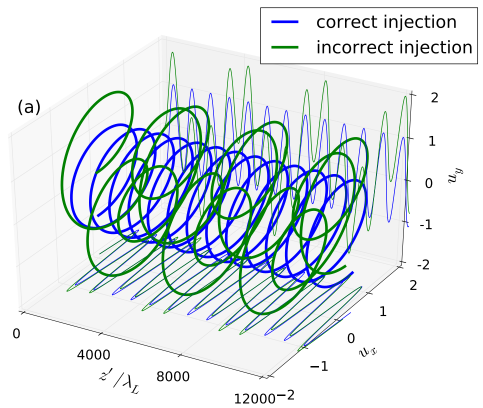

Figure 1: Trajectory of an electron injected into the plasma undulator correctly (blue line) and incorrectly (green line) as a function of propagation distance z'. In this figure, $u_x = p_x/mc$ and $u_y = p_y/mc$ with m the electron mass and c the speed of light in vacuum, respectively.

Here, we report on theoretical and numerical studies of the plasma undulator and its radiation properties. First, using the wave equation, the evolution of the laser pulse inside the parabolic channel (z axis is the channel axis) was studied. In the case of matched laser pulse injection off-x-axis and under a certain angle with respect to the y axis $\theta_y = x_i/Z_R$, where x_i is the initial centroid displacement along the x axis, the laser pulse centroid exhibits circular trajectory. Next, applying linear plasma theory, we have studied the wakefield structure and the trajectories of the particles injected therein. It has been shown that one has to inject particles with certain precision to avoid betatron contribution. This is summarized in Fig. 1, where the trajectory of the electron injected into the plasma undulator both correctly (assuming correct initial conditions given by solutions of the equations of motion) and incorrectly (assuming particle injected on and along the channel axis) are presented. In the case of the correct injection, particle trajectory is circularly polarized.

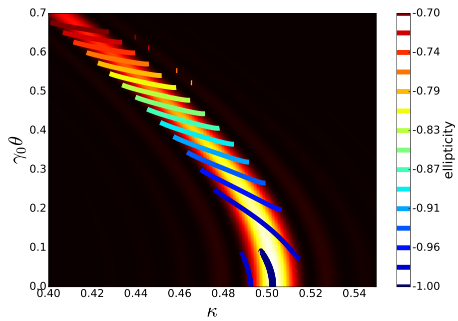

Figure 2: Normalized radiation intensity (color-coded image) as a function of both the normalized photon energy κ and normalized angle $\gamma_0\theta$, with γ_0 the relativistic Lorentz factor of injected electron. Ellipticity contours with corresponding colormap are also shown.

Radiation produced an electron beam has been calculated and compared with the analytical formulas, and the results agree very well. On Fig. 2, a typical energy-angular radiation spectrum is presented with normalized intensity shown with color-coded image and ellipticity of radiation shown with color-coded contour lines (colormap is to the right of the figure). On-axis radiation is perfectly circular.

Conclusions

We have performed theoretical and numerical studies of the plasma undulator, created by the laser pulse injected off-axis and under some angle with respect to the plasma channel axis. Polarization control of such an undulator is effortless, making it a promising way towards a "table-top" bright incoherent soft X-ray source, and a "table-top" FEL.

References

[1] S.G. Rykovanov, et al, "Plasma Undulator Based on Laser Excitation of Wakefields in a Plasma Channel", Physical Review Letters, 114, 145003 (2015)

* Work supported by Helmholtz Association (Helmholtz-Nachwuchsgruppe VH-NG-1037)

† S.Rykovanov@gsi.de

Many-electron effects on x-ray Rayleigh scattering by heliumlike ions *

A. V. Volotka†[1,2], *V. A. Yerokhin*[3], *A. Surzhykov*[1], *Th. Stöhlker*[1,4,5], *and S. Fritzsche*[1,5]

[1]Helmholtz-Institut Jena, Germany; [2]St. Petersburg State University, Russia; [3]Peter the Great St. Petersburg Polytechnic University, Russia; [4]GSI, Darmstadt, Germany; [5]Friedrich-Schiller-Universität Jena, Germany

The elastic scattering of a light by bound electrons is commonly known as Rayleigh scattering. It has been found a powerful and versatile tool for investigating the structure and dynamics of bound electrons as well as for probing the atomic environment. Experimentally, recent progress in exploring the Rayleigh scattering of hard x rays by atomic or solid-state targets has been achieved by a major improvement of the detection techniques as well as the quality of light sources. For example, a measurement of the linear polarization of the Rayleigh scattered light has been recently performed with the help of the segmented solid-state detectors at the PETRA III synchrotron at DESY. The advances in the Rayleigh scattering experiments nowadays also demand further and accurate predictions at the side of theory.

Recently, we provide a rigorous QED treatment of the Rayleigh scattering of light by highly charged helium-like ions [1]. The QED perturbation expansion with regard to the interelectronic interaction is applied up to the first-order for the Rayleigh scattering. In particular, formulas have been derived for the zeroth- and first-order interelectronic-interaction corrections to the scattering amplitude. This framework enables us to systematically investigate the many-electron effects beyond the independent particle approximation (IPA) as conventionally employed for describing the Rayleigh scattering.

The total and angle-differential cross sections are evaluated for the scattering of unpolarized and linearly polarized incoming x rays on the helium-like Ni^{26+}, Xe^{52+}, and Au^{77+} ions in their ground state. In Figure 1, we display the angle-differential cross sections for the Rayleigh scattering of linearly polarized incoming light scattered by helium-like Ni^{26+} (left column) and Au^{77+} (right column) ions. The two sets of IPA calculations (Coulomb and screening) are compared with the many-electron computations aiming to investigate the "many-electron" effects beyond the IPA. The relative differences between the Coulomb and many-electron computations are especially large at low Z and clearly demonstrate the importance of the interelectronic-interaction effects. However, the deviations are much less significant between the screening and many-electron computations, i.e. less than 2% for all the cases considered.

We found that the interelectronic-interaction effects are more important for photon energies below and just above of the ionization threshold. However, the major part of these many-electron contributions can be taken into account by IPA calculations with a screening potential. For photon energies well above the valence and sub-valence binding energies, this conclusion can be generalized also towards more complex atoms. For such atoms and ions, the Rayleigh scattering is typically dominated by the scattering from the closed-shell electrons. However, for photon energies compared with the valence and sub-valence binding energies, the Rayleigh scattering cross sections are strongly affected by the scattering from the outer-shell electrons and further care has to be taken in employing the IPA. The theoretical formalism developed now can be applied to such open-shell atoms, though further effort will be needed for its efficient numerical implementation.

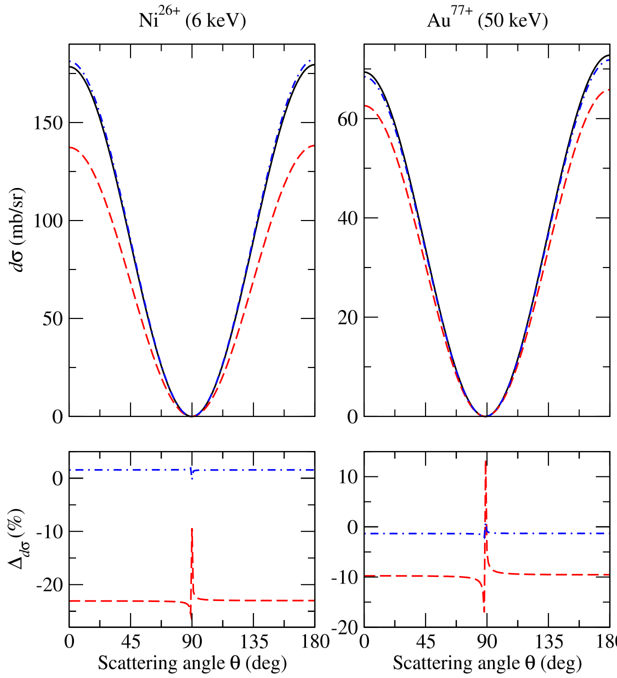

Figure 1: Angle-differential cross section for the Rayleigh scattering of linearly polarized incoming photons with energies 6 keV (left column) and 50 keV (right column) by helium-like Ni^{26+} and Au^{77+} ions, respectively. Results are shown for the three approximations: Coulomb (red dashed line), screening (blue dash-dotted line), and many-electron (black solid line). In the lower panel, the differences (in %) between the Coulomb (red dashed line) and screening results (blue dash-dotted line) are shown, just relative to the many-electron computations.

References

[1] A. V. Volotka, V. A. Yerokhin, A. Surzhykov, Th. Stöhlker, and S. Fritzsche, Phys. Rev. A **93**, 023418 (2016).

* Work supported by BMBF under the contract No. 05K13VHA.
† a.volotka@gsi.de

Temporal laser pulse shape in nonlinear Thomson scattering*

V. Yu. Kharin† 1, S. G. Rykovanov[1], and D. Seipt[1,2]

[1]Helmholtz-Institut, Jena, Germany; [2]Friedrich-Schiller-Universität, Theoretisch Physikalisches Institut, Jena, Germany

Nonlinear Thomson scattering (TS) has nowadays become a recognized tool for generation of tunable X- and γ-rays. The effect consists in Doppler up-shift in the frequency of the laser radiation scattered by the high γ electron beam. However, the relatively small cross-section of this scattering forces one to increase the laser intensity when the bright X-ray source is needed. High intensity of the incident pulse makes longitudinal ponderomotive drift of the electron (arising from $\mathbf{v} \times \mathbf{B}$ force) non-negligible. Drift, in turn, contributes to Doppler shift of the scattered light. Since drift velocity is intensity-dependent, one gets different scattered radiation frequencies provided by parts of the pulse with different intensities. Therefore, the scattered spectrum broadens with growing intensity of the incident pulse. Up to now it was considered as the flaw of TS generated X-rays, and there is number of papers devoted to possibilities of elimination of the effect ([1] and references therein). On the other side, ponederomotive broadening "spectrally resolves" the incident pulse intensity profile. Hence, if one is able to resolve the spectrum of the scattered radiation, one can gain information about the intensity profile of the incident pulse. Measurement of the intensity profile of relativistically strong laser pulse itself is a challenge at present, and use of TS for this purpose could be helpful.

Interference-averaged spectra

As a first step, one can move to the frame of reference where the electron is initially at rest. Note that all the spectra below are presented in this particular frame of reference. Second, we assume that the incident pulse can be represented by a plane wave with vector-potential $\mathbf{A}^L(\varphi)$. Third, here we constrain ourselves to the case of circularly polarized light. The equations of electron motion in this case can be solved analytically. Calculating Lienard-Wiechert potentials for on-axis back-scattered radiation yields

$$\mathbf{A}(\zeta) = \frac{1}{R} \frac{\mathbf{A}^L(\varphi(\zeta))}{1 + \mathbf{A}^L(\varphi(\zeta))^2}\,, \qquad (1)$$

with ζ being the detector time $\zeta = \varphi + \int \mathbf{A}^L(\varphi)^2 d\varphi$.

Taking the Fourier transform of Eq. 1 one can make sure that scattered spectrum factorizes into average spectral intensity, and interference factor provided by difference of optical paths traveled by light of the same frequency. For the interference-averaged spectrum of the scattered light with peak amplitude a_0 and normalized temporal intensity profile $f(\varphi)$ one has simple relation between scattered spectrum and pulse shape [2]:

$$\frac{d^2 I}{d\omega d\Omega} = \frac{\omega\tau}{\pi} \left| y \frac{df^{-1}(y)}{dy} \right|_{y=-a_0^{-2}(1-1/\omega)} . \qquad (2)$$

This relation demonstrates that for high a_0 the scattered spectrum is sensitive with respect to incident pulse shape (see Fig. 1).

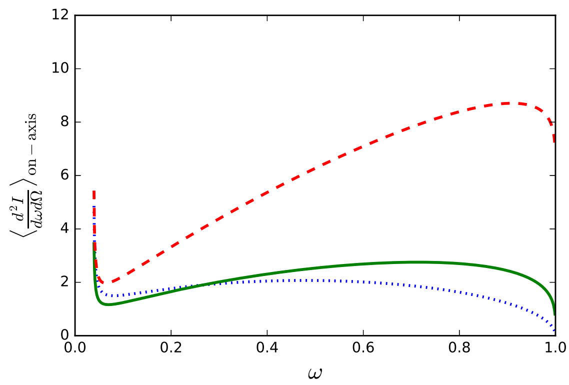

Figure 1: Interference-averaged scattered on-axis spectra. Gaussian (dashed), sine (solid) and sine-squared (dotted) incident pulses. $a_0 = 5$

Discussion

There are few remarkable properties of nonlinear TS that become explicit from our description. First, within the assumption that incident pulse is symmetric and multicycle, it could be possible to reconstruct its temporal intensity profile from measurement of TS spectrum in case of high a_0 even not resolving the interference structure. Second, passing to the detector time ζ greatly simplifies the calculation of electron response both in analytics and numerics.

References

[1] D. Seipt, S. G. Rykovanov, A. Surzhykov, and S. Fritzsche "Narrowband inverse Compton scattering x-ray sources at high laser intensities", PRA, 91, 033402 (2015)

[2] V. Yu. Kharin, D. Seipt and S. G. Rykovanov, "Temporal laser pulse shape effects in nonlinear Thomson scattering", arXiv:1602.03062 (2016)

* Work supported by Helmholtz Association (Helmholtz-Nachwuchsgruppe VH-NG-1037)

† v.kharin@gsi.de

Spectral caustics in laser-assisted x-ray Compton scattering

D. Seipt[* 1,2,3], *A. Surzhykov*[1,2], *S. Fritzsche*[1,3], *and B. Kämpfer*[4,5]

[1]Helmholtz-Institut Jena, Fröbelstieg 3, 07743 Jena; [2]GSI Darmstadt; [3]FSU Jena, Theoretisch-Physikalisches Institut; [4]Helmholtz Zentrum Dresden Rossendorf; [5]TU Dresden, Institut für Theoretische Physik

We study the process of laser-assisted Compton scattering: The Compton scattering of x-rays from an XFEL off electrons that are driven by a relativistically intense short optical laser pulse. The frequency spectrum of the laser-assisted Compton radiation shows a broad plateau in the vicinity of the laser-free Compton line due to a nonlinear mixing between x-ray and laser photons [1]. We observe sharp peak structures in the plateau region. These structures are interpreted as spectral caustics by using a semiclassical analysis of the laser-assisted QED matrix element, relating the caustic peak positions to the laser-driven electron motion [2].

Caustics are a well-known phenomenon in optics, occurring when diffracted or reflected light rays coalesce on a manifold of lower dimension, creating bright spots. For instance at the focal spot of an ideal lens all parallel light rays that impinge on the lens coalesce in a single point. Mathematically, caustics are described as singularities of differentiable mappings [3]. They can also occur in the spectral domain, where the roles of position and momentum space are exchanged.

The transition amplitude for laser assisted Compton scattering can be written as an integral over the laser phase ϕ:

$$\mathcal{M}(\ell,\vartheta) = \int \mathrm{d}\phi \, \mathcal{A}(\phi) e^{i\Psi(\phi,\ell,\vartheta)} \,. \qquad (1)$$

The phase $\Psi(\phi,\ell,\vartheta)$ depends on the laser momentum transfer ℓ, which is uniquely related to the frequency of the scattered photons [2]. For large frequency ratio $\omega_X/\omega_L \gg 1$ and high laser intensity $a_L \gtrsim 1$ the phase Ψ is large, and the integrand is a rapidly oscillating function of ϕ [2]. That means the matrix element (1) is determined at the stationary points, where $\dot{\Psi} = 0$. This saddle point condition—it is called the *ray-surface*—is plotted in Fig. 1 (a). It furnishes a semiclassical relation between a specific moment of scattering ϕ and the laser momentum transfer $\ell(\phi,\vartheta)$ as

$$\ell(\phi,\vartheta) = \frac{\omega_X}{\omega_L}\left(\frac{n'(\vartheta)\cdot v_L(-\infty)}{n'(\vartheta)\cdot v_L(\phi)} - 1\right) . \qquad (2)$$

Here, $v_L(\phi)$ denotes the four-velocity of the laser-driven electron as the solution of the classical Lorentz-force equation. It is projected onto the four-direction of the scattered photon $n'(\vartheta)$, depending on the scattering angle ϑ. (Note that the dependence on the azimuthal angle is suppressed here.)

The frequency spectrum of Compton scattered x-rays in the spectrum in Fig. 1 (b) for three scattering angles ϑ

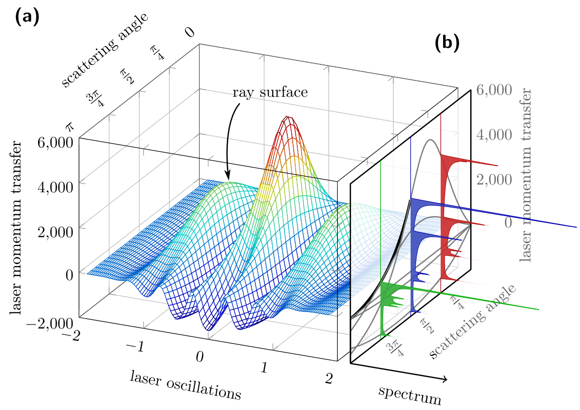

Figure 1: (a) The ray surface is the semiclassical solution determining a specific value of the laser momentum transfer ℓ for each laser phase and scattering angle ϑ. (b) When projected onto the ℓ–ϑ–plane the local extrema of the ray surface lead to the formation of large caustic peaks in the spectrum.

shows sharp and large peaks. Those peaks are interpreted as spectral caustics. The condition for the occurrence of caustics is the stationary of the phase to second order, $\ddot{\Psi} = 0$, or equivalently the singularity of the inverse $\phi(\ell,\vartheta)$ of (2) when projecting onto the ℓ–ϑ–plane, i.e. where several stationary points coalesce [2]. Moreover, by (2) this is equivalent to $n' \cdot \dot{v}_L = 0$, i.e. the four-acceleration is perpendicular to the observation direction.

In summary, we studied the occurrence of spectral caustic peaks in the frequency spectrum of the Compton scattered x-rays, which are related to the microscopic laser-driven electron motion. Loosely speaking, one can say that the spectral intensity is "focused" to the caustic peaks. Observing such features might serve as a novel tool for the investigation of high-intensity laser-matter interaction.

References

[1] D. Seipt, A. Surzhykov, S. Fritzsche, and B. Kämpfer, Phys. Rev. A **89**, 023433 (2014).

[2] D. Seipt, A. Surzhykov, S. Fritzsche, and B. Kämpfer, New J. Phys. **18**, 023044 (2016).

[3] Yu. A. Kravtsov, and Yu. I. Orolov, Sov. Phys. Usp. **26**, 1083 (1983).

* d.seipt@gsi.de

Critical Schwinger Pair Production

H. Gies[1,2] *and T. Torgrimsson*[3]

[1]Helmholtz Institute Jena, Germany; [2]Theoretisch-Physikalisches Institut, Abbe Center of Photonics, Friedrich Schiller University Jena, Germany; [3]Department of Applied Physics, Chalmers University, Gothenburg, Sweden

We investigate Schwinger pair production in spatially inhomogeneous electric backgrounds. A critical point for the onset of pair production can be approached by fields that marginally provide sufficient electrostatic energy for an off-shell long-range electron-positron fluctuation to become a real pair. Close to this critical point, we observe features of universality which are analogous to continuous phase transitions in critical phenomena with the pair-production rate serving as an order parameter: electric backgrounds can be subdivided into universality classes and the onset of pair production exhibits characteristic scaling laws. An appropriate design of the electric background field can interpolate between power-law scaling, essential BKT-type scaling and a power-law scaling with log corrections. The corresponding critical exponents only depend on the large-scale features of the electric background, whereas the microscopic details of the background play the role of irrelevant perturbations not affecting criticality.

Universality is an overarching concept in physics, signifying the independence of general gross properties of a physical system of the details of its microscopic realizations. Most prominently, critical phenomena near a continuous phase transition reveal a remarkably high degree of universality. As a consequence, critical systems can be associated with universality classes which are characterized by only a few properties such as the symmetries of the order parameter, the dimensionality, and the number and type of long-range degrees of freedom. It is therefore not surprising that universality and a notion of criticality can also be found beyond the realm of statistical physics. For instance, the onset of black-hole formation shows a surprising insensitivity to the initial data.

We have identified for the first time aspects of universality in the phenomenon of Schwinger pair production [1] in quantum electrodynamics (QED). Criticality occurs in this context, if the work done by an electric field on a virtual particle-antiparticle fluctuation equals the rest mass of the charged pair. This point of energetic criticality can be summarized in a dimensionless parameter γ approaching $\gamma \to 1$ at criticality. In the semi-classical critical regime, we have found a scaling law of the vacuum decay rate for a large-class of unidirectional electric fields that decay asymptotically with a power, $E(x) \sim \frac{1}{(x)^p}$ as $x \to \infty$. For instance for $p > 3$, the scaling law is of the form [2]

$$\mathrm{Im}\,\Gamma \sim (1-\gamma^2)^\beta, \quad \beta = \frac{5p+1}{4(p-1)}, \qquad (1)$$

independently of the microscopic details of the field profile.

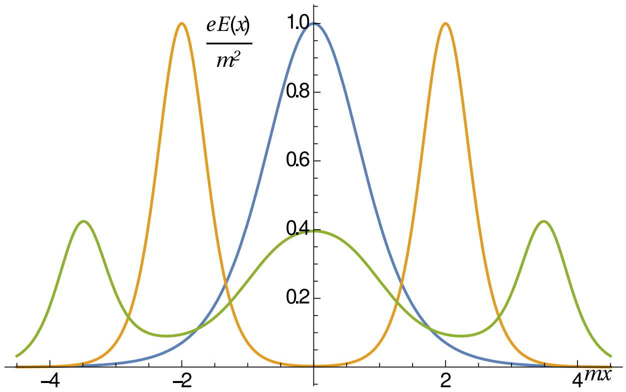

Figure 1: Various examples for critical field profiles with exponent $\beta = \frac{5}{4}$. The onset of criticality is determined by the asymptotic behavior ($p \to \infty$, i.e., exponential in these cases). The critical scaling law Eq. (1) is independent of the local details of the field profiles.

Upon variations of the asymptotic behavior of the field profile, the scaling law can acquire a variety of forms known from critical phenomena. A prominent example is given by essential scaling or BKT (or Miransky) scaling which occurs in systems exhibiting a transition from a conformal to a non-conformal phase. In the language of pair production, essential scaling turns out to be related to a dominance of electron-positron fluctuations at the largest length scales.

In summary, we have discovered an analogy between Schwinger pair production and continuous phase transitions. This analogy is quantitatively manifest in universal scaling laws for the onset of pair production in spatially inhomogeneous electric backgrounds. The scaling laws show a high degree of universality as the corresponding critical exponents only depend on the large-scale properties of the background (for monotonic potentials) but become insensitive to the microscopic details. Hence, localized electric backgrounds fall into universality classes each giving rise to a characteristic scaling law. As a particularly fascinating aspect, we discovered universality classes covering essentially all types of scaling laws familiar from continuous phase transitions.

References

[1] J. S. Schwinger, Phys. Rev. **82** (1951) 664.

[2] H. Gies and G. Torgrimsson, Phys. Rev. Lett. **116**, no. 9, 090406 (2016) doi:10.1103/PhysRevLett.116.090406 [arXiv:1507.07802 [hep-ph]].

Triple ionization of atomic Cd involving $4p^{-1}$ and $4s^{-1}$ inner-shell holes *

R. Beerwerth[† 1,2], *J. Andersson*[3], *P. Linusson*[4], *J. H. D. Eland*[3,5], *V. Zhaunerchyk*[3], *R. Feifel*[3,6], *and S. Fritzsche*[1,2]

[1]Helmholtz Institute Jena, Jena, Germany; [2]Theoretisch-Physikalisches Institut, Universität Jena, Jena, Germany; [3]Department of Physics, University of Gothenburg, Gothenburg, Sweden; [4]Department of Physics, Stockholm University, Stockholm, Sweden; [5]Department of Chemistry, Physical and Theoretical Chemistry Laboratory, Oxford University, Oxford, United Kingdom; [6]Department of Physics and Astronomy, Uppsala University, Uppsala, Sweden

The creation of inner-shell holes leads to a cascade of Auger decays if the binding energy of the hole is above the ionization threshold for at least two higher charge states. Experimentally, these processes can be investigated by Augerelectron photoelectron coincidence spectroscopy, where the emitted electrons are measured in coincidence. The total kinetic energy of the electrons associated to one event allows to obtain precise information on the spectrum of the final states. Additionally, the energy of individual electrons provides information about intermediate states and thus the decay pathways. We provided a theoretical analysis of the triple ionization of atomic cadmium, which was studied experimentally [1]. This study extends the previously performed analysis of the formation of doubly-ionized cadmium [2].

We performed numerical computations to understand the two-step Auger cascade that emerges upon the photo ionization of a $4s$ or $4p$ electron from the $4d^{10}5s^2$ ground-state configuration of atomic cadmium. To this end, we utilize the RATIP toolkit [3] to compute the photo-ionization cross sections as well as the Auger transition rates between all major intermediate states. As a result, we obtain spectral information about the emitted electrons and on the population of the final states in triply-charged cadmium.

Our computed final-state spectrum at a photon energy of $200\,eV$ is shown in figure 1. The lower part of the figure shows the computed spectrum, where the energy scale is relative to the ground-state energy of atomic cadmium.

We find that Auger cascades leading to triply-ionized final states are strongly influenced by shake-up transitions, where either the initial photo ionization or one of the Auger decays is accompanied by the excitation of a valence electron. Since the $4d^8 5p$ configuration does not appear in any pathway emerging from singly-ionized cadmium with an inner-shell hole, it is clear that the population of this configuration happens completely due to shake-up transitions. Computationally, we treat this by including configuration mixing between $5s^2$ and $5p^2$ configurations. As a result, as can be seen in figure 1, we find that $4d^8 5p$ states receive a similar population by shake-up transitions as the $4d^8 5s$ configuration.

Another important conclusion of our calculations is that a $4s$-hole predominantly decays to the excited state configuration $4d^7 5s^2$, while the ground configuration does almost

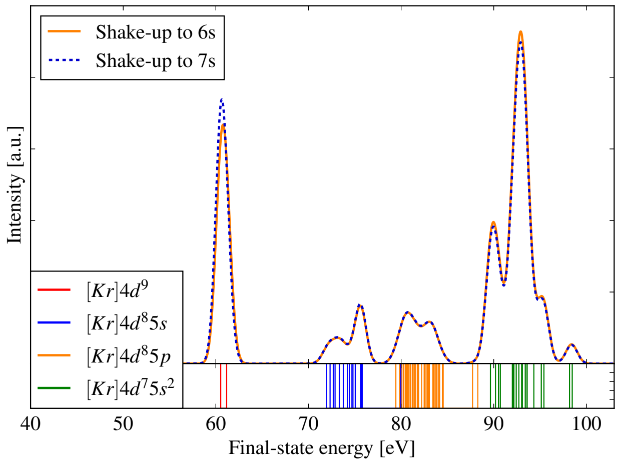

Figure 1: Calculated final-state spectrum of triply ionized cadmium. We consider two sequential Auger steps that follow the removal of an inner-shell $4s$ or $4p$ electron in atomic cadmium by a $200\,eV$ photon.

not get populated by this path. Furthermore, its population is energetically forbidden by any path emerging from a $4p$-hole, if no shake-up transition is involved. However, we find that if one of the valence $5s$ electrons is excited to a higher s-orbital, this path becomes energetically possible and also very likely, such that the ground-state configuration receives a significant population. To estimate the contribution of higher s-orbitals to this decay path, we performed the same calculation with additional shake-up transitions into the $7s$ orbital. In Fig. 1, it can be seen that the population of the ground configuration increases slightly, while the excited states get less populated. Higher shells are therefore expected to have almost negligible contribution, while other classes of shake-up transitions may be more important.

Our study shows that shake-up transitions are very important for the considered cascade processes. They become more important when longer decay paths, and hence higher ionization stages, are involved. In this particular case, we found that the population of the ground state of triply-ionized cadmium is predominantly driven by shake-up transitions in either the photo ionization or the first Auger step.

References

[1] Andersson, J. et al., Phys. Rev. A 92, 023414 (2015)
[2] Linusson, P. et al., Phys. Rev. A 83, 023424 (2011)
[3] Fritzsche, S., Comp. Phys. Comm. 183, 1525–1559 (2012)

* This work has been supported by the BMBF (Grant No. 05P15SJCIA).

† Randolf.Beerwerth@uni-jena.de

Vacuum birefringence in strong inhomogeneous electromagnetic fields

F. Karbstein[1,2], H. Gies[1,2], M. Reuter[1,3], and M. Zepf[1,3,4]

[1]Helmholtz-Institut Jena, Germany; [2]Theoretisch-Physikalisches Institut, FSU Jena, Germany; [3]Institut für Optik und Quantenelektronik, FSU Jena, Germany; [4]Queen's University, Belfast, United Kingdom

Birefringence is one of the fascinating properties of the vacuum of quantum electrodynamics (QED) in strong electromagnetic fields. The scattering of linearly polarized incident probe photons into a perpendicularly polarized mode provides a distinct signature of the optical activity of the quantum vacuum and thus offers an excellent opportunity for a precision test of non-linear QED. Precision tests require accurate predictions and thus a theoretical framework that is capable of taking the detailed experimental geometry into account. We derive analytical solutions for vacuum birefringence which include the spatio-temporal field structure of a strong optical pump laser field and an x-ray probe. We show that the angular distribution of the scattered photons depends strongly on the interaction geometry and find that scattering of the perpendicularly polarized scattered photons out of the cone of the incident probe x-ray beam is the key to making the phenomenon experimentally accessible with the current generation of FEL/high-field laser facilities.

One of the most famous optical signatures of vacuum nonlinearity in strong electromagnetic fields [1] is vacuum birefringence, which is so far searched for in experiments using macroscopic magnetic fields. A proposal to verify vacuum birefringence with the aid of high-intensity lasers has been put forward by [2], envisioning the combination of an optical high-intensity laser as pump and a linearly polarized x-ray pulse as probe (cf. also [3], which elaborates more on the experimental techniques). While [2] proposed the experimental scenario depicted in Fig. 1 for the first time, its theoretical description does not account for the possibility of momentum transfer from the pump field inhomogeneity. Incorporating this in our work [4] entails an enhancement of the birefringence signal-to-noise ratio of several orders of magnitude.

To arrive at these results we used new theoretical insights into photon propagation in slowly varying inhomogeneous electromagnetic fields [5], allowing us to overcome previous limitations and to calculate the angular divergence of the cross-polariz ed photons for the first time. Our study provides a new twist on the feasibility of future vacuum birefringence experiments. The key idea – so far completely unappreciated in this context – is to exploit the diffraction spreading of the outgoing signal photons. We focus on a realistic experimental setup combining a high-intensity laser system and an XFEL source as envisioned at the Helmholtz International Beamline for Extreme Fields (HIBEF) at the European XFEL at DESY.

To obtain realistic estimates for the numbers of induced photons for a state-of-the-art laser system, we assume the pump laser to be of the $1\mathrm{PW}$ class (pulse energy $W = 30\mathrm{J}$, pulse duration $\tau = 30\mathrm{fs}$ and wavelength $\lambda = 800\mathrm{nm}$) focused to $w_0 = 1\mu\mathrm{m}$. For the x-ray probe we choose $\omega = 12914\mathrm{eV}$, for which the presently most sensitive x-ray polarimeter [6] was benchmarked. Assuming the probe pulse to comprise $N = 10^{12}$ photons and a repetition rate of $1\mathrm{Hz}$, we expect to detect $N^{(\perp)} \approx 265$ perpendicularly polarized photons per hour.

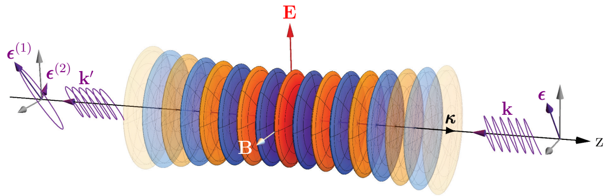

Figure 1: Sketch of the pump-probe type scenario intended to verify vacuum birefringence. A linearly polarized optical high-intensity laser pulse – wavevector $\boldsymbol{\kappa}$, electric (magnetic) field $\mathbf{E}$ ($\mathbf{B}$) – propagates along the positive z axis. Its strong electromagnetic field couples to the charged particle-antiparticle fluctuations in the quantum vacuum, and thereby effectively modifies its properties to be probed by a counter-propagating x-ray beam (wavevector $\mathbf{k}$, polarization $\boldsymbol{\epsilon}$). Vacuum birefringence manifests itself in an ellipticity of the outgoing x-ray photons (wavevector $\mathbf{k}'$, polarization components along $\boldsymbol{\epsilon}^{(1)}$ and $\boldsymbol{\epsilon}^{(2)}$).

In conclusion, we have demonstrated that vacuum birefringence can be verified experimentally with state-of-the-art technology. The key idea to making this phenomenon experimentally accessible is to exploit the scattering of perpendicularly polarized photons out of the cone of the incident probe x-ray beam. We are optimistic that our study can pave the way for an experimental verification of vacuum birefringence in an all-optical experiment.

References

[1] W. Heisenberg and H. Euler, Z. Phys. **98**, 714 (1936).

[2] T. Heinzl, B. Liesfeld, K. U. Amthor, H. Schwoerer, R. Sauerbrey and A. Wipf, Opt. Commun. **267**, 318 (2006).

[3] H. -P. Schlenvoigt, T. Heinzl, U. Schramm, T. Cowan and R. Sauerbrey, Physica Scripta **91**, 023010 (2016).

[4] F. Karbstein, H. Gies, M. Reuter and M. Zepf, Phys. Rev. D **92**, 071301 (2015)

[5] F. Karbstein and R. Shaisultanov, Phys. Rev. D **91**, 113002 (2015) and Phys. Rev. D **91**, 085027 (2015).

[6] B. Marx, *et al.*, Opt. Comm. **284**, 915 (2011) and Phys. Rev. Lett. **110**, 254801 (2013).

Linear polarization of fluorescence photons emitted from two-step radiative cascade via overlapping resonances of highly charged ions

Z. W. Wu[1,2]*, A. Surzhykov*[1]*, N. M. Kabachnik*[3,4]*, C. Z. Dong*[2]*, and S. Fritzsche*[1,5]

[1]Helmholtz Institute Jena, Germany; [2]Northwest Normal University, Lanzhou, China; [3]European XFEL, Hamburg, Germany; [4]Moscow State University, Moscow, Russia; [5]University of Jena, Germany

Angular distribution and polarization of characteristic fluorescence photons emitted from highly charged ions have been studied for many decades. In contrast to total decay rates, these angle- and polarization-resolved properties have been found much more sensitive to various atomic effects such as the Breit interaction, the hyperfine interaction, or the multipole mixing of radiation fields. However, until now, almost all the angular and polarization studies were made for photon emissions from well-isolated fine-structure levels of atoms or ions, while little attention was paid to their counterparts from (partially) overlapping resonances. Compared to the case of well-isolated energy levels, an overlap of two or more atomic resonances may lead to a depolarization of themselves due to the spin-spin and spin-orbit interactions. The effect of such a depolarization was studied very recently for angular distribution and angular correlation of the fluorescence photons emitted in a two-step radiative cascade $1s2p^2\ J_i = 3/2 \rightarrow 1s2s2p\ J = 1/2, 3/2 + \gamma_1 \rightarrow 1s^22s\ J_f = 1/2 + \gamma_1 + \gamma_2$ of lithium-like W^{71+} ions [1]. For this particular case, due to the depolarization, a quite strong dependence of angular anisotropy of the emitted fluorescence photons upon the splitting of the intermediate $1s2s2p\ J = 1/2, 3/2$ overlapping resonances were found.

In this contribution, we follow our previous work [1] and further study linear polarization of the fluorescence photons emitted in the same radiative cascade [2]. Special attention was paid how the splitting of the intermediate resonances affects the linear polarization and whether modifications of the linear polarization can be utilized for extracting such splittings, if analyzed along the isoelectronic sequence of lithium-like ions. For this purpose, we employed the density matrix theory to derive general expression for the linear polarization of the emitted fluorescence photons. While the derived formalism can be applied to any atomic or ionic system, we here consider again the two-step radiative cascade of lithium-like W^{71+} ions.

In Fig. 1, for example, we display linear polarization of the second-step γ_2 photons as functions of the level splitting of the intermediate $1s2s2p\ J = 1/2, 3/2$ overlapping resonances. Results are shown for photons that are emitted perpendicular to the quantization axis (as defined in the prior excitation process) and for assumed alignment parameters $\mathcal{A}_2 = -1.0$, -0.5, 0.5, and 1.0 of the initial $1s2p^2\ J_i = 3/2$ level. Similar to the case of angular distribution, a quite strong effect of the level splitting upon the linear polarization of the photons is obtained at small splittings $\Delta\omega \lesssim 0.2$ a.u. ≈ 5.4 eV. Moreover, for given small level splittings, the linear polarization also depends sensitively upon the initial alignment of the $1s2p^2\ J_i = 3/2$ level [2]. This finding strengthens our recent suggestion that angle-resolved measurements of characteristic fluorescence photons may help identify small level splittings.

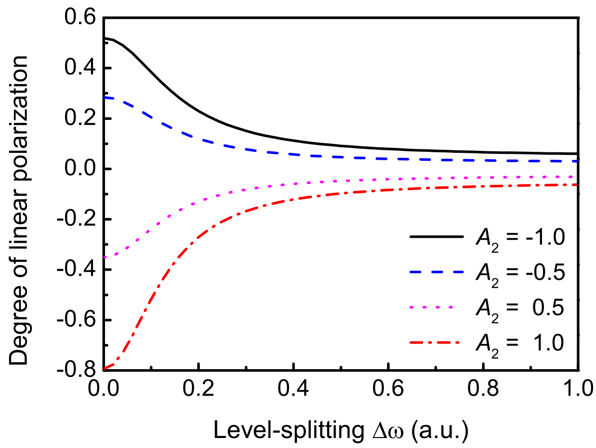

Figure 1: Degree of linear polarization of the second-step γ_2 photons as functions of the level splitting $\triangle\omega$ of the intermediate overlapping resonances. Results are shown for photons that are emitted perpendicular to the quantization axis and for assumed alignment parameters $\mathcal{A}_2$ of the initial $1s2p^2\ J_i = 3/2$ level: $\mathcal{A}_2 = -1.0$ (black solid line), -0.5 (blue dashed line), 0.5 (magenta dotted line), and 1.0 (red dash-dotted line).

Owing to this sensitivity of the linear polarization with regard to the level splitting of the intermediate overlapping resonances, we conclude that accurate measurements of photon polarization may alternatively serve as a tool as well for determining small level splittings in highly charged ions. Such measurements are experimentally accessible by using present-day solid-state or crystal-based photon detectors and could be carried out at heavy-ion storage rings or electron beam ion trap facilities.

References

[1] Z. W. Wu, N. M. Kabachnik, A. Surzhykov, C. Z. Dong and S. Fritzsche, *Phys. Rev. A* **90**, 052515 (2014).

[2] Z. W. Wu, A. Surzhykov, N. M. Kabachnik, C. Z. Dong and S. Fritzsche, *J. Phys. Conf. Ser.* **635**, 012020 (2015).

Photon merging and splitting in electromagnetic field inhomogeneities

Holger Gies[1,2], *Felix Karbstein*[1,2], *and Nico Seegert*[1,2]

[1]Helmholtz Institut Jena, Fröbelstieg 3, D-07743 Jena, Germany; [2]Theoretisch-Physikalisches Institut, FSU Jena, Max-Wien-Platz 1, D-07743 Jena, Germany

We theoretically investigate photon merging and splitting in inhomogeneous, slowly varying electromagnetic fields. Employing a set-up combining typical Terawatt/Petawatt-class lasers, we find that the combination of frequency upshifting, polarization dependence and scattering of signal photons into background-free regions renders photon merging an ideal candidate to experimentally verify quantum vacuum nonlinearities.

The vacuum of quantum electrodynamics (QED), permeated by virtual electron-positron fluctuations [1], facilitates a variety of nonlinear interactions between electromagnetic fields. These interactions depend on the electric (magnetic) field strengths involved, and are suppressed by powers of $\mathcal{E}/\mathcal{E}_{\rm cr}$, where $\mathcal{E}_{\rm cr} \approx 10^{18}\mathrm{V/m}$ ($\approx 10^9\mathrm{T}$). A promising route towards experimentally verifying signatures of QED vacuum nonlinearities, such as vacuum birefringence and light-by-light scattering, for the first time involves employing state-of-the-art high-intensity lasers, which have undergone a rapid development in recent years.

In light of these efforts, in [2] we investigated two prominent complementary signatures of quantum vacuum nonlinearities: photon merging and splitting. By employing the low-energy effective theory of QED in electromagnetic background fields [1] we were able to examine these signatures in slowly varying, but otherwise arbitrary electromagnetic field inhomogeneities, and identify deviations from the well-known constant-field results. Whereas splitting and merging amplitudes in constant fields are suppressed by $(\mathcal{E}/\mathcal{E}_{\rm cr})^3$, inhomogeneous background fields generically lower the suppression to only $\mathcal{E}/\mathcal{E}_{\rm cr}$.

We considered an experimental pump-probe type set-up, where both probe and pump beams are delivered by high-intensity lasers, cf. Fig. 1. The probe-photon beam(s), modeled as a plane wave with current density J (J', J''), hits the focal spot of the pump laser. Then, to lowest order in the pump field strength the differential number of signal photons per laser shot originating from the splitting (merging) of probe photons is given by

$$\begin{Bmatrix} \mathrm{d}^6\mathcal{N}^{p\to p'p''}_{\rm Split} \\ \mathrm{d}^3\mathcal{N}^{p'p''\to p}_{\rm Merg} \end{Bmatrix} \propto \begin{Bmatrix} \frac{J}{(2\pi)^3}\mathrm{d}^3k'\mathrm{d}^3k'' \\ J'J''\mathrm{d}^3k \end{Bmatrix} \left(\frac{\mathcal{E}}{\mathcal{E}_{\rm cr}}\right)^2 \omega\omega'\omega''$$
$$\times \left| c^{pp'p''}_{(1)} \sum_{\ell=\pm1} \mathrm{e}^{-\frac{1}{16}\left[w_0^2(q_{\rm x}^2+q_{\rm y}^2)+w_{\rm z}^2(q^0-q_{\rm z})^2+\tau^2(q^0+\ell\Omega)^2\right]}\right|^2 . \quad (1)$$

Eq. (1) implies that merging and splitting rates in inhomogeneous pump fields are mainly governed by two kinematical factors: The *polarization overlap function* $c^{pp'p''}_{(1)}$ encodes selection rules which only depend on the propagation direction and the polarizations $\{p, p', p''\}$ of the probe

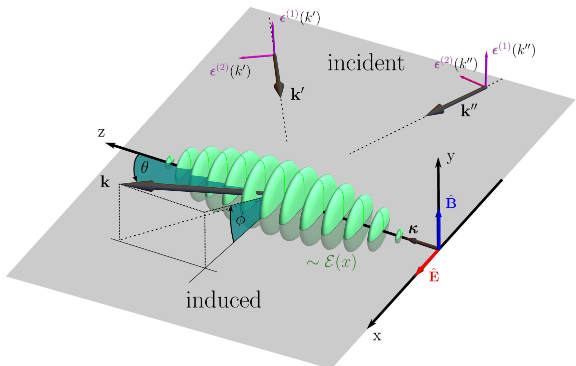

Figure 1: Schematic depiction of photon merging in a localized background field inhomogeneity. Two photons with four-momentum k' and k'', and polarization vectors $\boldsymbol{\epsilon}^{(p')}(k')$ and $\boldsymbol{\epsilon}^{(p')}(k')$, merge to yield one outgoing photon of four-momentum k. For photon splitting (not depicted) the roles are reversed: One photon of momentum k splits into two photons with k' and k''.

and signal photons. Conversely, the exponential term is a function of the four-momentum $q = k - k' - k''$, and causes an exponential drop in the number of signal photons for settings which violate four-momentum conservation between the inhomogeneity, probe and signal photons.

For numerical estimates we employed parameters of state-of-the-art high-intensity laser systems, assuming a 1PW pump beam of wavelength $\lambda = 800\mathrm{nm}$ being probed by two 250TW lasers of wavelength $\lambda/2$. These values can e.g. be achieved by the laser system to be installed at ELI-NP [3]. In this parameter regime splitting is greatly suppressed compared to merging, $\mathcal{N}_{\rm Split} \sim 10^{-16}\mathcal{N}_{\rm Merg}$, and can be neglected. By adjusting the propagation directions of the probe beams we identified a specific setting yielding a total of ≈ 37 merged photons per laser shot, which are furthermore predominantly emitted into the background-free area. Additionally, the distinct polarization of these signal photons, as well as their wavelength of $\lambda/3$, can be employed to discriminate them from stray background photons.

These promising results show the importance of accurately modeling the electromagnetic field inhomogeneities induced by the pump beam, and imply that photon merging in electromagnetic fields is ideally suited to experimentally verify and investigate the nonlinear nature of the quantum vacuum for the first time.

References

[1] W. Heisenberg and H. Euler, Z. Phys. **98**, 714 (1936).

[2] H. Gies, F. Karbstein and N. Seegert, arXiv:1603.00314 [hep-ph]

[3] https://eli-laser.eu/

Ionization of H_2^+ molecular ions by twisted Bessel light beam

A. A. Peshkov[*1], *S. Fritzsche*[1], *and A. Surzhykov*[2]
[1]Helmholtz Institute Jena, Germany; [2]University of Jena, Germany

Like in Young's well-known double-slit experiment with plane-wave light, interference effects have been observed and discussed also in the photoionization of diatomic molecules. These interferences in the photoelectron spectra can be understood in terms of the phase shift of the electrons, if they are emitted from different (atomic) centers of the molecule. Until the present, however, all molecular double-slit experiments have been performed only with incident plane-wave radiation, while very little is known about the photoionization of (diatomic) molecules by beams of twisted (or vortex) light. In contrast to plane-wave radiation, the twisted light carries a nonzero projection of the orbital angular momentum (OAM) upon their propagation direction. In addition, these twisted beams also exhibit a quite distinguished inhomogeneous intensity profile, if taken in the plane perpendicular to the propagation direction of the beam. One therefore expects that the OAM and intensity profile of such beams might affect also the angular distributions of the photoelectrons in the photoionization of molecules.

In a recent work [1], we have theoretically investigated the photoionization of H_2^+ molecular ions for a Bessel beam of twisted light. We hereby assumed that the beam propagates along the quantization axis and has well-defined longitudinal momentum k_z as well as absolute value of the transverse momentum $\varkappa$, which determine the so-called opening angle $\theta_k = \arctan(\varkappa/k_z)$. Non-relativistic first-order perturbation theory was applied, along with Born's approximation, in order to analyze the angular distributions of the emitted photoelectrons. We also restricted ourselves to just a macroscopic target of H_2^+ molecules that are uniformly-distributed but all aligned with regard to the propagation direction of the incident beam. For such a target, our analysis indicates that the photoelectron angular distribution is independent of the light's OAM but depends on the opening angle θ_k. In Fig. 1, we compare the azimuthal photoelectron angular distributions for incident plane-wave light with those of Bessel beams. As can be seen from this figure, the shapes of the angular distribution are almost identical for $\hbar\omega = 0.5$ keV. However, the angular distributions start to deviate from each other if either the photon energy or the opening angle θ_k increases. For a photon energy of $\hbar\omega = 10$ keV, the Bessel beam results in a quite isotropic distribution of the emitted photoelectrons and in contrast to the well-defined lobes for plane-wave radiation of the same energy [cf. Fig. 1(d)]. These modifications in the angular distribution can be understood from the inhomogeneity of intensity pattern for the Bessel beam: at high photon energies and large opening angles θ_k, the atomic centers of the molecules are exposed to the different intensity of the radiation field. For this reason then, the interference pattern gradually disappears, similar to Young's experiment for double slits of nonequal widths.

In summary, the main modifications in the angular distribution of the photoelectrons arise due to the intensity variation of Bessel beams relative to the size of the H_2^+ molecular ions. Hence, the photoionization of diatomic molecules opens up different possibilities of atomic double-slit phenomena. To use of twisted photons will allow one to perform a molecular analog of Young's experiment with two slits of unequal widths.

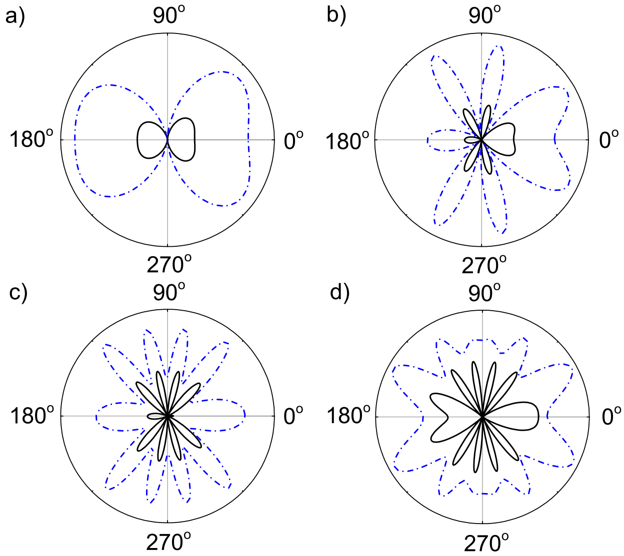

Figure 1: Comparison of the azimuthal photoelectron angular distribution for incident plane waves (black solid lines) and Bessel beams with opening angle $\theta_k = 30°$ (blue dashed-dotted lines). The H_2^+ molecular ions are assumed to be aligned again under the angle $45°$ with regard to the quantization axis. Results in arbitrary units are shown for four different photon energies: a) $\hbar\omega = 0.5$ keV; b) $\hbar\omega = 3$ keV; c) $\hbar\omega = 7$ keV; d) $\hbar\omega = 10$ keV. The polar angle of emitted electrons $20°$ is fixed.

References

[1] A. A. Peshkov, S. Fritzsche, and A. Surzhykov, Phys. Rev. A **92**, 043415 (2015).

* anton.peshkov@uni-jena.de

Comparison of semiclassical and Wigner function methods in pair production in rotating fields

Alexander Blinne [1,2] *and Eckhard Strobel* [3,4,5]

[1]Helmholtz Institut Jena, Fröbelstieg 1, D-07743 Jena, Germany; [2]Theoretisch-Physikalisches Institut, FSU Jena, Max-Wien-Platz 1, D-07743 Jena, Germany; [3]ICRANet, Piazzale della Repubblica 10, 65122 Pescara, Italy; [4]Dipartimento di Fisica, Università di Roma "La Sapienza", Piazzale Aldo Moro 5, 00185 Rome, Italy; [5]Université de Nice Sophia Antipolis, 28 Avenue de Valrose, 06103 Nice Cedex 2, France

We present a comparison of two methods to compute the momentum spectrum and the Schwinger pair creation rate for pulsed rotating electric fields: a numerical method based upon the real-time Dirac-Heisenberg-Wigner formalism and a semiclassical approximation based on a scattering ansatz. We find that the two numerical methods are complementary with respect to computation time as well as accuracy. We additionally find that the unequal production of pairs in different spin states reported for constant rotating fields with the scattering method is in agreement with the Wigner function method.

We compare [1] the results of the semiclassical scattering method and the Wigner method of [2] and [3] respectively for rotating electric field pulses of the form

$$\vec{E}(t) = \underbrace{\frac{E_{\mathrm{cr.}}\varepsilon}{\cosh^2\left({}^t/_\tau\right)}}_{E(t)} \begin{pmatrix} \cos(\Omega t) \\ \sin(\Omega t) \\ 0 \end{pmatrix} .$$

For a fair comparison, we mostly stay in the semiclassical regime. In contrast to the case of a constant rotating pulse, it is difficult to find an analytical solution for general $E(t)$ in the semiclassical scattering approach. We compared two different semiclassical methods. The first is to carry out the necessary computation numerically, the second is to perform an additional approximation which uses the analytic results for the constant rotating field. We refer to the latter as locally constant rotating field approximation (LCRFA).

As the semiclassical calculations are based on the ansatz

$$\psi_{\vec{q},s}(t) = C_s \begin{pmatrix} s\, m\, \psi_1^s(t) \\ m\, \psi_2^s(t) \\ -s(q_z + s\epsilon_\perp)\, \psi_1^s(t) \\ (q_z + s\epsilon_\perp)\, \psi_2^s(t) \end{pmatrix}$$

for $s = \pm 1$, the semiclassical result is the sum of two different states. These two states are given a clear interpretation and are reproduced in the Wigner formalism.

In addition to the full one-particle distribution function, the Wigner function gives access to information about the spinor degrees of freedom of the Dirac field. This is accomplished by applying projectors to the Wigner function before calculating the one-particle distribution function. Useful projectors turn out to be the chiral projections given by

$$P_{\mathrm{r/l}} = \frac{1}{2}\left(\mathbb{1} \pm \gamma_5\right)$$

and a combination of the projectors for charge and spin, which we call magnetic moment

$$P_{\mu_z^\pm} = P_Q P_{(0,0,\pm 1)} + P_{-Q} P_{(0,0,\mp 1)} .$$

These projectors give physical information about the produced particles. In order to bring the Wigner results in agreement with the semiclassical spectra, they have to be combined in a slightly peculiar way which follows directly from the semiclassical ansatz [1].

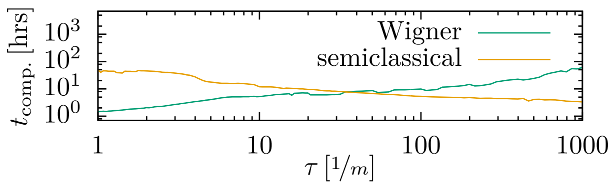

Figure 1: Comparison of computation times for the two methods with fixed $\sigma = \Omega \cdot \tau = 20$.

While the results agree for intermediate pulse lengths, for short pulses the semiclassical approximation breaks down and the computation time becomes high. The advantage of the semiclassical method is that one does not have to integrate numerically with respect to real time. This is especially useful for long pulse lengths since numerical problems arise in the Wigner method, which increase the required computation time and limit accuracy.

We also introduce the LCRFA for rotating field pulses and show that it has the same features as the numerical results and works especially well for pulse lengths $\tau \gg {}^1/_m$. This is intriguing since the parameters of current and near future laser systems fulfill this requirement. It can therefore be used to study different pulse shapes qualitatively.

As mentioned in [2] the fact that one of these solutions dominates the spectrum for a certain range of parameters might help to differentiate pairs produced by the Schwinger process from other particles detected in high energy experiments.

References

[1] A. Blinne and E. Strobel, Phys. Rev. D **93**, 025014 (2016)

[2] E. Strobel and S. S. Xue, Phys. Rev. D **91**, 045016 (2015)

[3] A. Blinne and H. Gies, Phys. Rev. D **89**, 085001 (2014)

The effect of bound-state dressing in laser-assisted radiative recombination*

R. A. Müller[† 1,2], *D. Seipt*[1], *S. Fritzsche*[1,2], *and A. Surzhykov*[1]
[1]Helmholtz-Institute Jena, Jena, Germany; [2]Friedrich-Schiller-University Jena, Jena, Germany

The radiative capture of a continuum electron into a bound state of an atom or ion in the presence of a laser field is commonly called *laser assisted radiative recombination* (LARR). This process can be observed for example as the last step in high harmonic generation (HHG) as well as in storage ring experiments [1, 2]. Besides the practical application in HHG there are moreover indications that LARR might support the generation of neutral antihydrogen [3].

While in most analytical treatments of LARR it is assumed that the incident electron moves solely in the laser field and recombines into a bound Coulomb state that is unaltered by the external laser, we attributed a recent work to the effects arising due to the laser dressing of the residual bound state [4]. In this work we performed calculations accounting for the influence of both, the laser and the Coulomb field on the initial continuum as well as the final bound state. We found that the angle-differential cross section can be split up into so called partial cross sections each describing LARR for a particular number of photons N exchanged between the recombining electron and the external laser field:

$$\frac{d\sigma_{1s}^{(N)}}{d\Omega_k} = \frac{4\pi^2}{c^2 p}\omega_k(N)\sum_{\lambda}\left|M^{(N)}\right|^2, \tag{1}$$

where $M^{(N)}$ is the matrix element of the process and $\omega_k(N) = E_i - E_{1s} + N\omega_L$ the *discrete* energy of the emitted recombination photon.

In Fig. 1 we display the cross section (1) as a function of the recombination photon energy $\omega_k(N)$ (solid lines and circles) for two laser intensities I_L. In comparison we show results where we artificially excluded the bound state dressing (dashed lines and triangles). It can be seen in Fig. 1 that the spectrum is not just a single line, as it would be for the laser-free radiative recombination, but a distribution of photon energies. The width of this distribution is approximatively given by $\Delta\omega_k = 2E_L p/\omega_L^2$ [4], therefore $\Delta\omega_k$ increases the stronger the laser becomes.

As seen from Fig. 1, the dressed and undressed results behave quite differently as a function of $\omega_k(N)$. The results obtained without bound-state dressing are almost symmetric around the field-free photon energy where $N = 0$. A slight increase of $d\sigma_{1s}^{(N)}/d\Omega_k$ towards higher photon energies is caused by the prefactor $\omega_k(N)$ in Eq. (1). If, in contrast, the bound-state dressing is included in the computations, the photon distribution becomes strongly asymmetric. For higher intensities these asymmetries become more pronounced. This can be explained by the fact that the influence of the bound-state dressing increases the more photons are involved in the process [4]. This number N, of course, is larger for a more intense external laser. However dressing effects are often neglected we have shown that they can become important even for medium laser intensities ($I_L \sim 10^{13}$W/cm^2).

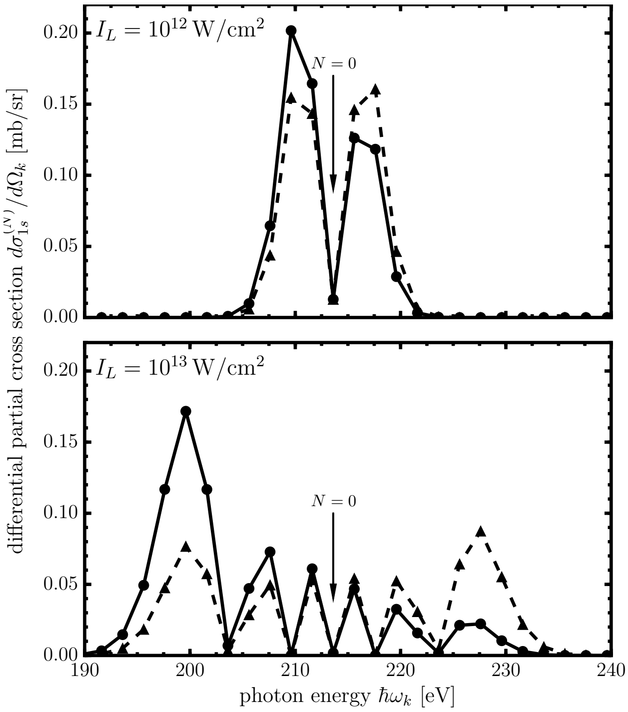

Figure 1: Angle-differential partial cross section for the laser-assisted recombination of a $E_i = 200$eV electron and a hydrogen nucleus as a function of the recombination photon energy $\omega_k(N)$. Dashed lines and triangles refer to results where the dressing of the target bound states is neglected. For details see text and Ref. [4]

References

[1] A. L'Huillier and Ph. Balcou, Phys. Rev. Lett. **70**, 774 (1993)

[2] U. Schramm, et al. Phys. Rev. Lett. **67**, 22 (1991).

[3] M. L. Rogelstad, F. B. Yousif, T. J. Morgan, and J. B. A. Mitchell, J. Phys. B **30**, 3913 (1997).

[4] R. A. Müller, D. Seipt, S. Fritzsche, and A. Surzhykov, Phys. Rev. A **92**, 053426 (2015)

* Work supported by HI Jena and Studienstiftung des Deutschen Volkes.

† robert.alex.mueller@gmail.com

Publications

A. Akber, M. W. Reed, P. M. Walker, Yu. A. Litvinov, G. J. Lane, T. Kibédi, K. Blaum, F. Bosch, C. Brandau, J. J. Carroll, D. M. Cullen, I. J. Cullen, A. Y. Deo, B. Detwiler, C. Dimopoulou, G. D. Dracoulis, F. Farinon, H. Geissel, E. Haettner, M. Heil, R. S. Kempley, R. Knöbel, C. Kozhuharov, J. Kurcewicz, N. Kuzminchuk, S. Litvinov, Z. Liu, R. Mao, C. Nociforo, F. Nolden, W. R. Plass, Zs. Podolyak, A. Prochazka, C. Scheidenberger, D. Shubina, M. Steck, Th. Stöhlker, B. Sun, T. P. D. Swan, G. Trees, H. Weick, N. Winckler, M. Winkler, P. J. Woods, and T. Yamaguchi
Increased isomeric lifetime of hydrogen-like ^{192m}Os
Physical Review C **91**, 031301 (2015).

J. Andersson, R. Beerwerth, P. Linusson, J. H. D. Eland, V. Zhaunerchyk, S. Fritzsche, and R. Feifel
Triple ionization of atomic Cd involving $4p^{-1}$ and $4s^{-1}$ inner-shell holes
Phyical Review A **92**, 023414 (2015).

A. N. Artemyev, and A. Surzhykov
Quantum Electrodynamical Corrections to Energy Levels of Diatomic Quasimolecules
Physical Review Letters **114**, 243004 (2015).

D. Atanasov, K. Blaum, F. Bosch, C. Brandau, P. Bühler, X. Chen, I. Dillmann, T. Faestermann, B. Gao, H. Geissel, R. Gernhäuser, S. Hagmann, T. Izumikawa, P.-M. Hillenbrand, C. Kozhuharov, J. Kurcewicz, S. Litvinov, Y. Litvinov, X. Ma, G. Münzenberg, M. Najafi, F. Nolden, T. Ohtsubo, A. Ozawa, F. Ozturk, Z. Patyk, M. Reed, R. Reifarth, M. Sanjari, D. Schneider, M. Steck, T. Stöhlker, B. Sun, F. Suzaki, T. Suzuki, C. Trageser, X. Tu, T. Uesaka, P. Walker, M. Wang, H. Weick, N. Winckler, P. Woods, H. Xu, T. Yamaguchi, X. Yan, and Y. Zhang
Between atomic and nuclear physics: radioactive decays of highly-charged ions
Journal of Physics B: Atomic, Molecular and Optical Physics **48**, 144024 (2015).

B. Aurand, S. Kuschel, C. Rödel, O. Jäckel, J. Polz, B. Elkin, H. Zhao, A. Karmakar, P. Gibbon, M. Kaluza, and T. Kühl
Reduction of X-ray generation in high-intensity laser ion acceleration
Applied Physics B **118**, 247 (2015).

D. Banaś, M. Pajek, A. Surzhykov, Th. Stöhlker, C. Brandau, A. Gumberidze, C. Kozhuharov, H. F. Beyer, S. Böhm, F. Bosch, M. Czarnota, S. Chatterjee, J.-C. Dousse, S. Fritzsche, S. Hagmann, D. Liesen, P. H. Mokler, A. Müller, A. Kumar, R. Reuschl, D. Sierpowski, U. Spillmann, J. Szlachetko, S. Tashenov, S. Trotsenko, P. Verma, and A. Warczak
Subshell-selective x-ray studies of radiative recombination of U^{92+} ions with electrons for very low relative energies
Phyical Review A **92**, 032710 (2015).

D. Bernhardt, C. Brandau, Z. Harman, C. Kozhuharov, S. Böhm, F. Bosch, S. Fritzsche, J. Jacobi, S. Kieslich, H. Knopp, F. Nolden, W. Shi, Z. Stachura, M. Steck, Th. Stöhlker, S. Schippers, and A. Müller
Electron-ion collision spectroscopy: Lithium-like xenon ions
Phyical Review A **91**, 012710 (2015).

D. Bernhardt, C. Brandau, Z. Harman, C. Kozhuharov, S. Böhm, F. Bosch, S. Fritzsche, J. Jacobi, S. Kieslich, H. Knopp, F. Nolden, W. Shi, Z. Stachura, M. Steck, T. Stöhlker, S. Schippers, and A. Müller
Spectroscopy of berylliumlike xenon ions using dielectronic recombination
Journal of Physics B: Atomic, Molecular and Optical Physics **48**, 144008 (2015).

H. Bernhardt, R. Diener, P. Sungur, C. Katzer, G. Schmidl, U. Hübner, I. Uschmann, W. Fritzsche, and F. Schmidl
Engineering crystalline Au nanoparticles of anisotropic shape in epitaxially grown high-index $SrTiO_3$
Journal of Materials Science **50**, 5562 (2015).

H. Bernhardt, C. Katzer, A. Undisz, M. Drüe, M. Rettenmayr, I. Uschmann, and F. Schmidl
Characterization of self-organized crystalline Au nanoparticles embedded in epitaxially grown $SrTiO_3$
Journal of Materials Research **30**, 973 (2015).

H. F. Beyer, T. Gassner, M. Trassinelli, R. Hess, U. Spillmann, D. Banaś, K.-H. Blumenhagen, F. Bosch, C. Brandau, W. Chen, C. Dimopoulou, E. Förster, R. E. Grisenti, A. Gumberidze, S. Hagmann, P.-M. Hillenbrand, P. Indelicato, P. Jagodzinski, T. Kämpfer, C. Kozhuharov, M. Lestinsky, D. Liesen, Y. A. Litvinov, R. Loetzsch, B. Manil, R. Märtin, F. Nolden, N. Petridis, M. S. Sanjari, K. S. Schulze, M. Schwemlein, A. Simionovici, M. Steck, Th. Stöhlker, C. I. Szabo, S. Trotsenko, I. Uschmann, G. Weber, O. Wehrhan, N. Winckler, D. F. A. Winters, N. Winters, and E. Ziegler
Crystal optics for precision x-ray spectroscopy on highly charged ions–conception and proof
Journal of Physics B: Atomic, Molecular and Optical Physics **48**, 144010 (2015).

J. Bierbach, M. Yeung, E. Eckner, C. Roedel, S. Kuschel, M. Zepf, and G. G. Paulus
Long-term operation of surface high-harmonic generation from relativistic oscillating mirrors using a spooling tape
Optics Express **23**, 12321 (2015).

J. Bieron, C. F. Fischer, S. Fritzsche, G. Gaigalas, I. P. Grant, P. Indelicato, P. Jönsson, and P. Pyykkö
Ab initio MCDHF calculations of electronnucleus interactions
Physica Scripta **90**, 054011 (2015).

J. H. Bin, W. J. Ma, H. Y. Wang, M. J. V. Streeter, C. Kreuzer, D. Kiefer, M. Yeung, S. Cousens, P. S. Foster, B. Dromey, X. Q. Yan, R. Ramis, J. Meyer-ter-Vehn, M. Zepf, and J. Schreiber
Ion Acceleration Using Relativistic Pulse Shaping in Near-Critical-Density Plasmas
Physical Review Letters **115**, 064801 (2015).

K.-H. Blumenhagen, A. Gumberidze, R. Märtin, N. Schell, U. Spillmann, G. Weber, and Th. Stöhlker
Characterization of a double-sided Si(Li) strip Compton polarimeter
Journal of Physics: Conference Series **583**, 012043 (2015).

K.-H. Blumenhagen, U. Spillmann, T. Gassner, A. Gumberidze, R. Märtin, N. Schell, S. Trotsenko, G. Weber, and T. Stöhlker
Identification and reduction of unwanted stray radiation using an energy- and position-sensitive Compton polarimeter
Physica Scripta **T166**, 014032 (2015).

C. Brabetz, S. Busold, T. Cowan, O. Deppert, D. Jahn, O. Kester, M. Roth, D. Schumacher, and V. Bagnoud
Laser-driven ion acceleration with hollow laser beams
Physics of Plasmas **22**, 013105 (2015).

C. Brandau, C. Kozhuharov, M. Lestinsky, A. Müller, S. Schippers, and T. Stöhlker
Storage-ring experiments on dielectronic recombination at the interface of atomic and nuclear physics
Physica Scripta **T166**, 014022 (2015).

J. Braun, S. Finkbeiner, F. Karbstein, and D. Roscher
Search for inhomogeneous phases in fermionic models
Physical Review D **91**, 116006 (2015).

S. Breitkopf, T. Eidam, A. Klenke, H. Carstens, S. Holzberger, E. Fill, T. Schreiber, F. Krausz, A. Tünnermann, I. Pupeza, and J. Limpert
Stack and dump: Peak-power scaling by coherent pulse addition in passive cavities
European Physical Journal - Special Topics **224**, 2573 (2015).

S. Busold, D. Schumacher, C. Brabetz, D. Jahn, F. Kroll, O. Deppert, U. Schramm, T. Cowan, A. Blazevic, V. Bagnoud, and M. Roth
Towards highest peak intensities for ultra-short MeV-range ion bunches
Scientific Reports **5**, 1 (2015).

W. Cayzac, V. Bagnoud, M. M. Basko, A. Blazevic, A. Frank, D. O. Gericke, L. Hallo, G. Malka, A. Ortner, An. Tauschwitz, J. Vorberger, and M. Roth
Predictions for the energy loss of light ions in laser-generated plasmas at low and medium velocities
Physical Review E **92**, 053109 (2015).

H. X. Chang, B. Qiao, Z. Xu, X. R. Xu, C. T. Zhou, X. Q. Yan, S. Z. Wu, M. Borghesi, M. Zepf, and X. T. He
Generation of overdense and high-energy electron-positron-pair plasmas by irradiation of a thin foil with two ultraintense lasers
Physical Review E **92**, 053107 (2015).

X. Chen, M. S. Sanjari, J. Piotrowski, P. Hülsmann, Y. A. Litvinov, F. Nolden, M. Steck, and T. Stöhlker
Report on a computer-controlled automatic test platform for precision RF cavity characterizations
Physica Scripta **T166**, 014061 (2015).

D. T. Doherty, P. J. Woods, Y. A. Litvinov, M. Ali Najafi, S. Bagchi, S. Bishop, M. Bo, C. Brandau, T. Davinson, I. Dillmann, A. Estrade, P. Egelhof, A. Evdokimov, A. Gumberidze, M. Heil, C. Lederer, S. A. Litvinov, G. Lotay, N. Kalantar-Nayestanaki, O. Kiselev, C. Kozhuharov, T. Kröll, M. Mahjour-Shafei, M. Mutterer, F. Nolden, N. Petridis, U. Popp, R. Reifarth, C. Rigollet, S. Roy, M. Steck, T. Stöhlker, B. Streicher, S. Trotsenko, M. von Schmid, X. L. Yan, and J. C. Zamora
Nuclear transfer reaction measurements at the ESR—for the investigation of the astrophysical $^{15}O(\alpha,\gamma)^{19}Ne$ reaction
Physica Scripta **T166**, 014007 (2015).

D. Doria, S. Kar, H. Ahmed, A. Alejo, J. Fernandez, M. Cerchez, R. J. Gray, F. Hanton, D. A. MacLellan, P. McKenna, Z. Najmudin, D. Neely, L. Romagnani, J. A. Ruiz, G. Sarri, C. Scullion, M. Streeter, M. Swantusch, O. Willi, M. Zepf, and M. Borghesi
Calibration of BAS-TR image plate response to high energy (3-300 MeV) carbon ions
Review of Scientific Instruments **86**, 123302 (2015).

B. Ecker, B. Aurand, D. C. Hochhaus, P. Neumayer, B. Zielbauer, E. Oliva, L. Li, T. T. T. Le, Q. Jin, H. Zhao, K. Cassou, S. Daboussi, O. Guilbaud, S. Kazamias, D. Ros, P. Zeitoun, and T. Kühl
Double-stage soft x-ray laser pumped by multiple pulses applied in grazing incidence
Journal of Physics B: Atomic, Molecular and Optical Physics **48**, 144009 (2015).

T. Eidam, M. Kienel, A. Klenke, J. Limpert, and A. Tünnermann
Divided-pulse amplification for terawatt-class fiber lasers
European Physical Journal - Special Topics **224**, 2567 (2015).

E. Eliav, S. Fritzsche, and U. Kaldor
Electronic structure theory of the superheavy elements
Nuclear Physics A **944**, 518 (2015).

S. Fritzsche, A. Surzhykov, and A. Volotka
Relativistically prolonged lifetime of the 2s2p $^3P_0$ level of zero nuclear-spin beryllium-like ions
New Journal of Physics **17**, 103009 (2015).

N. Frommgen, D. L. Balabanski, M. L . Bissell, J. Bieron, K. Blaum, B. Cheal, K. Flanagan, S. Fritzsche, C. Geppert, M. Hammen, M. Kowalska, K. Kreim, A. Krieger, R. Neugart, G. Neyens, M. M. Rajabali, W. Nörtershäuser, J. Papuga, and D. T. Yordanov
Collinear laser spectroscopy of atomic cadmium Extraction of nuclear magnetic dipole and electric quadrupole moments
European Physical Journal D **69**, 164 (2015).

C. Gaida, M. Gebhardt, F. Stutzki, C. Jauregui, J. Limpert, and A. Tünnermann
Self-compression in a solid fiber to 24 MW peak power with few-cycle pulses at 2 μm wavelength
Optics Letters **40**, 5160 (2015).

C. Gaida, M. Kienel, M. Müller, A. Klenke, M. Gebhardt, F. Stutzki, C. Jauregui, J. Limpert, and A. Tünnermann
Coherent combination of two Tm-doped fiber amplifiers
Optics Letters **40**, 2301 (2015).

T. Gassner, and H. F. Beyer
Spatial characterization of the internal gas target at the ESR for the FOCAL experiment
Physica Scripta **T166**, 014052 (2015).

M. Gebhardt, C. Gaida, S. Hädrich, F. Stutzki, C. Jauregui, J. Limpert, and A. Tünnermann
Nonlinear compression of an ultrashort-pulse thulium-based fiber laser to sub-70 fs in Kagome photonic crystal fiber
Optics Letters **40**, 2770 (2015).

M. Gebhardt, C. Gaida, F. Stutzki, S. Hädrich, C. Jauregui, J. Limpert, and A. Tünnermann
Impact of atmospheric molecular absorption on the temporal and spatial evolution of ultra-short optical pulses
Optics Express **23**, 13776 (2015).

R. Geithner, F. Kurian, H. Reeg, M. Schwickert, R. Neubert, P. Seidel, and T. Stöhlker
A squid-based beam current monitor for FAIR/CRYRING
Physica Scripta **T166**, 014057 (2015).

H. Gies, F. Karbstein, and N. Seegert
Quantum reflection of photons off spatio-temporal electromagnetic field inhomogeneities
New Journal of Physics **17**, 043060 (2015).

M. Guerra, T. Stöhlker, P. Amaro, J. Machado, and J. P. Santos
Electron impact ionization cross-sections for few-electron uranium ions
Journal of Physics B: Atomic, Molecular and Optical Physics **48**, 144027 (2015).

A. Gumberidze, T. Stöhlker, and Y. Litvinov
Atomic physics at the future facility for antiproton and ion research: status report 2014
Physica Scripta **T166**, 014076 (2015).

A. Gumberidze, D. B. Thorn, C. J. Fontes, B. Najjari, H. L. Zhang, A. Surzhykov, A. Voitkiv, S. Fritzsche, D. Banaś, H. Beyer, W. Chen, R. D. DuBois, S. Geyer, R. E. Grisenti, S. Hagmann, M. Hegewald, S. Hess, C. Kozhuharov, R. Märtin, N. Petridis, R. Reuschl, A. Simon, U. Spillmann, M. Trassinelli, S. Trotsenko, G. Weber, D. F. A. Winters, N. Winters, D. Yu, and Th. Stöhlker
Ground-state excitation of heavy highly-charged ions
Journal of Physics B: Atomic, Molecular and Optical Physics **48**, 144006 (2015).

S. Hädrich, M. Krebs, A. Hoffmann, A. Klenke, J. Rothhardt, J. Limpert, and A. Tünnermann
Exploring new avenues in high repetition rate table-top coherent extreme ultraviolet sources
Light: Science & Applications **4**, e320 (2015).

T. Hahn, J. Bierbach, C. Rödel, D. Hemmers, M. Yeung, B. Dromey, S. Fuchs, A. Galestian, S. Kuschel, M. Zepf, G. Paulus, and G. Pretzler
Broadband XUV polarimetry of high harmonics from plasma surfaces using multiple Fresnel reflections
Applied Physics B **118**, 241 (2015).

K. Heeg, J. Haber, D. Schumacher, L. Bocklage, H.-C. Wille, K. Schulze, R. Loetzsch, I. Uschmann, G. Paulus, R. Rüffer, R. Röhlsberger, and J. Evers
Tunable Subluminal Propagation of Narrow-band X-Ray Pulses
Physical Review Letters **114**, 203601 (2015).

D. Hengstler, M. Keller, C. Schötz, J. Geist, M. Krantz, S. Kempf, L. Gastaldo, A. Fleischmann, T. Gassner, G. Weber, R. Märtin, Th. Stöhlker, and C. Enss
Towards FAIR: first measurements of metallic magnetic calorimeters for high-resolution x-ray spectroscopy at GSI
Physica Scripta **T166**, 014054 (2015).

P.-M. Hillenbrand, S. Hagmann, D. H. Jakubassa-Amundsen, J. M. Monti, D. Banaś, K.-H. Blumenhagen, C. Brandau, W. Chen, P. D. Fainstein, E. De Filippo, A. Gumberidze, D. L. Guo, M. Lestinsky, Yu. A. Litvinov, A. Müller, R. D. Rivarola, H. Rothard, S. Schippers, M. S. Schöffler, U. Spillmann, S. Trotsenko, X. L. Zhu, and Th. Stöhlker
Electron-capture-to-continuum cusp in U^{88+}+N_2 collisions
Phyical Review A **91**, 022705 (2015).

P.-M. Hillenbrand, S. Hagmann, K. E. Stiebing, S. Schippers, Y. A. Litvinov, and T. Stöhlker
Experimental concepts of positron spectroscopy at HESR
Physica Scripta **T166**, 014026 (2015).

A. Hoffmann, M. Zürch, and C. Spielmann
Extremely Nonlinear Optics Using Shaped Pulses Spectrally Broadened in an Argon-or Sulfur Hexafluoride-Filled Hollow-Core Fiber
Applied Sciences **5**, 1310 (2015).

J. Holmberg, A. N. Artemyev, A. Surzhykov, V. A. Yerokhin, and Th. Stöhlker
QED corrections to radiative recombination and radiative decay of heavy hydrogenlike ions
Phyical Review A **92**, 042510 (2015).

H. Höppner, A. Hage, T. Tanikawa, M. Schulz, R. Riedel, U. Teubner, M. J. Prandolini, B. Faatz, and F. Tavella
An optical parametric chirped-pulse amplifier for seeding high repetition rate free-electron lasers
New Journal of Physics **17**, 053020 (2015).

M. Hornung, G. Becker, A. Seidel, J. Reislöhner, H. Liebetrau, L. Bock, S. Keppler, A. Kessler, M. Zepf, J. Hein, and M. Kaluza
Generation of 25-TW Femtosecond Laser Pulses at 515 nm with Extremely High Temporal Contrast
Applied Sciences **5**, 1970 (2015).

C. Jauregui, H.-J. Otto, F. Stutzki, J. Limpert, and A. Tünnermann
Simplified modelling the mode instability threshold of high power fiber amplifiers in the presence of photodarkening
Optics Express **23**, 20203 (2015).

C. João, F. Wagner, J. Körner, J. Hein, T. Gottschall, J. Limpert, and V. Bagnoud
A 10-mJ-level compact CPA system based on Yb:KGW for ultrafast optical parametric amplifier pumping
Applied Physics B **118**, 401 (2015).

E. Jordan, G. Cerchiari, S. Fritzsche, and A. Kellerbauer
High-Resolution Spectroscopy on the Laser-Cooling Candidate La^-
Physical Review Letters **115**, 113001 (2015).

H. Jörg, Z. Hu, H. Bekker, M. Blessenohl, D. Hollain, S. Fritzsche, A. Surzhykov, J. Crespo López-Urrutia, and S. Tashenov
Linear polarization of x-ray transitions due to dielectronic recombination in highly charged ions
Phyical Review A **91**, 042705 (2015).

F. Karbstein, H. Gies, M. Reuter, and M. Zepf
Vacuum birefringence in strong inhomogeneous electromagnetic fields
Physical Review D **92**, 071301 (2015).

F. Karbstein, and R. Shaisultanov
Stimulated photon emission from the vacuum
Physical Review D **91**, 113002 (2015).

F. Karbstein, and R. Shaisultanov
Photon propagation in slowly varying inhomogeneous electromagnetic fields
Physical Review D **91**, 085027 (2015).

C. Kern, M. Zürch, and C. Spielmann
Limitations of Extreme Nonlinear Ultrafast Nanophotonics
Nanophotonics **4**, 303 (2015).

M. Kienel, M. Müller, A. Klenke, T. Eidam, J. Limpert, and A. Tünnermann
Multidimensional coherent pulse addition of ultrashort laser pulses
Optics Letters **40**, 522 (2015).

J. Körner, J. Reiter, J. Hein, and M. Kaluza
Temporal Shaping of High Peak Power Pulse Trains from a Burst-Mode Laser System
Applied Sciences **5**, 1790 (2015).

O. Kovalenko, O. Dolinskii, Yu. A. Litvinov, R. Maier, D. Prasuhn, and Th. Stöhlker
Investigation of the heavy-ion mode in the FAIR High Energy Storage Ring
Physica Scripta **T166**, 014042 (2015).

O. Kovtun, V. Tioukine, A. Surzhykov, V. Yerokhin, B. Cederwall, and S. Tashenov
Spin-orbit interaction in bremsstrahlung and its effect on the electron motion in a strong Coulomb field
Phyical Review A **92**, 062707 (2015).

D. Kraus, J. Vorberger, J. Helfrich, D. O. Gericke, B. Bachmann, V. Bagnoud, B. Barbrel, A. Blazevic, D. C. Carroll, W. Cayzac, T. Döppner, L. B. Fletcher, A. Frank, S. Frydrych, E. J. Gamboa, M. Gauthier, S. Göde, E. Granados, G. Gregori, N. J. Hartley, B. Kettle, H. J. Lee, B. Nagler, P. Neumayer, M. M. Notley, A. Ortner, A. Otten, A. Ravasio, D. Riley, F. Roth, G. Schaumann, D. Schumacher, W. Schumaker, K. Siegenthaler, C. Spindloe, F. Wagner, K Wünsch, S. H. Glenzer, M. Roth, and R. W. Falcone
The complex ion structure of warm dense carbon measured by spectrally resolved x-ray scattering
Physics of Plasmas **22**, 056307 (2015).

T. Krings, U. Spillmann, D. Protić, C. Ross, Th. Stöhlker, G. Weber, L. Bombelli, R. Alberti, and T. Frizzi
Multi-element readout of structured HPGe-detectors for high-resolution x-ray spectroscopy using CUBE-preamplifiers
Journal of Instrumentation **10**, C02043 (2015).

A. G. Krygier, J. T. Morrison, S. Kar, H. Ahmed, A. Alejo, R. Clarke, J. Fuchs, A. Green, D. Jung, A. Kleinschmidt, Z. Najmudin, H. Nakamura, P. Norreys, M. Notley, M. Oliver, M. Roth, L. Vassura, M. Zepf, M. Borghesi, and R. R. Freeman
Selective deuterium ion acceleration using the Vulcan petawatt laser
Physics of Plasmas **22**, 053102 (2015).

S. Kuhn, M. Tiegel, A. Herrmann, J. Körner, R. Seifert, F. Yue, D. Klöpfel, J. Hein, M. C. Kaluza, and C. Rüssel
Effect of hydroxyl concentration on Yb^{3+} luminescence properties in a peraluminous lithium-alumino-silicate glass
Optical Materials Express **5**, 430 (2015).

S. Kuhn, M. Tiegel, A. Herrmann, C. Rüssel, S. Engel, C. Wenisch, S. Gräf, F. Müller, J. Körner, R. Seifert, F. Yue, D. Klöpfel, J. Hein, and M. Kaluza
Photo-acoustic spectroscopy and quantum efficiency of Yb3+ doped alumino silicate glasses
Journal of Applied Physics **118**, 103104 (2015).

B. Landgraf, A. Hoffmann, D. Kartashov, F. Gärtner, Z. Samsonova, P. Polynkin, J. Jacoby, T. Kühl, and C. Spielmann
Generation of multi-millijoule red-shifted pulses for seeding stimulated Raman backscattering amplifiers
Optics Express **23**, 7400 (2015).

W. Liu, D. N. Schimpf, T. Eidam, J. Limpert, A. Tünnermann, F. X. Kärtner, and G. Chang
Pre-chirp managed nonlinear amplification in fibers delivering 100 W, 60 fs pulses
Optics Letters **40**, 151 (2015).

S. X. Luan, W. Yu, M. Y. Yu, S. M. Weng, J. W. Wang, H. Xu, H. B. Zhuo, and A. Y. Wong
Trapping of intense light in hollow shell
Physics of Plasmas **22**, 093110 (2015).

I. A. Maltsev, V. M. Shabaev, I. I. Tupitsyn, A. I. Bondarev, Y. S. Kozhedub, G. Plunien, and Th. Stöhlker
Electron-positron pair creation in low-energy collisions of heavy bare nuclei
Phyical Review A **91**, 032708 (2015).

B. Manschwetus, N. Lin, J. Rothhardt, R. Guichard, T. Auguste, A. Camper, P. Breger, J. Caillat, M. Géléoc, T. Ruchon, R. Taïeb, B. Carré, and P. Salières
Self-Probing Spectroscopy of the SF 6 Molecule: A Study of the Spectral Amplitude and Phase of the High Harmonic Emission
The Journal of Physical Chemistry A **119**, 6111 (2015).

B. Marx-Glowna, K. Schulze, I. Uschmann, T. Kämpfer, G. Weber, C. Hahn, H.-C. Wille, K. Schlage, R. Röhlsberger, E. Förster, Th. Stöhlker, and G. Paulus
Influence of higher harmonics of the undulator in X-ray polarimetry and crystal monochromator design
Journal of Synchrotron Radiation **22**, 1151 (2015).

B. Mei, T. Aumann, S. Bishop, K. Blaum, K. Boretzky, F. Bosch, C. Brandau, H. Bräuning, T. Davinson, I. Dillmann, C. Dimopoulou, O. Ershova, Z. Fülöp, H. Geissel, J. Glorius, G. Gyürky, M. Heil, F. Käppeler, A. Kelic-Heil, C. Kozhuharov, C. Langer, T. Le Bleis, Y. Litvinov, G. Lotay, J. Marganiec, G. Münzenberg, F. Nolden, N. Petridis, R. Plag, U. Popp, G. Rastrepina, R. Reifarth, B. Riese, C. Rigollet, C. Scheidenberger, H. Simon, K. Sonnabend, M. Steck, T. Stöhlker, T. Szücs, K. Sümmerer, G. Weber, H. Weick, D. Winters, N. Winters, P. Woods, and Q. Zhong
First measurement of the ^{96}Ru(p,γ)^{97}Rh cross section for the p process with a storage ring
Physical Review C **92**, 035803 (2015).

S. R. Mirfayzi, S. Kar, H. Ahmed, A. G. Krygier, A. Green, A. Alejo, R. Clarke, R. R. Freeman, J. Fuchs, D. Jung, A. Kleinschmidt, J. T. Morrison, Z. Najmudin, H. Nakamura, P. Norreys, M. Oliver, M. Roth, L. Vassura, M. Zepf, and M. Borghesi
Calibration of time of flight detectors using laser-driven neutron source
Review of Scientific Instruments **86**, 073308 (2015).

R. Müller, D. Seipt, S. Fritzsche, and A. Surzhykov
Effect of bound-state dressing in laser-assisted radiative recombination
Phyical Review A **92**, 053426 (2015).

A. Ortner, S. Faik, D. Schumacher, M. Basko, A. Blazevic, S. Busold, S. Bedacht, W. Cayzac, A. Frank, D. Kraus, T. Rienecker, G. Schaumann, An. Tauschwitz, F. Wagner, and M. Roth
A novel double hohlraum target to create a moderately coupled plasma for ion stopping experiments
Nuclear Instruments and Methods in Physics Research Section B: Beam Interactions with Materials and Atoms **343**, 123 (2015).

A. Ortner, A. Frank, A. Blazevic, and M. Roth
Role of charge transfer in heavy-ion-beam-plasma interactions at intermediate energies
Physical Review E **91**, 023104 (2015).

A. Otto, D. Seipt, D. Blaschke, S. A. Smolyansky, and B. Kämpfer
Dynamical Schwinger process in a bifrequent electric field of finite duration: Survey on amplification
Physical Review D **91**, 105018 (2015).

A. Otto, D. Seipt, D. Blaschke, B. Kämpfer, and S. Smolyansky
Lifting shell structures in the dynamically assisted Schwinger effect in periodic fields
Physics Letters B **740**, 335 (2015).

H.-J. Otto, N. Modsching, C. Jauregui, J. Limpert, and A. Tünnermann
Impact of photodarkening on the mode instability threshold
Optics Express **23**, 15265 (2015).

A. A. Peshkov, S. Fritzsche, and A. Surzhykov
Ionization of H_2^+ molecular ions by twisted Bessel light
Phyical Review A **92**, 043415 (2015).

N. Petridis, R. E. Grisenti, Y. A. Litvinov, and T. Stöhlker
Prototype internal target design for storage ring experiments
Physica Scripta **T166**, 014051 (2015).

S. Ringleb, M. Vogel, S. Kumar, W. Quint, G. G. Paulus, and Th. Stöhlker
HILITE—ions in intense photon fields
Physica Scripta **T166**, 014067 (2015).

J. Rothhardt, S. Hädrich, S. Demmler, M. Krebs, D. Winters, T. Kuehl, T. Stöhlker, J. Limpert, and A. Tünnermann
Prospects for laser spectroscopy of highly charged ions with high-harmonic XUV and soft x-ray sources
Physica Scripta **T166**, 014030 (2015).

S. Rykovanov, C. Schroeder, E. Esarey, C. Geddes, and W. Leemans
Plasma Undulator Based on Laser Excitation of Wakefields in a Plasma Channel
Physical Review Letters **114**, 145003 (2015).

R. Sanchez, J. Ullmann, J. Vollbrecht, Z. Andelkovic, A. Dax, W. Geithner, C. Geppert, C. Gorges, M. Hammen, V. Hannen, S. Kaufmann, K. König, Y. A. Litvinov, M. Lochmann, B. Maass, J. Meisner, T. Murböck, W. Nörtershäuser, S. Schmidt, M. Schmidt, M. Steck, T. Stöhlker, R. C. Thompson, and C. Weinheimer
Hyperfine transition in $^{209}Bi^{80+}$ – one step forward
Physica Scripta **T166**, 014021 (2015).

M. S. Sanjari, X. Chen, P. Hülsmann, Y. A. Litvinov, F. Nolden, J. Piotrowski, M. Steck, and T. Stöhlker
Conceptual design of elliptical cavities for intensity and position sensitive beam measurements in storage rings
Physica Scripta **T166**, 014060 (2015).

G. Sarri, M. E. Dieckmann, I. Kourakis, A. Di Piazza, B Reville, C. H. Keitel, and M. Zepf
Overview of laser-driven generation of electron-positron beams
Journal of Plasma Physics **81**, 23 (2015).

G. Sarri, K. Poder, J. M. Cole, W. Schumaker, A. Di Piazza, B. Reville, T. Dzelzainis, D. Doria, L. A. Gizzi, G. Grittani, S. Kar, C. H. Keitel, K. Krushelnick, S. Kuschel, S. P. D. Mangles, Z. Najmudin, N. Shukla, L. O. Silva, D. Symes, A. G. R. Thomas, M. Vargas, J. Vieira, and M. Zepf
Generation of neutral and high-density electron-positron pair plasmas in the laboratory
Nature Communications **6**, 6747 (2015).

A. Sävert, S. P. D. Mangles, M. Schnell, E. Siminos, J. M. Cole, M. Leier, M. Reuter, M. B. Schwab, M. Möller, K. Poder, O. Jäckel, G. G. Paulus, C. Spielmann, S. Skupin, Z. Najmudin, and M. C. Kaluza
Direct Observation of the Injection Dynamics of a Laser Wakefield Accelerator Using Few-Femtosecond Shadowgraphy
Physical Review Letters **115**, 055002 (2015).

A. M. Sayler, M. Arbeiter, S. Fasold, D. Adolph, M. Möller, D. Hoff, T. Rathje, B. Fetić, D. B. Milošević, T. Fennel, and G. G. Paulus
Accurate determination of absolute carrier-envelope phase dependence using photo-ionization
Optics Letters **40**, 3137 (2015).

S. Schippers, A. Borovik Jr., T. Buhr, J. Hellhund, K. Holste, A. L. D. Kilcoyne, S. Klumpp, M. Martins, A. Müller, S. Ricz, and S. Fritzsche
Stepwise contraction of the nf Rydberg shells in the 3d photoionization of multiply-charged xenon ions
Journal of Physics B: Atomic, Molecular and Optical Physics **48**, 144003 (2015).

S. Schmidt, U. Lippmann, M. M. Günther, and H. Gross
Diffraction effects in laser beam shaping systems
Proceedings of SPIE **9626**, 962610 (2015).

M. Schnell, A. Sävert, I. Uschmann, O. Jansen, M. C. Kaluza, and C. Spielmann
Characterization and application of hard x-ray betatron radiation generated by relativistic electrons from a laser-wakefield accelerator
Journal of Plasma Physics **81**, 1 (2015).

D. Seipt, S. G. Rykovanov, A. Surzhykov, and S. Fritzsche
Narrowband inverse Compton scattering x-ray sources at high laser intensities
Phyical Review A **91**, 033402 (2015).

V. Serbo, I. P. Ivanov, S. Fritzsche, D. Seipt, and A. Surzhykov
Scattering of twisted relativistic electrons by atoms
Phyical Review A **92**, 012705 (2015).

J. Seres, E. Seres, B. Landgraf, B. Aurand, T. Kuehl, and C. Spielmann
Quantum Path Interference and Multiple Electron Scattering in Soft X-Ray High-Order Harmonic Generation
Photonics **2**, 104 (2015).

C. Shah, H. Jörg, S. Bernitt, S. Dobrodey, R. Steinbrügge, C. Beilmann, P. Amaro, Z. Hu, S. Weber, S. Fritzsche, A. Surzhykov, J. Crespo López-Urrutia, and S. Tashenov
Polarization measurement of dielectronic recombination transitions in highly charged krypton ions
Phyical Review A **92**, 042702 (2015).

Y. Shamir, J. Rothhardt, S. Hädrich, S. Demmler, M. Tschernajev, J. Limpert, and A. Tünnermann
High average power 2 μm few-cycle optical parametric chirped pulse amplifier at 100-kHz repetition rate
Optics letters **40**, 5546 (2015).

S. Stock, A. Surzhykov, S. Fritzsche, and D. Seipt
Compton scattering of twisted light: Angular distribution and polarization of scattered photons
Phyical Review A **92**, 013401 (2015).

Th. Stöhlker, V. Bagnoud, K. Blaum, A. Blazevic, A. Bräuning-Demian, M. Durante, F. Herfurth, M. Lestinsky, Y. Litvinov, S. Neff, R. Pleskac, R. Schuch, S. Schippers, D. Severin, A. Tauschwitz, C. Trautmann, D. Varentsov, and E. Widmann
APPA at FAIR: From fundamental to applied research
Nuclear Instruments and Methods in Physics Research Section B: Beam Interactions with Materials and Atoms **365**, 680 (2015).

T. Stöhlker, and Y. A. Litvinov
Atomic physics experiments at the high energy storage ring
Physica Scripta **T166**, 014025 (2015).

F. Stutzki, C. Gaida, M. Gebhardt, F. Jansen, C. Jauregui, J. Limpert, and A. Tünnermann
Tm-based fiber-laser system with more than 200 MW peak power
Optics Letters **40**, 9 (2015).

A. Surzhykov, D. Seipt, V. G. Serbo, and S. Fritzsche
Interaction of twisted light with many-electron atoms and ions
Phyical Review A **91**, 013403 (2015).

A. Surzhykov, V. A. Yerokhin, T. Stöhlker, and S. Fritzsche
Rayleigh x-ray scattering from many-electron atoms and ions
Journal of Physics B: Atomic, Molecular and Optical Physics **48**, 144015 (2015).

S. Tashenov, D. Banas, H. Beyer, C. Brandau, S. Fritzsche, A. Gumberidze, S. Hagmann, P.-M. Hillenbrand, H. Jörg, I. Kojouharov, C. Kozhuharov, M. Lestinsky, Y. A. Litvinov, A. V. Maiorova, H. Schaffner, V. M. Shabaev, U. Spillmann, T. Stöhlker, A. Surzhykov, and S. Trotsenko
Coherent population of magnetic sublevels of $2p_{3/2}$ state in hydrogenlike uranium by radiative recombination
Physica Scripta **T166**, 014027 (2015).

C. Trageser, C. Brandau, C. Kozhuharov, Y. A. Litvinov, A. Müller, F. Nolden, S. Sanjari, and T. Stöhlker
A new data acquisition system for Schottky signals in atomic physics experiments at GSI's and FAIR's storage rings
Physica Scripta **T166**, 014062 (2015).

S. Trotsenko, A. Gumberidze, Y. Gao, C. Kozhuharov, S. Fritzsche, H. F. Beyer, S. Hagmann, P.-M. Hillenbrand, N. Petridis, U. Spillmann, A. Surzhykov, D. B. Thorn, G. Weber, and T. Stöhlker
Experimental study of the dielectronic recombination into Li-like uranium
Physica Scripta **T166**, 014024 (2015).

J. Ullmann, Z. Andelkovic, A. Dax, W. Geithner, C. Geppert, C. Gorges, M. Hammen, V. Hannen, S. Kaufmann, K. König, Y. Litvinov, M. Lochmann, B. Maass, J. Meisner, T. Murböck, R. Sánchez, M. Schmidt, S. Schmidt, M. Steck, T. Stöhlker, R. C. Thompson, J. Vollbrecht, C. Weinheimer, and W. Nörtershäuser
An improved value for the hyperfine splitting of hydrogen-like $^{209}Bi^{82+}$
Journal of Physics B: Atomic, Molecular and Optical Physics **48**, 144022 (2015).

M. Vogel, G. Birkl, M. Ebrahimi, D. von Lindenfels, A. Martin, G. Paulus, W. Quint, S. Ringleb, Th. Stöhlker, and M. Wiesel
Extreme-field physics in Penning traps
Hyperfine Interactions **1**, 1 (2015).

J. Vollbrecht, Z. Andelkovic, A. Dax, W. Geithner, C. Geppert, C. Gorges, M. Hammen, V. Hannen, S. Kaufmann, K. König, Y. Litvinov, M. Lochmann, B. Maass, J. Meisner, T. Murboeck, W. Nörtershäuser, R. Sánchez, S. Schmidt, M. Schmidt, M. Steck, T. Stöhlker, R. C. Thompson, J. Ullmann, and C. Weinheimer
Laser spectroscopy of the ground-state hyperfine structure in H-like and Li-like bismuth
Journal of Physics: Conference Series **583**, 012002 (2015).

O. de Vries, T. Saule, M. Plötner, F. Lücking, T. Eidam, A. Hoffmann, A. Klenke, S. Hädrich, J. Limpert, S. Holzberger, T. Schreiber, R. Eberhardt, I. Pupeza, and A. Tünnermann
Acousto-optic pulse picking scheme with carrier-frequency-to-pulse-repetition-rate synchronization
Optics Express **23**, 19586 (2015).

F. Wagner, S. Bedacht, V. Bagnoud, O. Deppert, S. Geschwind, R. Jaeger, A. Ortner, A. Tebartz, B. Zielbauer, D. H. H. Hoffmann, and M. Roth
Simultaneous observation of angularly separated laser-driven proton beams accelerated via two different mechanisms
Physics of Plasmas **22**, 063110 (2015).

H. Y. Wang, B. Liu, X. Q. Yan, and M. Zepf
Gamma-ray emission in near critical density plasmas at laser intensities of 10^{21} W/cm^2
Physics of Plasmas **22**, 033102 (2015).

H. Y. Wang, X. Q. Yan, and M. Zepf
High-energy monoenergetic proton beams from two stage acceleration with a slow laser pulse
Physical Review ST - Accelerators and Beams **18**, 021302 (2015).

H. Y. Wang, X. Q. Yan, and M. Zepf
Signatures of quantum radiation reaction in laser-electron-beam collisions
Physics of Plasmas **22**, 093103 (2015).

G. Weber, K.-H. Blumenhagen, H. Bräuning, H. Ding, S. Fritzsche, S. Hess, R. Märtin, U. Spillmann, A. Surzhykov, S. Trotsenko, D. F. A. Winters, V. A. Yerokhin, and T. Stöhlker
Compton polarimetry using double-sided segmented x-ray detectors
Journal of Physics: Conference Series **583**, 012041 (2015).

G. Weber, H. Bräuning, A. Surzhykov, C. Brandau, S. Fritzsche, S. Geyer, R. E. Grisenti, S. Hagmann, C. Hahn, R. Hess, S. Hess, C. Kozhuharov, M. Kühnel, R. Märtin, N. Petridis, U. Spillmann, S. Trotsenko, D. F. A. Winters, and Th. Stöhlker
Combined linear polarization and angular distribution measurements of x-rays for precise determination of multipole-mixing in characteristic transitions of high-Z systems
Journal of Physics B: Atomic, Molecular and Optical Physics **48**, 144031 (2015).

G. Weber, H. Ding, M. O. Herdrich, and A. Surzhykov
Towards a fast calculator for the radiation characteristics of radiative recombination and radiative electron capture
Journal of Physics: Conference Series **599**, 012040 (2015).

G. Weber, M. Herdrich, R. DuBois, P.-M. Hillenbrand, H. Beyer, L. Bozyk, T. Gassner, R. Grisenti, S. Hagmann, Y. Litvinov, F. Nolden, N. Petridis, M. Sanjari, D. Winters, and Th. Stöhlker
Total projectile electron loss cross sections of U^{28+} ions in collisions with gaseous targets ranging from hydrogen to krypton
Physical Review ST - Accelerators and Beams **18**, 034403 (2015).

L. Willingale, S. Nagel, A. Thomas, C. Bellei, R. Clarke, A. Dangor, R. Heathcote, M. Kaluza, C. Kamperidis, S. Kneip, K. Krushelnick, N. Lopes, S. P. D. Mangles, W. Nazarov, P. M. Nilson, and Z. Najmudin
Characterization of laser-driven proton beams from near-critical density targets using copper activation
Journal of Plasma Physics **81**, 365810102 (2015).

D. Winters, T. Beck, G. Birkl, C. Dimopoulou, V. Hannen, T. Kühl, M. Lochmann, M. Loeser, X. Ma, F. Nolden, W. Nörtershäuser, B. Rein, R. Sánchez, U. Schramm, M. Siebold, P. Spiller, M. Steck, T. Stöhlker, J. Ullmann, T. Walther, W. Wen, J. Yang, D. Zhang, and M. Bussmann
Laser cooling of relativistic heavy-ion beams for FAIR
Physica Scripta **T166**, 014048 (2015).

Z. W. Wu, S. Fritzsche, and A. Surzhykov
Nuclear magnetic dipole moment effect on the angular distribution of the K-alpha lines
Physica Scripta **T166**, 014029 (2015).

Z. W. Wu, A. Surzhykov, N. M. Kabachnik, C. Z. Dong, and S. Fritzsche
Linear polarization of x-rays emitted in the decay of highly-charged ions via overlapping resonances
Journal of Physics: Conference Series **635**, 012020 (2015).

Z. W. Wu, Y. Z. Zhang, Y. B. Fu, A. Surzhykov, S. Fritzsche, and C. Dong
Dielectronic recombination rate coefficients of initially rubidium-like tungsten
European Physical Journal D **69**, 140 (2015).

P. Wustelt, M. Möller, T. Rathje, A. M. Sayler, T. Stöhlker, and G. G. Paulus
Momentum-resolved study of the saturation intensity in multiple ionization
Phyical Review A **91**, 031401 (2015).

V. A. Yerokhin, A. N. Artemyev, V. M. Shabaev, Th. Stöhlker, A. Surzhykov, and S. Fritzsche
Target effects in negative-continuum-assisted dielectronic recombination
Phyical Review A **92**, 042708 (2015).

V. A. Yerokhin, A. Surzhykov, and S. Fritzsche
Relativistic configuration-interaction calculation of Kα transition energies in beryllium-like argon
Physica Scripta **90**, 054003 (2015).

M. Yeung, J. Bierbach, E. Eckner, S. Rykovanov, S. Kuschel, A. Sävert, M. Förster, C. Rödel, G. Paulus, S. Cousens, M. Coughlan, B. Dromey, and M. Zepf
Noncollinear Polarization Gating of Attosecond Pulse Trains in the Relativistic Regime
Physical Review Letters **115**, 193903 (2015).

U. Zastrau, P. Sperling, C. Fortmann-Grote, A. Becker, T. Bornath, R. Bredow, T. Döppner, T. Fennel, L. B. Fletcher, E. Förster, S. Göde, G. Gregori, M. Harmand, V. Hilbert, T. Laarmann, H. J. Lee, T. Ma, K. H. Meiwes-Broer, J. P. Mithen, C. D. Murphy, M. Nakatsutsumi, P. Neumayer, A. Przystawik, S. Skruszewicz, J. Tiggesbäumker, S. Toleikis, T. G. White, S. H. Glenzer, R. Redmer, and T. Tschentscher
Ultrafast electron kinetics in short pulse laser-driven dense hydrogen
Journal of Physics B: Atomic, Molecular and Optical Physics **48**, 224004 (2015).

V. A. Zaytsev, S. Tashenov, A. V. Maiorova, V. M. Shabaev, and T. Stöhlker
Parity nonconservation effect in the resonance elastic electron scattering on heavy He-like ions
Journal of Physics B: Atomic, Molecular and Optical Physics **48**, 165003 (2015).

M. Zürch, and C. Spielmann
Extreme ultraviolet digital in-line holography using a tabletop source
Applied Optics **54**, 5992 (2015).